Abrasive Impact Wear:
Tester, Wear and Grindability Studies

RIHO TARBE

TALLINN UNIVERSITY OF TECHNOLOGY
Faculty of Mechanical Engineering
Department of Materials Engineering

Dissertation was accepted for the defence of the degree of Doctoral of Philosophy in Engineering on 23.04.2009

Supervisor: Prof. Priit Kulu, Department of Materials Engineering, Tallinn University of Technology

Co-supervisor: Prof. Helmo Käerdi, Department of Mathematics, Estonian Public Service Academy

Opponents: Prof. Michal Besterci, Institute of Materials Research, Slovak Academy of Sciences, Košice, Slovakia

Irina Hussainova D. Eng., Department of Materials Engineering, Tallinn University of Technology

Prof. Rein Laaneots, Department of Mechatronics, Tallinn University of Technology

Defence of the thesis: 4.06.2009 at 14:00
Room No.: V-215
Tallinn University of Technology
Ehitajate tee 5, Tallinn, Estonia

Declaration

Hereby I declare that this doctoral thesis, my original investigation and achievement, submitted for the doctoral degree at Tallinn University of Technology has not been submitted for any academic degree.

/töö autori nimi ja allkiri/

Abrasiivlöökkulumine: seade, kulumise ja jahvatatavuse uuringud

RIHO TARBE

CONTENTS

INTRODUCTION

As [1] claims, size reduction – the oldest engineering process – had its beginnings in prehistoric times, when early humans pounded grains and nuts with stones to free edible inner parts from the hard protective shells. It shows a wide historical background of size reduction, although we focus on milling of abrasive mineral materials. There is a lot of truth in saying that all that moves, wears. Always should be a reason for investigating wear.

Impact-based milling tends to produce a favourable cubical product, ensuring particle breakage chiefly along the planes of weakness; thereby the resultant product is free of weak zones. The drawback of impact-based milling is a high wear rate of the mills, which raises the importance of a good testing apparatus for studying the behaviour of the crusher materials.

The two most commonly used working principles of erosion testers are gas-blasting or centrifugal-accelerating. In the testers built so far is not possible to test with erosion particles bigger than 2 mm. Due to the need for abrasive impact wear tester enabling to test bigger particles than 2 mm, and considering good properties of centrifugal-accelerators, focuses this work to disintegrator type tester development for testing two-body wear process in the conditions of impact wear as well as grindability of abrasive mineral materials.

The present study focuses on design of universal impact wear tester, on testing method, wear study of materials for grinding media as well on study of gindability and abrasivity of abrasive mineral materials.

The developed impact wear tester has gained an interest from abroad, as Metso Powdermet AB from Finland and Swedish Steel AB from Sweden have ordered several test series from us, and hopefully our collaboration continues in the future.

Acknowledgements

ABBREVIATONS, TERMS AND SYMBOLS

A	average active surface area of the specimen
A_c	abrasivity
AEW	Abrasive Erosive wear
AIW	Abrasive Impact Wear
$\vec{a}_r$	acceleration relative to the second reference frame
$a(x_i)$	the half-with of the interval
b	impact zone width
b_{st}	standard impact zone width
C	Cohran's C test value
C_1, C_2	constants of integration
CAK	Centrifugal Accelerator of Kleis
c_i	sensitivity coefficient for input quantity X_i
COF	coefficient of friction
COR	coefficient of restitution
$C_{Crp}(K, J)$	Cohran's critical values
DESI	the name of the disintegrator, which was the basis for impact wear tester
d	calculated wear crater diameter
D_2	the mean diameter of the erodent particle
d_{50}	median particle size
e	mathematical constant
E_k^p	kinetic energy of a particle
E_s	specific energy of treatment
E'	the reduced modulus of elasticity
E_1 and E_2	Young's modulus of the target material and the abrasive particle
F	fusion
FSF	flame spray fusion
$\vec{\Phi}_c$	Coriolis inertial force
$\vec{\Phi}_e$	inertial force relative to second reference frame
$\vec{F}_\alpha$	active forces and bond reactions
GG	granite gravel
GOST	state standard of former USSR
GS	Granite Sand
H_a	abrasive hardness
H_1	the hardness of the material
h	impact zone height
$\bar{h}$	average impact zone height
h_p	the depth of the wear crater after single impact of the particle
h_{st}	standard impact zone height
HV	Vickers hardness

HV'	weighted Vickers hardness
HVOFS	High Velocity Oxy-Fuel Spray
I_g	wear rate, mg/kg
I_v	volumetric wear rate, mm^3/kg
J ($j = 1, 2, \ldots, J$)	series of measurement
K	correction
K ($k = 1, 2, \ldots, K$)	repetitions in the series of measurement
$\boldsymbol{K}_i$ and $\boldsymbol{K}_f$	initial and final kinetic energy of a particle
k	coverage factor
L.A.	Los Angeles
M	total number of sets of repeated measurements
m	mass
m_a	mass of the specimen after the test
m_{abr}	total mass of abrasive
m_b	mass of the specimen before the test
MMC	Metal Matrix Composite
m_p	mass of a particle,
Δm	specimen mass loss,
Δm_{unit}	unit mass loss in mg/mm^2, calculated by dividing mass loss of each specimen with impacted zone area in mm^2
n	counted number of particles
p	confidence level
Q	abrasive amount
QG	quartzite gravel
QS	quartzite sand
R	turning radius, m
$r(x_i, x_k)$	correlation
SSAB	Swedish Steel AB
SP	spike value
s_p	pooled standard deviation (that is the combination of experimental standard deviations)
SPQ	Spike Parameter – Quadratic fit
$s(x_i)$	experimental standard deviation
$s(\bar{x}_i)$	experimental standard deviation of arithmetic mean
t	time
T	frictional force
TUT	Tallinn University of Technology
$u_i(h)$	instrument's uncertainty
$u_m(\bar{h})$	method uncertainty (it takes into account width variations of the specimens)
$u(x_i)$	standard measurement uncertainty
$u(\bar{x}_i)$	standard measurement uncertainty of arithmetic mean
$u(x_i, x_k)$	covariance
v_{ej}	ejection velocity from the impeller

v_{fin}	real velocity acting on the specimen at the end of the collision phase
v_{fin}^{n}, v_{st}^{n}, v_{pin}^{n}	velocity components normal to the work surface area of the specimens
v_{fin}^{τ}, v_{st}^{τ}, v_{pin}^{τ}	velocity components tangential to the work surface area of the specimens
v_{impst}	impingement velocity from the outer side of the 1st specimens ring
v_{impfin}	impingement velocity from the inner side of the 1st specimens ring
v_{pin}	linear velocity of the 1st circle of pins.
$\bar{v}_{r}$	particle velocity in the second reference frame
v_{st}	real velocity acting on the specimen at the beginning of the collision phase
v_{τ}	tangential velocity
v_{2max} circle	maximal theoretical impact velocity during the contact with 2nd of specimens
VSI	vertical shaft impact
ΔV	volume loss (mm^3), calculated by dividing average mass loss of standard size specimen with the density
X_i, $(i = 1, \ldots, N)$ input quantities	
x_i, $(i = 1, \ldots, N)$ estimates of the input quantities	
Y	measurand, a particular quantity that is the subject of the measurement
y	estimate of the measurand
$\bar{y}$	arithmetic mean of the estimate of measurand
W_{net}	mechanical work
3D	three dimensional
α	ejection angle
β	imaginary impact angle
β_{fin}	final imaginary impact angle formed at the end of collision phase
β_{st}	starting imaginary impact angle formed at the beginning of collision phase
γ_{fin}	real impact angle formed at the end of the collision phase
γ_{st}	real impact angle formed at the beginning of the collision phase
ε_v	relative volumetric wear resistance
θ_{st}	impingement angle from the outer side of the 1st circle of specimens
θ_{fin}	impingement angle from the inner side of the 1st circle of specimens
μ	frictional coefficient
μ_1 and μ_2	Poisson's ratios for target material and abrasive particle
v_i	degrees of freedom

ξ	indicate axle originating from the tip of the impeller and is equal with the length of the impeller, its derivate $\dot{\xi}$ is equal with relative velocity
ρ	density
ρ_2	the density of erodent particle
τ_0 / e_s	a dimensionless universal parameter used to determine wear resistance of metals
χ	abrasive fraction allocated for a specimen
ω	angular velocity, rad/s

1 REVIEW OF THE LITERATURE

1.1 Modes of wear

Wear is mostly a problem and an inevitable cause of any useful engineering process. In the [2] is claimed, that wear testing has traditionally been used by material engineers and scientists to rank wear resistance of materials for the purpose of optimizing materials selection or development for a given application. Wear is not a basic material property, but a system response of the material. Wear is generally defined as a progressive loss or displacement of material from a surface as a result of relative motion between that surface and another. Engel in [3] describes wear in a similar way. However, Bayer in [4] emphasizes, that nowadays material wear is not limited to loss of material. An example would be the change in the geometry or dimension of a part as the result of plastic deformation, such as from repeated hammering, or the development of a network of cracks in a surface. Bayer in [4] categorises wear into following categories:
- adhesion,
- single-cycle deformation,
- repeated-cycle deformation,
- oxidation (corrosion, chemical),
- thermal,
- tribofilm,
- atomic,
- abrasion.

The most relevant for us is abrasion, because impact wear tester developed under this work can be characterised by abrasive erosion. Engel claims in [3], that abrasion is sometimes indiscriminately associated with erosion, so that the erosive particles are often referred to as "abrasives". Bayer agrees in [4, 5] that particle erosion and slurry erosion may be considered forms of abrasive wear; just the major difference is how the abrasives are forced against the surface. In erosion the particles are not trapped between two solid particles, but impact the surface as free bodies. Bayer in [5] classifies one body-contact, when single body is in contact with a fluid or stream of particles. Engel in [3] adds that one-body contact is if only one body is under consideration, in two-body contact the wear of both parts is under investigation (as it is in impact wear tester).

According to the [6] is impingement erosion or impact erosion erosive wear where motion of the solid particles is nearly normal to the solid surface. From a wear mechanism point of view, impact wear can be considered as equal to erosive wear, but in erosive wear the impacting particles are small compared to the surface being impacted. If abrasive particles are bigger than 2 mm then we call it impact wear. If impact angle is not normal to the work surface, it induces

relative velocity parallel to the interface and according to [5] this is called compound impact.

Mechanical contact between solids may result from various basic models of relative motion and impact is one of them. Other models are sliding, and rolling. In each case, large contact stresses may arise, but their character, distribution and variation in time are unique (Figure 1.1).

a

b

c
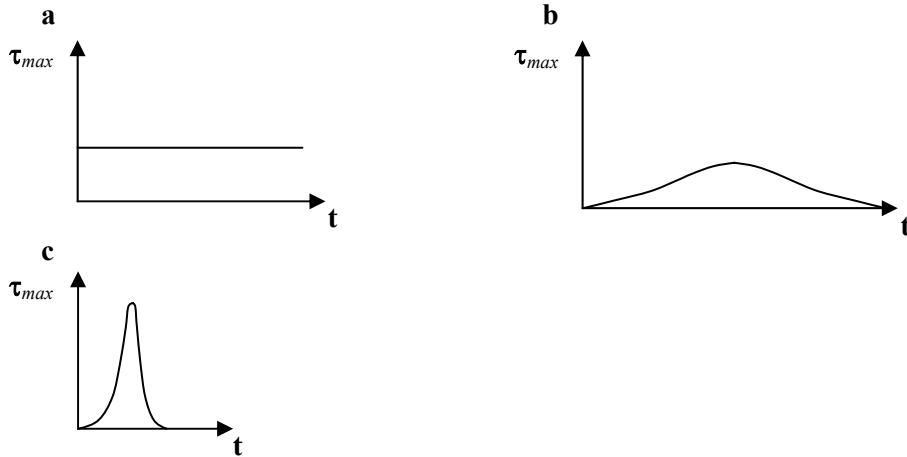
Figure 1.1 Maximum shear stress τ_{max} variation in time in three types of contact: a − sliding (the shear stress on the slider is shown); b − rolling; c − impact [3]

Impact wear is characterized by narrow and high peak of stress because of very short duration of impact. The force **F** during impact is very big and this is the reason for using momentums instead of forces in kinematical calculations of impacts [7]:

$$\mathbf{I} = \int_{t_i}^{t_f} \mathbf{F} dt = \Delta p, \qquad (1.1)$$

where

$\Delta \mathbf{p} = \mathbf{p}_f - \mathbf{p}_i,$

$\mathbf{p}_i$ and $\mathbf{p}_f$ − initial and final momentum of a particle,

$\mathbf{I}$ − impulse of the particle,

t_i and t_f −initial and final time,

Bayer explains in [8], that single-cycle and repeated-cycle wear mechanisms can be associated with tribosystems. With a low angle of impingement, abrasion mechanisms tend to become more predominant, but as the angle increases, repeated-cycle deformation becomes more significant. The same trend was confirmed by Kleis and Kulu in [9]. If the number of cycles in repeated-cycle deformation is small, it is called low cyclic fatigue.

Finally it is good to finish with lines of [2], which says that wear test simulation does not require that an application be replicated to provide valid data. For example, the dry-sand rubber wheel test, useful in ranking material

wear situations involving dry, low-stress scratching abrasion, is not typical of the situations to which the results are applied.

1.2   Grinding equipment

The purpose of a crushing process is to reduce the size of natural or blasted rock to desired size fractions [10]. Grinding itself is not the same as crushing: in the [11] is claimed, that grinding is the process when size reduction of below (5−20) mm is needed. In the [10] is shown that in grinding is the final product size below 10 mm and that grinding is the same as milling. In the [11] is added, that grinding is a powdering or pulverizing process. As a conclusion can be said, that if the final product is smaller than about 15 mm, the comminution process is grinding, if it is bigger, the process is crushing.

In this chapter, various well-known crushing and grinding methods are briefly introduced. They are divided according to the principle to impact-based milling and compression-based milling, like it was done in [10]. Roller milling (the simplest form is arrastra) and tumbling milling (present in ball mills and rod mills) discussed in [1] and [11] are found to be too far from present work and have not been covered here.

1.2.1   Impact-based milling

Impact-based milling is a direct scope of this thesis, because impact wear tester basing on a disintegrator DESI (chapter 2) belongs to this group. Impact-based milling will be introduced more thoroughly than compression-based milling.

As it is explained in [1], impact-based milling comprises milling processes, where crushable particles are propelled to the collision with breaker plate or each other. Shattering occurs due to the high energy of collision. In the [12] is brought out an important positive side of impact based milling: the high energy interparticle and particle-to-rock-bed collisions produce a particle breakage chiefly along planes of weakness, such as mineral boundaries, jointing and micro fractures. The resultant product is free of weak zones, and often has the valuable mineral exposed or liberated [12].

In both [1] and [10] is claimed, that impact-based milling tends to produce a cubical/round product. As [13] claims, cubical shape is favourable in the construction industry; because the consumption of cement can be minimized if the rock is round/cubical. Svensson in [14] found additionally, that cubical rock pumping characteristics are much better. Here a parallel with thermal powder spraying can be drawn, where the shape of the powder must be also cubical due to flowability reasons [15]. A practical example on the favour of final cubical abrasive product concerning road building is given in [10], where is presented the fact that the wear resistance of road surface is better with cubical product, especially in the countries where studded tires are used.

In both [1] and [10] is concluded, that highly favourable cubical shape of the product is the reason, why impact based milling is used despite high wear of the machines: [10] specifies that the wear cost can be up to 10 times higher than for a cone crusher, representing compression based milling. Additionally impact-based milling can provide higher crushing rations than jaw and gyratory crushers (see subchapter 1.2.2).

The shape of final product depends also from feed material: flaky feeds have a tendency to give better shaped product than cubical feed, because then flaky product is broken in the middle there will be two cubical pieces of rock. The general opinion is that a higher speed gives better cubicity, because higher speed results in higher impact on the rock which thus breaks into more cubical product [10].

Hammer mill impact crushers
The material in a hammer mill is fed uniformly to the breakage zone (Figure 1.2).
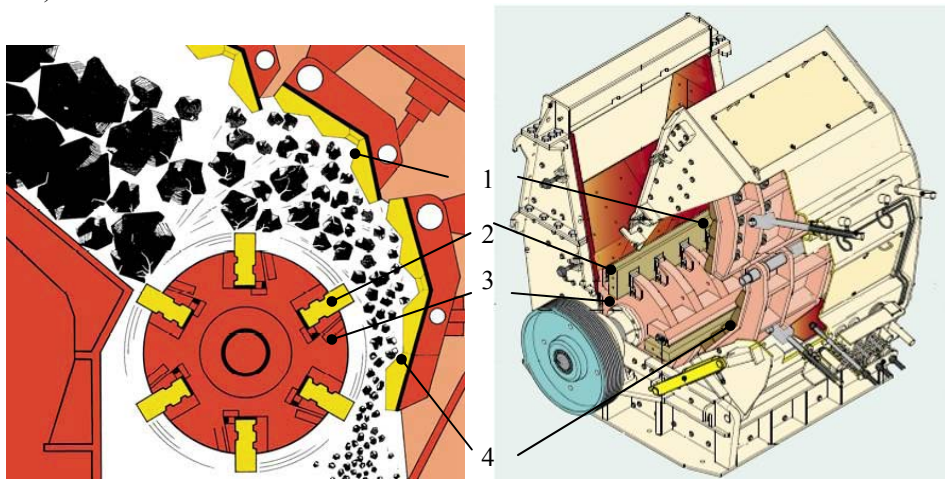
Figure 1.2 Hammer mill impact crusher. 1 – 1st breaker plate, 2 – hammer, 3 – rotor, 4 – 2nd breaker plate [17, 18]

The hammers are attached to the shaft. They deliver heavy blows, shattering the rock and throwing it against the breaker plate. Broken pieces rebound, and the procedure is repeated until the fragments leave the mill through a grate in the bottom of the machine. The capacity of a hammer mill is more dependent on the nature of the material than is the case for most other crushers. It also relies on the velocity of the hammers and the aperture of ejection grate. The energy in the hammers is maintained by the kinetic energy in the rotor shaft, often supplemented by heavy flywheels attached to the ends of the shaft [1]. Hammer mills are used for primary, secondary, and fine crushing [16].

The reduction ratio in a hammer mill is very high, up to 20:1 in open circuit and much more in closed circuit. The potentially high wear rates of the hammers and side plates generally limit the use of hammer mills to the crushing

of soft, nonabrasive rocks such as limestone, coal or gypsum, or for the grinding of hay and grains for chopped feed. It also suits very well for crushing mineral based medium hard abrasives, like asphalt and concrete [1].

A rule of thumb has been that hammer mills are suitable for materials containing not more than 5% silica, doubtful for a silica content of 10%–15%, dangerous if 20%–25%, and prohibitive if it exceeds 30%. However, for example Metso's Nordberg NP Series impact crusher suits for crushing minerals having Los Angeles (L.A.) test coefficient smaller than 12 [1, 18, 16].

Vertical-shaft impact crushers
The shattering can also be caused by the collision of a rock travelling at high velocity with another rock or a breaker plate. This is the concept of Barmac vertical-shaft impact (VSI) crusher invented by Jim Macdonald in 1970. His approach was [1]:
- stones will break if you bang them together hard enough (thus saving wear on metal parts),
- steel will be protected from abrasive wear if covered by a layer of trapped stones.

Figure 1.3 shows a Barmac VSI crusher, where the crushing rock protects anvils. Barmac VI vertical shaft impact crushers are used for crushing materials ranging from those of low abrasion to extremely abrasive products in industry [19].
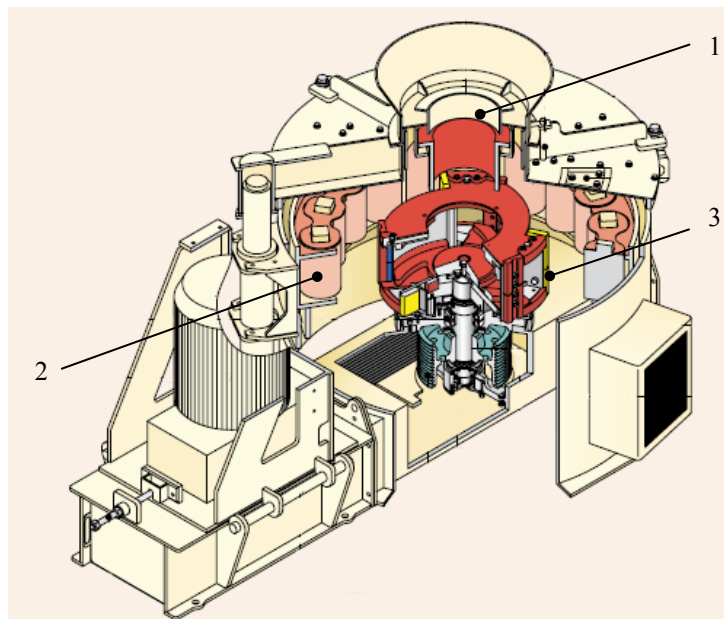
Figure 1.3 Barmac VI series VSI Crusher: 1 – feed tube, 2 – anvils, 3 – rotor [19]

The feed material is accelerated to speeds of up to 80 m/s before being discharged into the crushing chamber (Figure 1.3).

For decreasing machine wear and energy consumption, a modified rock-on-rock crusher with two feed streams (Duopactor) has been developed (Figure 1.4) [12].
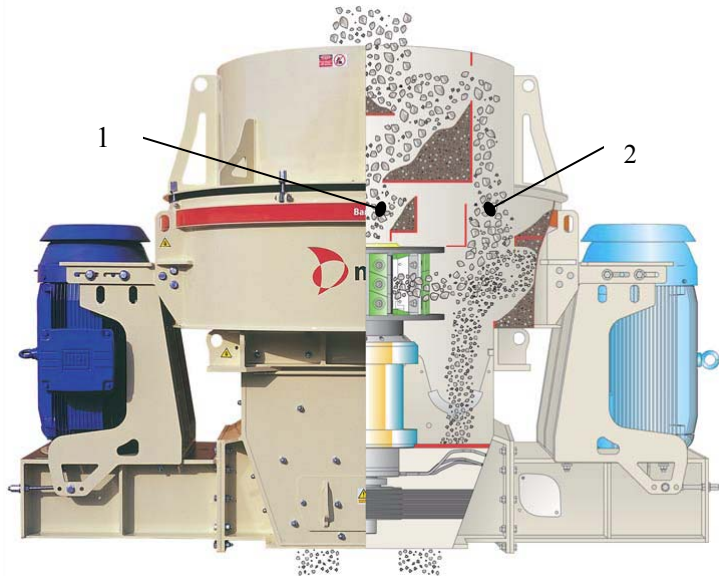
Figure 1.4 A modified Barmac B-Series VSI crusher made by Metso Minerals: 1 – rotor feed, 2 – cascade feed [12]

The primary path for feed material is through the rotor where material is accelerated to speeds of up to 80 m/s before being discharged into the crushing chamber. The second stream of material may be introduced into the crushing chamber via cascade, thus bypassing the rotor. Up to 10% cascade can be utilised with no measurable change in product gradation or quality. That means 10% extra product for no extra power use or wear part consumption. Further increase of the cascade percentage will have a detrimental effect on product shape [11, 12].

Disintegrators
Centrifugal acceleration principle is used in disintegrator mills (Figure 1.5).

Probably the first disintegrator mill was made by Alpine in 1898, the first disintegrators in Estonia were taken into use in 1951 for grinding sand-lime mixtures for the production of silicate concrete [9]. J. Hint, who founded enterprise "Disintegrator" was the pioneer in the disintegrator technology area in Estonia was [20]. In TUT the initiator in the field of disintegrators was Aleksander Tymanok [21].
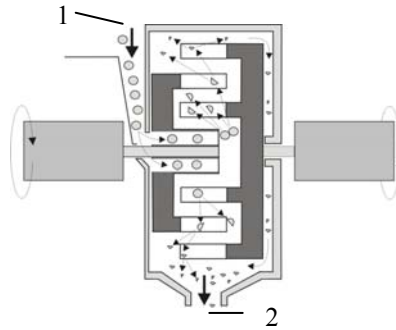
Figure 1.5 Disintegrator working pinciple. 1 – abrasive feed, 2 – abrasive out

Abrasive erosion particles in the disintegrators can be relatively big. Their maximum size depends from the model of a disintegrator and can be more than 10 mm. Their main disadvantage is that they are built for refining abrasive material and not for investigating wear phenomena of working parts.

1.2.2 Compression-based milling

This subchapter deals with compression-based milling methods where shattering is done by employing brutal force on working surfaces of the crusher, which, in its turn, break the particles in pressing action. According to the working principle, the crushers can be divided into two categories: a) crushing elements which employ back and forth motion, b) crushing elements which employ circular motion.

Although compression-based milling is not directly focused on in this work, it is a commonly used method for crushing in mining industry.

Jaw crushers
Before 1855, when the jaw crusher was invented, the hammers, drills and chisels used to break rocks were powered by hand. The jaw crusher Blake designed in 1853 and patented in 1958 was one of the great inventions of size-reduction machines. The early Blake crushers were extensively used in road building, but soon gained success in mineral processing plants [1]. Nowadays jaw crushers are mostly used for primary crushing [16, 22].
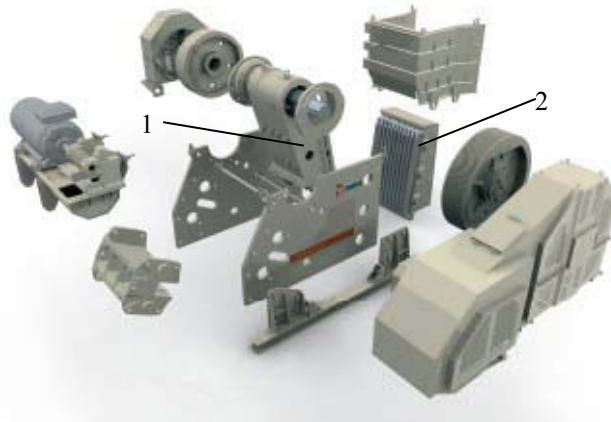
Figure 1.6 Present day C series jaw crusher from Metso Powdermet: 1 – a fixed jaw, 2 – a moving jaw [22]

Gyratory crushers

Philetus Gates patented a successful gyratory crusher in 1881. The Gates crusher consisted of a vertical cone suspended at the top and held by an eccentric sleeve at the bottom that gyrated within a fixed cone. Crushing occurred around the periphery as the movable crushing surface, named the mantle, approached to and receded from the fixed crushing surface, called the concave – that is the rocks are squeezed between an eccentrically gyrating spindle. As rock enters the top of the crusher, it becomes wedged and squeezed between the mantle and the bowl liner or concave. Large pieces of ore are broken once, and then fall to a lower position (because they are now smaller) where they are broken again. This process continues until the pieces are small enough to fall through the narrow opening at the bottom of the crusher [1, 23].

The Blake jaw crusher and the Gates gyratory crusher are still the preferred primary crushers today, and their designs have changed little compared to the originals [1]. In Figure 1.7 (a) a modern gyratory crusher can be seen.

Cone crushers

The aggregate producers' demand for a machine that would control the size distribution and shape of pebbles at a high production rate offered the incentive to build cone crushers (Figure 1.7 (b)), which had specially designed crushing chambers to minimize blockage. In a cone crusher, the closed side settings could be adjusted to control the product size during operation. A cone crusher is
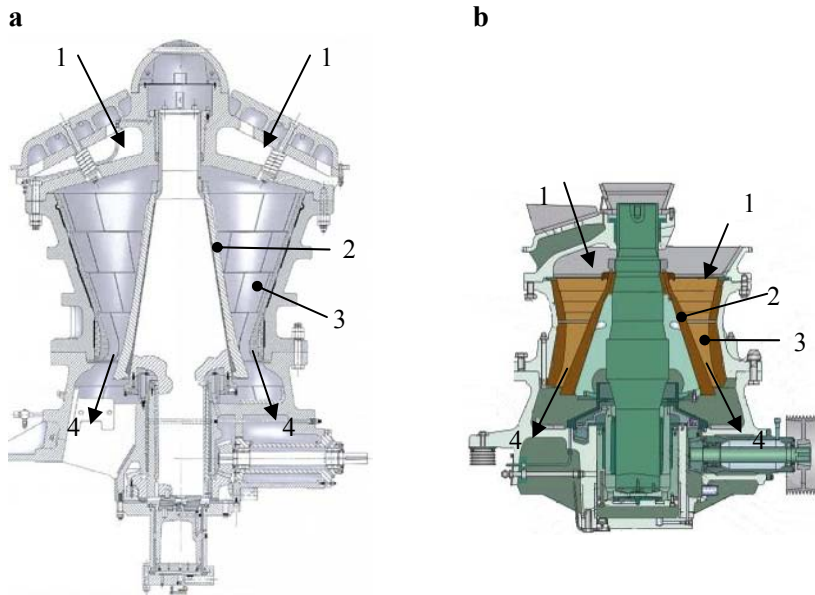
Figure 1.7 A cross-sectional view of Metso Nordberg Superior$^{®}$ gyratory crusher (a) and Metso Nordberg GP series cone crusher (b): 1- feed area, 2 – mantle, 3 – concave, 4 – ejection area [24, 25]

similar in operation to a gyratory crusher. Compared to the gyratory crusher, the cone crusher is characterized by higher speed and a flat (less steep) crushing chamber design, which is intended to give a high capacity and reduction ration for materials suitable for this type of processing. The aim is to retain material longer in the crushing chamber to do more work on material as it is being processed [1].

The cone crusher has been widely used in the mining industry for 70 years to prepare feed for rod and ball mills and to crush critical-size pebbles that have been removed from autogenous or semiautogenous mills because they are too small to be effective as grinding media and too large to be broken by the larger rocks [1].

1.2.3 Common testing equipment for testing materials in erosive wear conditions

The testing equipments used so far can be distinguished by the way how the erosive particles are accelerated. The main options are by gas stream, (Figure 1.8 (a)) or centrifugal acceleration (Appendix 1) [9, 26, 27].

Free-fall test rig (Figure 1.8 (b)) has also been in use, but it allows only limited particle impact speeds [9], and has largely fallen into disuse [26]. As Deng et al. mention in [26], other not so common testers are gas gun impact tester, and whirling arm tester.
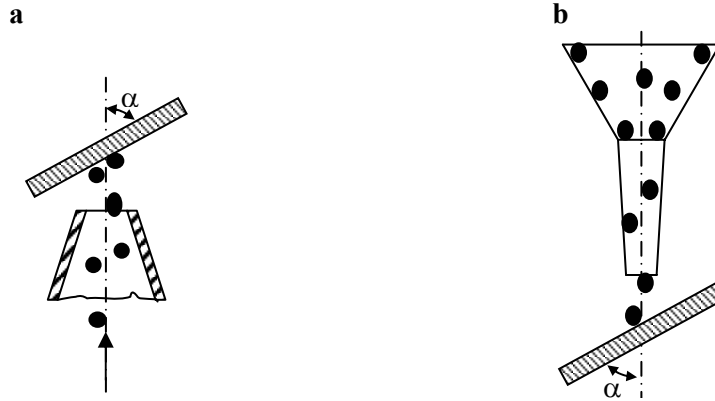
Figure 1.8 Erosion testers where particles are accelerated: a − by gas stream; b − by gravitation [9]

   Gas stream and centrifugal acceleration testers have been the subject of standardization; ASTM G76-83 in the USA and DIN 50332 of the Federal Republic of Germany based on gas stream, and GOST 23201-78 of the former Soviet Union centrifugal acceleration principle. GOST standard 23.201-78 was developed under supervision of Kleis for CAK testing (see Appendix 1).

   ASTM G76-83 and DIN 50332 base on gas stream technology, and allow testing of specimens one by one. The productivity of testing with such equipment is low and it is impossible to test the material under study and reference material simultaneously. CAK allows testing both materials simultaneously, but the size of abrasive is limited to 2 mm [9].

1.3   Materials for crushers

The predominant wear mechanisms associated with impact motion are deformation mechanisms, either single cycle or repeated cycle. If stresses are beyond the elastic limit of the material, single-cycle deformation mechanisms tend to dominate. With lower stresses, repeated-cycle deformation mechanisms dominate [5]. The working surfaces of crushers and grinding mills are lined with wear-resistant materials to protect the permanent parts. A well-known fact emphasised in [8] is that wear tends to decrease with increasing hardness. Materials used in mill liners include impact-resistant alloyed cast iron, abrasion- and impact-resistant alloyed cast steel, rolled alloy steel, and rubber [1].

   Already in the 1880s, the first cast-wearing parts were made from Hadfield manganese steel for crushers and mills. Hadfield steel is tough, and according to [8], ductile and brittle materials experience less wear in impact and single-cycle deformation mechanisms. If manganese steel castings are exposed to continuous impacting, they grow sideways as they wear. When the wear rate of the castings is lower than the rate of their growth, the intermittent operation of primary crushers allows time to remove the growth. Consequently, replaceable

manganese steel castings have proved to be satisfactory wearing surfaces for jaw and gyratory crushers. [1].

Bayer in [8] mentions, that for single-cycle deformation mechanisms in abrasive wear situations, wear tends to decrease with increasing modulus, but for rolling, impact, and sliding situation, wear tends to decrease with increasing modulus.

In impact and rolling situations the ratio of contact pressure to compression yield stress is important. Wear and wear rates tend to decrease with decreasing values of this ratio. Experience indicates that if these ratios exceed 1, wear is typically severe and wear rates generally too large for most applications. Experience also indicates that acceptable behaviour in rolling and impact situations generally require that this ratio be between 0.5 and 1 [8]. Where heavy impacting occurs, chrome-molybdenum alloyed steel castings are used. Iron castings containing nickel resist abrasive wear but are brittle and break under impact. For example impact-resistant shell liners made of nickel-hardened cast irons have long lives in rod mills, but the end (head) liners, which are subjected to pounding by the lateral movement of rods, are made from chrome-molybdenum steel. Cast or rolled wear-resistant alloyed steel liners are used in ball and semiautogeneous mills [1].

Because of the general trend for wear resistance to increase with increasing hardness, ceramics and carbides can provide improved wear resistance over hardened steels in many cases. However, because of the complexities of wear, it is possible for steels and other materials to provide better wear resistance in many cases as well, because ceramics and carbides tend to be brittle [8]. The brittleness plays an important role in case of normal impact angle.

In the 1960s, Swedish and American companies used rubber for mill liners. The rubber had the advantage of being much lighter in weight, easier to install, and less noisy [1]. Bayer in [8] claims also, that elastomers can out perform harder materials in erosion by solid particles and three-body abrasion. Rubber is just a representative of elastomer. In the case of erosion the particles are held until they rebound from the surface, and more severe sliding situation is thereby avoided.

1.4   Wear testing uncertainty

Nowadays every technical field student is taught that a proper measurement has three parts: firstly, the measurement itself, secondly, the margin of uncertainty, and thirdly, the confidence level – that is, the probability that the actual property of the physical object is within the margin of error [28]. A value without included uncertainty and confidence lever does not describe anything. As under this study a new impact wear apparatus is developed, we need to calculate uncertainty values for its main parameters – impact angles and velocities (subchapter 2.2), and to the wear characteristics (subchapter 3.3) A

short theoretical background for the route of uncertainty calculation is given here.

Based on [29] the physical relationship called m*easurement model* establishes relation between input quantities $X_1, X_2, ..., X_i, ..., X_N$ and measurand Y (*the output quantity*). It can formally be expressed as

$$Y = f(X_1, X_2, ..., X_i, ..., X_N) \tag{1.2}$$

To obtain an estimate y of the output quantity Y, we insert the estimates x_i of the N input quantities X_i into the theoretical measurement model, equation (1.2) [29]:

$$y = f(x_1, x_2, ..., x_i, ..., x_N). \tag{1.3}$$

Determination of arithmetic mean $\bar{y}$ depends on if the function f is linear or not. If we have carried out n sets of repeated measurements of all X_i (i.e. $n = n_1 = n_2 = ...n_i = ...n_N$) under repeatability conditions and our function f is linear, $\bar{y}$ can be calculated by

$$\bar{y} = f(\bar{x}_1, \bar{x}_2, ..., \bar{x}_i, ..., \bar{x}_N). \tag{1.4}$$

If the function f is non-linear, we will have to use [29]

$$\bar{y} = \frac{1}{n}\sum_{j=1}^{n} y_i = \frac{1}{n}\sum f(x_{1j}, x_{2j}, ..., x_{ij}, ..., x_{Nj}). \tag{1.5}$$

Our measurement model for determining relative volumetric wear resistance is linear (equation (3.3)).

The uncertainty of experimental results depends on the uncertainties of multiple input quantities [29]. The calculation starts from the calculation of the uncertainties of input quantities. Combined standard uncertainty can be calculated after calculating uncertainties of input values by taking positive square root of the combined variance, which is the weighted sum of the experimental variances and covariances of all input quantities considered in the measurement model [29]

$$u^2(y) = \sum_{i=1}^{N} u_i^2(y) = \sum_{i=1}^{N} c_i^2 u^2(x_i). \tag{1.6}$$

The weighing factor c_i is called the *sensitivity coefficient* for input quantity X_i. Sensitivity coefficients are usually obtained as partial derivatives, which characterise the dependence of the estimate y of the output random variable Y on changes in the estimate x_i of the input random variable X_i [29]

$$c_i = \frac{\partial f}{\partial x_i} = \left(\frac{\partial f}{\partial X_i}\right)_{X_i=x_i, ..., X_N=x_N}. \tag{1.7}$$

If the model is too complicated for direct derivation, or if it is only available as an algorithm, the partial derivatives can be obtained by numerical methods [30, 31]. Sensitivity coefficients can also be found experimentally by observing the change in the estimate y of the output random variable Y when the estimate x_i of one of the input random variables X_i is changed by a known amount, and all other input random variables are kept constant [29].

The uncertainty of an input quantity is expressed by a standard deviation which can be considered equal to experimental standard deviation [29]

$$u(x_i) = s(x_i) = \sqrt{\frac{1}{(n_i - 1)}\sum_{j=1}^{n_i}(x_{ij} - \bar{x}_i)^2} \ . \tag{1.8}$$

Equation (1.8) should not be used if the number n_i of repeated measurements is smaller than ten. The reliability of the estimate $s(x_i)$ is poor when n_i is small. The experimental standard deviation of arithmetic mean is [29]

$$s(\bar{x}_i) = \frac{s(x_{ij})}{\sqrt{n_i}} . \tag{1.9}$$

If it is not practicable to increase the number of measurements, but the same or a similar quantity has been measured before, one way out is to build up standard deviation estimation of the process by combining all available results. The prerequisite is that the measurements have been carried out according to the same, well-defined measurement method and are all under statistical control (the standard deviation that describes the measurement process is not time-dependent). The combination of experimental standard deviations is called pooling, and the resulting estimate is called the pooled standard deviation s_p [29]:

$$s_{i,p} = \frac{\sqrt{\sum_{m=1}^{M} v_{im} s^2(x_{im})}}{\sqrt{\sum_{m=1}^{M} v_{im}}}, \tag{1.10}$$

where
$s(x_{im}) -$ experimental standard deviation obtained from the m-th set of repeated measurements of quantity X_i,
$v_{im} -$ degrees of freedom associated with the m-th set of measurements,
$M -$ total number of sets of repeated measurements,
$\sum_{m=1}^{M} v_{im}$ degrees of freedom $v_{i,p}$ of pooled standard deviation $s_{i,p}$.

In case of few repeated measurements and if standard deviation is not time-dependent, pooled standard deviation $s_{i,p}$ can be used instead of the experimental standard deviation to obtain a better estimate of the uncertainty $u(\bar{x}_i)$ of the arithmetic mean $\bar{x}_i$ of the n_i observations according to

$$u(\bar{x}_i) = \frac{s_{i,p}}{\sqrt{n_i}} . \tag{1.11}$$

In the cases where we do not have earlier test results for the calculation of pooled standard deviation, the number of test specimens for each material is less than ten and we cannot use experimental standard uncertainty. The solution is to use rectangular distribution (also called uniform distribution) by assuming that

intervals constraining the distribution are equal with max and min values of the measurand [29]

$$\sigma(x_i) = \frac{a(x_i)}{\sqrt{3}},$$ (1.12)

where

$a(x_i)$ is the half-width of the interval.

Covariance $u(x_i, x_k)$ is the measure of how much two variables vary together (as distinct from variance, which measures how much a single variable varies). If two variables tend to vary together (that is, when one of them is above its expected value, then the other variable tends to be above its expected value too), then the covariance between the two variables will be positive [32].

Correlation (also called correlation coefficient) indicates the strength and direction of a linear relationship between two random variables. In general statistical usage, *correlation* or co-relation refers to the departure of two variables from independence, although correlation does not imply causation. Correlation is determined by [33]:

$$r(x_i, x_k) = \frac{u(x_i, x_k)}{u(x_i)u(x_k)}.$$ (1.13)

If quantities X_i and X_k are in correlative relation, then general equation for $u^2(y)$ is [33]   :

$$u^2(y) = \sum_{i=1}^{N} c_i^2 u^2(x_i) + 2\sum_{i=1}^{N-1} \sum_{k=i+1}^{N} c_i c_k u(x_i)u(x_k)r(x_i, x_k),$$ (1.14)

if $r(x_i, x_k) = 1$ we get

$$u^2(y) = \left[\sum_{i=1}^{N} c_i u(x_i) \right]^2$$ (1.15)

In the modern treatment of uncertainty, the half-width of an interval having a stated level of confidence is called the expanded uncertainty of measurement. In principle the half-width is obtained by multiplying the standard uncertainty of measurement by a factor, known as the coverage factor k. Consequently, the probability associated with this stated level of confidence is called expanded uncertainty of measurement [29]

$$U(y) = k \cdot u(y).$$ (1.16)

It must be noted that in all experiments made under this thesis, uncertainty calculation is not performed in a traditional way that the measurand is measured for a certain amount of times. All specimens have been measured for one time only, for example, for making ten measurements, ten specimens are measured. Such approach allows to take into account the uncertainty component caused by the inhomogeneity of the specimens.

Variance analysis of the results of measurement
Repeated measurement can be carried out either under repeatability conditions or under reproducibility conditions. Bayer writes in [4] that wear tests in general

have large scatter and poor repeatability because of the complex nature of wear. The repeatability in standardized tests has to be found to be within 25% of deviation. For estimating the reliability of our impact wear testing we need to evaluate the repeatability of the tests.

In first case, care is taken to keep all conditions that may affect the result as constant as possible, only time varies unavoidably. According to the definition of repeatability condition, it is required that repetitions should be made during a short period of time. In contrast to that, reproducibility conditions imply that some conditions are deliberately changed during the series of measurements. The statistical procedure employed is known as analysis of variance. It is important in testing when analysing large amounts of measurement data [29].

One-factor analysis of variance based on the F-test
Let us have an object (realisation of the measurand), and assume that for this object J (j = 1, 2, …, J) series of measurements have been made, each with K (k = 1, 2, …, K) repetitions. Consider the repeated measurement of a variable Y, and let y_{jk} be the (usually corrected) result obtained at the k-th repetition in the j-th series of measurement [29].

Suppose that we are interested in testing the hypothesis that all the means are equal. As there are J arithmetic means $\bar{y}_j$, the final result $\bar{y}$ can be expressed as [29]

$$\bar{y} = \frac{1}{J} \sum_{j=1}^{J} \bar{y}_j = \frac{1}{JK} \sum_{j=1}^{J} \sum_{k=1}^{K} y_{jk} \; . \qquad (1.17)$$

Analogously with equation (1.8), the experimental variance of the K observations in the j-th series of measurement is [29]

$$s^2(y_{jk}) = \frac{1}{K-1} \sum_{k=1}^{K} (y_{jk} - \bar{y}_j)^2 \; , \qquad (1.18)$$

and the experimental variance of the arithmetic means $\bar{y}_j$ of the J series of measurement is [29]

$$s^2(\bar{y}_j) = \frac{1}{J-1} \sum_{j=1}^{J} (\bar{y}_j - \bar{y})^2 \; . \qquad (1.19)$$

To see whether the cause of variability of the results within a series of measurement and between the series of measurement is the same, we can compare two independent estimates of the variance σ_w^2 of the observations within a series. We obtain the first estimate s_a^2 from the variability of the arithmetic means $\bar{y}_j$ of all series. Because $\bar{y}_j$ is the arithmetic mean of K observations, its experimental variance $s^2(\bar{y}_j)$ is an estimate of the variance σ_W^2 / K. We thus find from equation (1.19) that the estimate s_a^2, having $v_a = J - 1$ degrees of freedom, is [29]

$$s_a^2 = K \cdot s^2(\bar{y}_j) = \frac{K}{J-1}\sum_{j=1}^{J}(\bar{y}_j - \bar{y})^2 \,. \tag{1.20}$$

The second estimate s_b^2 is the overall estimate of σ_W^2, obtained from the J estimates of experimental variance $s^2(y_{jk})$, where each of them has been calculated from equation (1.18) with $v_j = K - 1$ degrees of freedom [29].

$$s_b^2 = \frac{1}{J}\sum_{j=1}^{J} s^2(y_{jk}) = \frac{1}{J(K-1)}\sum_{j=1}^{J}\sum_{k=1}^{K}(y_{jk} - \bar{y}_j)^2 \tag{1.21}$$

As the first estimate s_a^2 of σ_W^2 is based on the variability of the arithmetic means $\bar{y}_j$, while the second estimate s_b^2 is based on the variability of the individual observations y_{jk}, their ratio may point to an effect that varies between the series. Such effect examined by what is known as the F-test [29].

The F distribution is the probability distribution of the ration F of two independent estimates $s_a^2(v_a)$ and $s_b^2(v_b)$ of the variance σ^2 of a normally distributed random variable [29],

$$F(v_a, v_b) = \frac{s_a^2(v_a)}{s_b^2(v_b)} \,. \tag{1.22}$$

The parameters v_a and v_b are the degrees of freedom of the estimates, and $0 \leq F(v_a, v_b) \leq \infty$. The values of $F_p(v_a, v_b)$ are given in the tables for the probability of $p = 0.95$ and $p = 0.99$ [29].

The null hypothesis of the F test (the assumption that $s_a^2(v_a)$ and $s_b^2(v_b)$ are estimates of the same variance σ^2) is rejected on the confidence level p if $F(v_a, v_b) > F_p(v_a, v_b)$. Therefore the interpretation of this inequality is that it is statistically certain that the estimate $s_a^2(v_a)$ is larger than $s_b^2(v_b)$ [29].

The experimental variance $s^2(\bar{y})$ of $\bar{y}$, based on the assumption that all observations y_{jk} are samples taken from the same distribution, is [29]

$$s^2(\bar{y}) = \frac{1}{JK(JK-1)}\sum_{j=1}^{J}\sum_{k=1}^{K}(y_{jk} - \bar{y}_j)^2 = \frac{(J-1)s_a^2 + J(K-1)s_b^2}{JK(JK-1)} \,. \tag{1.23}$$

If we admit that there is a variation between the series, the experimental variance $s^2(\bar{y}_j)$ does not estimate σ_W^2 / K but the variance $\sigma_W^2 / K + \sigma_B^2$, where σ_B^2 is the variance that represents the random component of the variability between the series [29],

$$s^2(\bar{y}_j) = \frac{s_b^2}{K} + s_B^2 \,. \tag{1.24}$$

From equation (1.24) we see that $s^2(\bar{y}_j)$ contains both the within-the-series and between-the-series components of experimental variance. This means that

using equation (1.11) we obtain the estimate $s^2(\bar{y})$ of the variance of the result $\bar{y}$ as [29]

$$s^2(\bar{y}) = \frac{s^2(\bar{y}_j)}{J}. \qquad (1.25)$$

The above analysis can be used to test a given result for the presence of an effect that influences is, such as the time of measurement, the equipment used, the method of measurement, or the laboratory [29]. In our case it was used for evaluating the effect of the time for measurement (subchapter 3.5).

One-factor analysis of variance using Cochran's C test
In practice, the number of observations K (k = 1, 2, …, K) in a series of repeated measurements may turn out to be rather small. If this is the case, the F test discussed in a previous subchapter, should be employed with care. The reason is that the experimental variances of some of the series may be very small by chance, making the F test extremely sensitive. When series have a small number of observations, there may easily be series with experimental variances that are much larger than the remainder. Cochran's C test is designed to test the homogeneity of a set of experimental variances, which should all be based on the same number of observations, K. The test statistic [29, 34],

$$C = \frac{s^2(y_{jk})_{max}}{\sum_{j=1}^{J} s^2(y_{jk})} \qquad (1.26)$$

is the ratio of the largest experimental variance $s^2(y_{jk})_{max}$ to the sum of all experimental variances $s^2(y_{jk})$. The ratio C is compared with a relevant quantile of Cochran's distribution, which is a function of the number of observations in each series, K, and the number of series, J. Handbooks give Cochran's critical values of the 5% and 1% significance levels. If $C_{Cr\,0.01}(K, J) > C > C_{Cr\,0.05}(K, J)$, the reason for the existence of the maximum experimental variance should be analysed and care should be taken when using the data. If $C > C_{Cr\,0.01}(K, J)$, the series of measurement with the maximum experimental variance should be considered an outlier and disregarded in the calculation of the final result [29].

1.5   Conclusions of the chapter and objectives of the study

Impact-based milling tends to produce a favourable cubical product, ensuring particle breakage chiefly along the planes of weakness, thereby the resultant product is free of weak zones. The drawback of impact-based milling is a high wear rate of the mills, which raises the importance of a good testing apparatus for studying the behaviour of the crusher materials.

The two most commonly used working principles of erosion testers are gas-blasting or centrifugal-accelerating (subchapter 1.2.3). In the testers built so far

is not possible to test with erosion particles bigger than 2 mm (that is in abrasive impact wear conditions).

The impact velocity of particles has such a strong influence on the erosion rate that it is important to know its value accurately. Deng et al in their extensive study in [27] proved, that in the gas-blast testers have both particle velocity and the dispersion angle of the particle jet more scatter than in centrifugal-accelerator tester. Later testers are relatively insensitive to particle characteristics while the influence for former testers is quite high. Particle characteristics are their size, shape, and concentration. Although particle rotation is an issue in the centrifugal-accelerator tester [35], is its effect minimal in big impact angles [36].

Due to the need for abrasive impact wear tester enabling to test bigger particles than 2 mm, and considering abovementioned good properties of centrifugal-accelerators the main aim of this work was to develop disintegrator type test rig for testing two-body wear process in the conditions of impact wear as well as grindability of abrasive mineral materials.

Other main objectives of the study are:
1. to determine appropriate testing parameters ensuring reliable results with moderate uncertainty of powder materials and coatings,
2. to study the wear resistance of different groups of materials at impact wear for the selection of prosperous materials to be used in the similar working conditions (in impact-based milling devices),
3. to study grindability and abrasivity of different widely used minerals.
   For fulfilling these goals the following activities were planned:
   1) designing the impact tester, determination of particles movement and calculation of wear parameters in the impact tester,
   2) uncertainty focused wear resistance study of the powder materials (steels and cermets) and thermally sprayed coatings,
   3) comparison materials behaviour with abrasive erosive wear (AEW) results,
   4) investigation of the grindability and abrasivity of different mineral materials (granite and quartzite gravels, etc.).

2 EXPERIMENTAL EQUIPMENT AND TEST METHOD

2.1 Design of impact wear tester

Impact wear tester is a centrifugal type impact-based milling tester based on a disintegrator DESI. With this tester is possible to test two-body wear process in the conditions of impact wear as well as the grindability of used abrasive materials. The main components of impact wear tester are two rotors rotating in opposite directions (Figure 2.1). Some parts in the abrasive intake area of the 3D model of the right rotor are turned transparent to facilitate understanding.
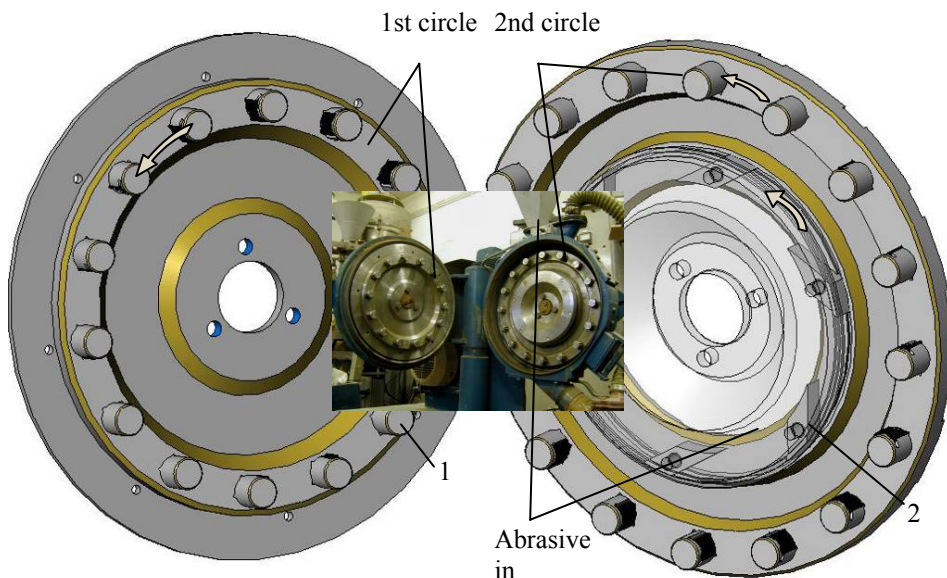
Figure 2.1 A photo of impact wear tester beside a 3D view of rotors: 1 – pin (specimen holder); 2 – impeller.

Both rotors are driven by electric motors. Pins holding the specimens are attached annularly to the rotors. The attachment of the specimens is unique and protected by the Estonian utility model no U200600001 [37].

The machine operates in the open circuit mode. The abrasive enters into the centre of the right rotor, where it is accelerated on the impellers (Figure 2.2) by the centrifugal force. Abrasive feed rate depends slightly on the abrasive and is usually kept 3 kg/min.

After the ejection from the impellers, abrasive impacts pins/specimens of the 1st circle.

30
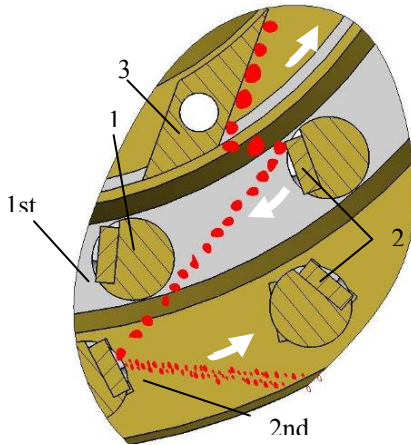
Figure 2.2 Simplified scheme of particles moving in DESI: 1 – pin (specimen holder), 2 – specimen, 3 – impeller

There are 14 samples fixed to the 1st circle. Usually 2 pins are occupied with the reference material, and 12 places are free for materials to be tested. 16 pins/samples are on the outer circle. Reference material is steel C 45.

Impact angles and velocities between the specimens of both circles and particles are determined by the numerical and graphical method. The real impact angles between the abrasive jet and the specimens are close to normal. A complete algorithm for the calculation of impact angles and velocities is given in subchapter 2.2.

The impact angle and velocity between the 2nd circle of specimens and particles originating from the 1st circle of specimens is influenced by many factors. Compared to the 1st circle, additional uncertainty factor is added by the impingement angle from the 1st circle of pins, which depends:

− on the shape and coefficient of restitution (COR) of each particle,
− on the impingement position of particles (does the impingement happen from the inner or the outer side of the 1st circle of pins) (see Figure 2.5).

Additional scattering is caused by rebounding from the inner body of the tester (after the impact with the 2nd circle of pins, the abrasive hits the inner body of the tester, bounds back and at least some of it collides again with the specimens).

Due to all of these considerations, the 2nd circle of pins is optional, which means that these can be removed for the test. The second circle of pins is mainly used for grindablity studies (subchapter 4.1).

Rotational velocity of rotors can be changed by the belt drive mechanism. It is possible is to have 5 different rotational velocities for both rotors. Twenty additional velocity combinations are possible if both rotors turn with different rotational velocities (Table 2.1).

Table 2.1. Possible rotors rotational velocities of impact wear tester

Turning mode	Impellers, the 2nd circle of specimens, min^{-1}	The 1st circle of specimens, min^{-1}
Both rotors have equal rotational velocity	2025	2025
	2830	2830
	3965	3965
	4960	4960
	5880	5880
Both rotors have different rotational velocity	2025	2830
	2020	3965
	2020	4960
	2020	5880
	2830	2025
	2830	3965
	2830	4960
	2830	5880
	3965	2025
	3965	2830
	3965	4960
	3965	5880
	4960	2025
	4960	2830
	4960	3965
	4960	5880
	5880	2025
	5880	2830
	5880	3965
	5880	4960

2.2 Impact angles and velocities in the impact wear tester

The main parameters of impact – impact angles and velocities between abrasive jet and specimens – are calculated theoretically by the main equation of relative movement in dynamics. The calculation of these parameters was made according to the theory given in [38–40]. Theory given in [41, 42] was basically the same with a slightly different approach: the calculation on the first reference frame (inertial primary reference frame) and the second reference frame (body fixed reference frame) was viewed together while in [38–40] they were viewed separately. A good reference example was given in [43].

The main equation of relative movement in dynamics is:

$$m\,\vec{a}_r = \sum \vec{F}_\alpha + \vec{\Phi}_e + \vec{\Phi}_c, \qquad (2.1)$$

where

$\vec{a}_r$ – acceleration relative to the second reference frame,

m – mass,

$\vec{F}_\alpha$ – active forces and bond reactions,

$\vec{\Phi}_e$ – inertial force relative to second reference frame (centrifugal force),

$\vec{\Phi}_c$ – Coriolis inertial force.

$$\vec{\Phi}_e = -m\omega^2 R , \qquad (2.2)$$

where

ω – angular velocity,

R – turning radius,

$$\vec{\Phi}_c = -2m\vec{\omega} \times \vec{v}_r , \qquad (2.3)$$

where

$\vec{v}_r$ - velocity of the particle in the second reference frame.

2.2.1   Impact angles and velocities between the 1st circle of specimens and abrasive jet

The main forces acting on particles are given in Figure 2.3. Gravitational force has not been taken into account as in comparison with other forces it is negligible.

In these calculations $O\xi\eta$ is a body fixed reference frame.

The projections on the indicate axles ξ and η are correspondingly

$$\mathrm{m}\ddot{\xi} = \Phi_e \cos\theta - T \qquad (2.4)$$

$$0 = N_2 - \Phi_c + \Phi_e \sin\theta, \qquad (2.5)$$

where $T = \mu N_2$, is the frictional force, and N_2 is the normal force.

Angle θ is calculated from a triangle ACS. The length of line segment AB is necessary for the calculation of AS. The length of BO is assumed to be in interval (0.025–0.031) m. BO is taken to be 0.028 m

$$AB = BC \cos 50°$$
$$AO = AB - BO = 0.113 \cos 50° - 0.028 \approx 0.045 \text{ m}$$
$$AC = BC \sin 50° = 0.113 \sin 50° \approx 0.087 \text{ m}$$

Here and in all other calculations the numbers are rounded for illustrative reasons only, because all actual calculations have been done in Microsoft Excel program with Excel accuracy. The final rounding to reasonable numbers of digits in correlation of input values accuracy is made at the end of the calculations (Table 2.2).

$$\cos\theta = \frac{AS}{CS} = \frac{AO + OS}{CS} = \frac{AO + \xi}{CS} = \frac{0.045 + \xi}{CS} \qquad (2.6)$$

$$\sin\theta = \frac{AC}{CS} = \frac{86.56 \cdot 10^{-3}}{CS} \qquad (2.7)$$

Figure 2.3 The forces acting on abrasive particle S necessary for the calculation of impact speed and angle between the impeller and the first circle

To equations (2.2), (2.3), and (2.5) follows:

$$N_2 = -\Phi_e \sin\theta + \Phi_c = -mCS\omega^2 \frac{86.56 \cdot 10^{-3}}{CS} + 2m\omega\dot{\xi} = -86.56 \cdot 10^{-3}\, m\omega^2 + m\omega\dot{\xi} =$$

$$= m\omega(-86.56 \cdot 10^{-3}\,\omega + 2\dot{\xi}) \qquad (2.8)$$

To equation (2.4) follows:

$$m\ddot{\xi} = \Phi_e \cos\theta - \mu N_2 = mCP\omega^2 \frac{\xi + 44.63 \cdot 10^{-3}}{CP} - \mu m\omega(-86.56 \cdot 10^{-3}\omega + 2\dot{\xi})$$

$$(2.9)$$

$$\ddot{\xi} = \omega^2\xi + 44.63\,\omega^2 + 86.56 \cdot 10^{-3}\,\mu\omega^2 - 2\mu\omega\dot{\xi} \qquad (2.10)$$

$$\ddot{\xi} + 2\mu\omega\dot{\xi} - \omega^2\xi - (44.63 + 86.56\mu) \cdot 10^{-3} \cdot \omega^2 = 0 \qquad (2.11)$$

The coefficient of friction (COF) for solving equation (2.11) is not known, but in the appendix 1 it is calculated for CAK by taking its particle ejection angle as a base. Particle ejection angle of centrifugal accelerator was also certified by Deng in [44].

The COF is assumed to be the same as it is calculated for CAK. However, uncertainty calculations in the subchapter 2.2.4 and Deng et al in [27] proved, that frictional coefficient has only a minor influence on particle acceleration in the centrifugal-accelerator tester.

Abrasives used in impact wear tester and CAK have different composition and different particle size. Standard abrasive mineral material in CAK is (0.5–0.9) mm quartz sand [9], but all practical experiments in TUT have been

made with (0.1−0.3) mm sand. Impact wear tester is designed for testing various abrasives with particle size up to 7 mm. However, abrasives (4.0−5.6) mm have been used in the tests of this thesis.

If we assume the friction coefficient in impact wear tester to be the same as in CAK and angular velocity of the rotors is 296.7 s^{-1} (2830 min^{-1}), it follows from equation (2.11):

$$\ddot{\xi} + 213.6\,\dot{\xi} - 296.7^2\xi = 7.579 \cdot 10^{-2} \cdot 296.7^2. \tag{2.12}$$

This is a second order nonhomogeneous linear differential equation with constant coefficients, and can be solved by variation of parameters [45]. Linear differential equation is solved by adding general solution of the related homogeneous equation and particular solution [46]

$$\xi = \bar{\xi} + \xi^*. \tag{2.13}$$

Homogeneous differential equation is

$$\ddot{\xi} + 213.6\,\dot{\xi} - 296.7^2\xi = 0. \tag{2.14}$$

Corresponding characteristic equation is

$$\lambda^2 + 213.6\lambda - 296.7^2 = 0. \tag{2.15}$$

The solution of the above equation is

$\lambda_1 = 208.5$

$\lambda_2 = -422.1.$

A general solution to the homogeneous equation is

$$\bar{\xi} = C_1\,e^{208.5t} + C_2\,e^{-422.1t}, \tag{2.16}$$

where C_1 and C_2 are constants.

The right side of nonhomogeneous equation (2.12) is in the form of $Q_0(t)e^{0t}$, therefore the solution can be found in the form

$$\xi^* = Q_0(t)e^{0t} = A_0.$$

After substituting ξ^*, $(\xi^*)'$ and $(\xi^*)''$ into equation (2.12)

$$-296.7^2 A_0 = 0.08 \cdot 296.7^2 \qquad A_0 = -7.579 \cdot 10^{-2}$$

$$\xi = \bar{\xi} + \xi^* = C_1\,e^{208.5t} + C_2\,e^{-422.1t} - 7.579 \cdot 10^{-2} \tag{2.17}$$

The constants C_1 and C_2 can be found from the initial conditions: if $t = 0$, $\xi = 0$ and $\dot{\xi} = 0$

$$\begin{cases} C_1 e^{208.5 \cdot 0} + C_2 e^{-422.1 \cdot 0} - 7.579 \cdot 10^{-2} = 0 \\ 208.5 C_1 e^{208.5 \cdot 0} - 422.1 C_2 e^{-422.1 \cdot 0} = 0 \end{cases} \Rightarrow \begin{cases} C_1 + C_2 - 7.579 \cdot 10^{-2} = 0 \\ 208.5 C_1 - 422.1 C_2 = 0 \end{cases} \Rightarrow$$

$$\begin{cases} C_2 = \dfrac{7.579 \cdot 10^{-2}}{3.025} = 2.505 \cdot 10^{-2} \\ C_1 = \dfrac{422.1}{208.5} C_2 = 2.025 C_2 = 2.025 \cdot 2.505 \cdot 10^{-2} = 5.074 \cdot 10^{-2} \end{cases}$$

The final equation of displacement in correlation with initial conditions is

$$\xi = 5.074 \cdot 10^{-2}\,e^{208.5t} + 2.505 \cdot 10^{-2}\,e^{-422.1t} - 7.579 \cdot 10^{-2}. \tag{2.18}$$

The length of the displacement ξ of abrasive particles is equal with AL

$$2.8 \cdot 10^{-2} = 5.074 \cdot 10^{-2}\,e^{208.5t} + 2.505 \cdot 10^{-2}\,e^{-422.1t} - 7.579 \cdot 10^{-2}$$
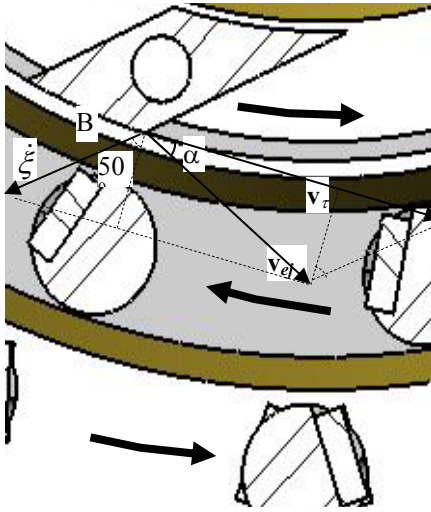
Figure 2.4 Velocity of the abrasive particles in point B while leaving the impeller

Time t cannot be revealed so easily. It can be found by trial method with the help of computer programs. With the help of Microsoft Excel program [47] it was found that if $t = 3.11 \cdot 10^{-3}$, then $AL = 2.80 \cdot 10^{-2}$ m.

The velocity relative to the second reference frame is equal with derivation from the displacement equation (2.18)

$$\dot{\xi} = 208.5 \cdot 5.074 \cdot 10^{-2} \, e^{208.5t} - 422.1 \cdot 2.505 \cdot 10^{-2} \, e^{-422.1t} . \qquad (2.19)$$

After substituting the value of t,

$$\dot{\xi} = 10.58 \, e^{208.5 \cdot 0.00311} - 10.57 \cdot e^{-422.1 \cdot 0.00311} \approx 17.4 \text{ m/s.}$$

The velocity of the second reference frame $O\xi\eta$ in point B relative to the primary reference frame Cxy is

$$v_\tau = \omega r = 296.7 \cdot \frac{0.226}{2} \approx 33.5 \text{ m/s.} \qquad (2.20)$$

Velocities acting on the particles ejecting from impellers are given in Figure 2.4. The general velocity or in another words, velocity in primary reference frame, is the ejection velocity from the impeller.

$$v_{ej} = \sqrt{(33.5 - 17.4\sin 50°)^2 + (17.4\cos 50°)^2} \approx 23.1 \text{ m/s.} \qquad (2.21)$$

From the same cinematic scheme we can calculate ejection angle α.

$$\alpha = \arctan\left(\frac{17.4\cos 50°}{33.5 - 17.4\sin 50°}\right) \approx \approx 29.0°.$$

Angle between axle ξ and $\mathbf{v}_{ej}$ is

$$40° + 29.0° = 69.0°$$

Collision phase starts from the outer side of the 1st circle of specimens (Figure 2.5) and finishes on the inner side. Such behaviour causes scattering of imaginary impact angle β (formed by imaging pins in "standstill" position).

Imaginary impact angle β was measured in the computer design program Solid Works [48], and ranged from 62.1° to 71.5° (Figure 2.5).

The designation is:

β_{st} – starting imaginary impact angle formed at the beginning of collision phase,

β_{fin} – final imaginary impact angle formed at the end of collision phase,

γ_{st} – real impact angle formed at the beginning of the collision phase,

γ_{fin} – real impact angle formed at the end of the collision phase,

v_{st} – real velocity acting on the specimen at the beginning of the collision phase,

Figure 2.5 Initial phase of impact (a) and final phase of impact (b)

v_{fin} – real velocity acting on the specimen at the end of the collision phase,
v_{pin} – linear velocity of the 1st circle of pins.

The movement of pins have been taken into account in a real impact angle γ.

The velocity $\mathbf{v}$ can be calculated by dividing $\mathbf{v}_{ej}$ and $\mathbf{v}_{pin}$ into normal and tangential components relative to the work surface area of the specimen.

$$v_{pin} = \omega r = 296.7 \cdot \frac{0.265}{2} \approx 39.3 \text{ m/s} \tag{2.22}$$

$$v_{st}^n = v_{ej} \sin 62.1° + v_{pin} \cos 20° = 23.1 \cdot \sin 62.1° + 39.3 \cdot \cos 20° \approx 57.4 \text{ m/s}$$

$$v_{fin}^n = v_{ej} \sin 71.5° + v_{pin} \cos 20° \approx 58.8 \text{ m/s}$$

$$v_{st}^\tau = v_{pin}^\tau - v_{ej}^\tau = 39.3 \cdot \sin 20° - 23.1 \cdot \cos 62.1° \approx 2.6 \text{ m/s} \tag{2.23}$$

$$v_{fin}^\tau \approx 6.1 \text{ m/s}$$

$$v_{st} = \sqrt{\left(v_{st}^n\right)^2 + \left(v_{st}^\tau\right)^2} = \sqrt{57.4^2 + 2.6^2} \approx 57.4 \text{ m/s} \tag{2.24}$$

$$v_{fin} \approx 59.2 \text{ m/s}$$

$$\gamma_{st} = \arctan\left(\frac{v_{st}^n}{v_{st}^\tau}\right) = \arctan\left(\frac{57.4}{2.6}\right) \approx 87.4°. \tag{2.25}$$

$$\gamma_{fin} \approx 84.1°.$$

In the above calculations the rotational velocity of the rotors was 2830 min^{-1}. The same calculations were made by rotational velocity 5880 min^{-1}. As it was expected, ejection angle α, imaginary impact angles β, and real impact angles γ were not changed. The velocities ($\mathbf{v}_{ej}$, $\mathbf{v}_{pin}$, $\mathbf{v}$) were in proportional relation with the increase of turning speed.

Impact angles and velocities for other rotational velocities of rotors were found by the above proved linear relationship for v_{ej} and by repeating the calculations from equation (2.22) to equation (2.25). The results with expanded uncertainties (coverage probability 95%) are given together in Table 2.2, where v and γ are the mean values of two pairs: v_{st}, v_{fin} and γ_{st}, γ_{fin}. Expanded uncertainties are calculated in a subchapter 2.2.4.

2.2.2 Impact angles and velocities between the 2nd circle of specimens and abrasive jet

As it was mentioned in subchapter 2.1, impact angle and velocity between the 2nd circle of pins and abrasive jet is influenced by numerous factors. That is why only maximum theoretical velocity is calculated. In the calculations of the maximum theoretical impact velocity the COR between the 1st circle of pins and abrasive jet is assumed to be equal to one and abrasive shape is assumed to be spherical.

Once again, this is only theoretical assumption and only a fraction of abrasive particles stay intact in reality.

The impingement from the 1st circle of pins does not happen according to the angles of γ_{st}, γ_{fin}, because in this case tangential components v^τ_{pin} and v^τ_{ej} have to be added instead of subtraction in equation (2.23).

$$v^\tau_{1impst} = v^\tau_{pin} + v^\tau_{ej} = 39.3 \cdot \sin 20° + 23.1 \cos 62.1° \approx 24.2 \text{ m/s}, \qquad (2.26)$$

$$v^\tau_{1impfin} \approx 20.7 \text{ m/s},$$

where
v_{impst} – impingement velocity from the outer side of the 1st specimens ring,
v_{impfin} – impingement velocity from the inner side of the 1st specimens ring.

As the COR was assumed to be equal to one,

$$v^n_{1impst} = v^n_{st} \text{ and } v^n_{1impfin} = v^n_{fin}$$

$$v_{1impst} = \sqrt{\left(v^n_{1impst}\right)^2 + \left(v^\tau_{1impst}\right)^2} = \sqrt{57.4^2 + 24.2^2} \approx 62.3 \text{ m/s}.$$

$$v_{1impfin} \approx 62.3 \text{ m/s}$$

$$v_{1impst} = v_{1impfin} = v_{imp}$$

$$\theta_{st} = \arctan\left(\frac{v^n_{1impst}}{v^\tau_{1impst}}\right) = \arctan\left(\frac{57.4}{24.2}\right) \approx 67.1°$$

$$\theta_{fin} \approx 70.6°.$$

θ_{st} – impingement angle from the outer side of the 1st circle of specimens.
θ_{fin} – impingement angle from the inner side of the 1st circle of specimens.

As it can be seen, v_{1impst} and $v_{1impfin}$ values are equal (a simplification was made and the difference of the turning radius of inner and outer side of the specimens was neglected). The COR was assumed to be equal to one, which means it is a perfectly elastic collision where the total kinetic energy is constant and, if the mass stays constant, the speed must be also constant, only its direction changes [7]. Although scalar values $v_{1impst} = v_{1impfin}$, their projections relative to the work surface area of the 2nd circle of specimens are different (Figure 2.6).
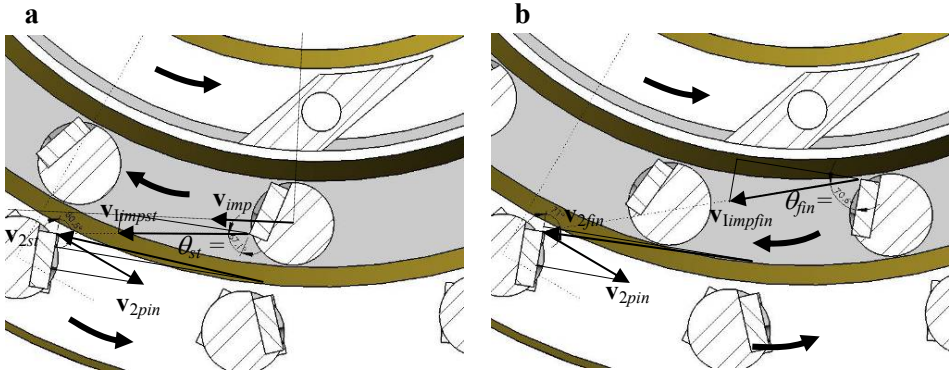
Figure 2.6 Kinematic schemes of theoretical real impact velocities acting on the 2nd circle of specimens: abrasive originates from the outer side of the 1st circle of specimens (a), and, abrasive originates from the inner side of the 1st circle of specimens (b)

Theoretical impact velocity v_2 is calculated from normal and tangential components (Figure 2.6).

$$v_{2pin} = \omega r = 296.7 \cdot \frac{0.325}{2} \approx 48.2 \text{ m/s}$$

$$v_{2st} = \sqrt{(v_{2pin}^n + v_{1impst}^n)^2 + (v_{2pin}^\tau - v_{1impst}^\tau)^2} =$$

$$= \sqrt{(48.2\cos 20° + 62.3\sin 80.5°)^2 + (48.2\sin 20° - 62.3\cos 80.5°)^2} \approx$$

$$\approx 106.9 \text{ m/s}$$

$$v_{2fin} = \sqrt{(v_{2pin}^n + v_{1impfin}^n)^2 + (v_{2pin}^\tau - v_{1impfin}^\tau)^2} \approx 104.4 \text{ m/s}$$

The abrasive is ejected from the outer side of the 1st circle of specimens and after colliding with the inner side of the 2nd circle of specimens, it achieves the maximum normal component of theoretical impact velocity v_2.

Abrasive jet originating from the inner side of the 1st circle of specimens (Figure 2.6 (b)) does not hit with the pin in front, because for the time being the pin has moved forward.

Further calculations proved that if the impingement velocity $\mathbf{v}_{1imp}$ is parallel with linear velocity $\mathbf{v}_{pin}$, the theoretical real velocity v_2 is maximal regardless of the shape of abrasive particles. It is shown in Figure 2.6 (a) is shown that $\mathbf{v}_{2st}$ is almost parallel with $\mathbf{v}_{pin}$, therefore

$$v_{2st} = v_{2max}.$$

An error made by assuming that $\mathbf{v}_{1imp}$ and $\mathbf{v}_{pin}$ are parallel is negligible, because imaginary impact angle ϕ has changed only 0.6 degrees (compare Figure 2.6 and Figure 2.7).

Maximal real impact velocity values for all rotational velocities between the 2nd circle of specimens and abrasive jet are given together in Table 2.2.
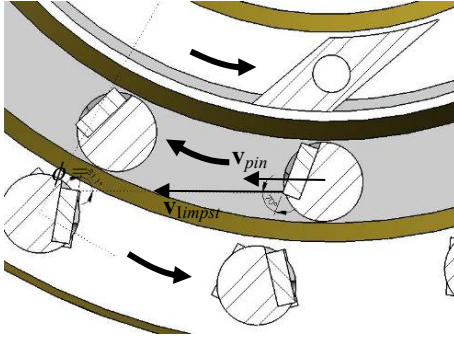
Figure 2.7 Imaginary impact angle calculation then $\boldsymbol{v}_{imp}$ and $\boldsymbol{v}_{1impst}$ are strictly parellel

2.2.3 Impact energy

The standard testing mineral material is granite gravel. For the calculation of kinetic energy, 50 g of granite gravel was weighed and contained particles were counted. It was found, that 50 g of granite gravel contained 318 particles.

Average mass per particle was determined by

$$m_p = \frac{m_{abr}}{n} \qquad (2.27)$$

m_p – mass of a particle,

m_{abr} – total mass of abrasive,

n – counted number of particles

The kinetic energy of a particle by contacting the 1st circle of the pins is

$$E_k^p = \frac{m_p v^2}{2} = \frac{50 \cdot 10^{-3} \cdot 58.3^2}{318 \cdot 2} \approx 0.27 \text{ J} \qquad (2.28)$$

Kinetic energies for other rotational velocities are calculated in the same way and are given together in Table 2.2 with expanded uncertainties (coverage probability 95%), which are calculated in a subchapter 2.2.4.

The values in Table 2.2 are theoretical, that is to say they are not measured in practice. However, the test made for SSAB proved, that theoretically calculated real impact angles γ_{st} and γ_{fin} presented in Figure 2.5 are valid.

SSAB produced custom made pins (which were specimens and pins in one unit), which were tested in the 1st circle setup. Working surfaces of these pins were asided with 90° inclined facets (Figure 2.8).

The pins were set up in such a way that the direction of their working surfaces coincided with the direction that standard pins would have had. Angular velocity of both rotors in the test was 2025 min⁻¹.

As can be seen from Figure 2.8, outer facet 3 has worn more than inner facet 2. From the same side of inner facet 2 and working surface 1, a material has deformed plastically and has been smeared to the inner facet.

It shows directly, that impacting particles have come from the outer side to the inner side, like it is shown in Figure 2.5. That is why outer facet has worn more and the material has been smeared to the inner facet. A small wear of the inner facet was also allowed by the calculations, because theoretical impact angle was found to be 86° ± 5° (Table 2.2). The maximal clockwise measured impact angle γ_{fin} is then 91° (Figure 2.5 (b)).

Table 2.2. Possible impact angles, impact velocities and kinetic energies in impact wear tester

Turning mode	Impellers and the 2nd circle of specimens, min⁻¹	The 1st circle of specimens, min⁻¹	v, m/s	γ, °	E_k^p, J	v_{2max}, m/s
Both rotors have equal rotational velocity	2025 ± 70	2025 ± 70	42 ± 5	86 ± 6	0.14 ± 0.08	80
	2830 ± 95	2830 ± 95	58 ± 7	86 ± 6	0.27 ± 0.17	110
	3965 ± 135	3965 ± 135	82 ± 9	86 ± 6	0.52 ± 0.33	150
	4960 ± 165	4960 ± 165	102 ± 12	86 ± 6	0.82 ± 0.51	190
	5880 ± 200	5880 ± 200	121 ± 14	86 ± 6	1.15 ± 0.72	220
Both rotors have different rotational velocity	2025 ± 70	2830 ± 95	53 ± 6	82 ± 6	0.22 ± 0.13	90
	2020 ± 70	3965 ± 135	68 ± 7	80 ± 5	0.36 ± 0.22	100
	2020 ± 70	4960 ± 165	82 ± 9	78 ± 5	0.52 ± 0.32	120
	2020 ± 70	5880 ± 200	94 ± 10	77 ± 4	0.70 ± 0.42	130
	2830 ± 95	2025 ± 70	48 ± 6	89 ± 4	0.18 ± 0.11	100
	2830 ± 95	3965 ± 135	74 ± 8	82 ± 6	0.43 ± 0.26	120
	2830 ± 95	4960 ± 165	87 ± 10	80 ± 5	0.60 ± 0.37	140
	2830 ± 95	5880 ± 200	100 ± 11	79 ± 5	0.78 ± 0.48	150
	3965 ± 135	2025 ± 70	56 ± 7	93 ± 2	0.25 ± 0.15	120
	3965 ± 135	2830 ± 95	67 ± 8	90 ± 4	0.35 ± 0.22	130
	3965 ± 135	4960 ± 165	95 ± 11	84 ± 6	0.71 ± 0.44	160
	3965 ± 135	5880 ± 200	107 ± 12	82 ± 5	0.91 ± 0.56	180
	4960 ± 165	2025 ± 70	64 ± 8	96 ± 3	0.32 ± 0.20	150
	4960 ± 165	2830 ± 95	74 ± 9	92 ± 1	0.43 ± 0.27	160
	4960 ± 165	3965 ± 135	89 ± 10	88 ± 7	0.62 ± 0.39	170
	4960 ± 165	5880 ± 200	114 ± 13	84 ± 6	1.03 ± 0.64	200
	5880 ± 200	2025 ± 70	71 ± 8	98 ± 3	0.40 ± 0.25	170
	5880 ± 200	2830 ± 95	81 ± 10	94 ± 2	0.52 ± 0.32	180
	5880 ± 200	3965 ± 135	96 ± 11	90 ± 3	0.72 ± 0.45	200
	5880 ± 200	4960 ± 165	109 ± 13	88 ± 7	0.93 ± 0.58	210

The uncertainties in columns 2 and 3 have uniform distribution
All angles are measured clockwise as in *Figure 2.5*

41
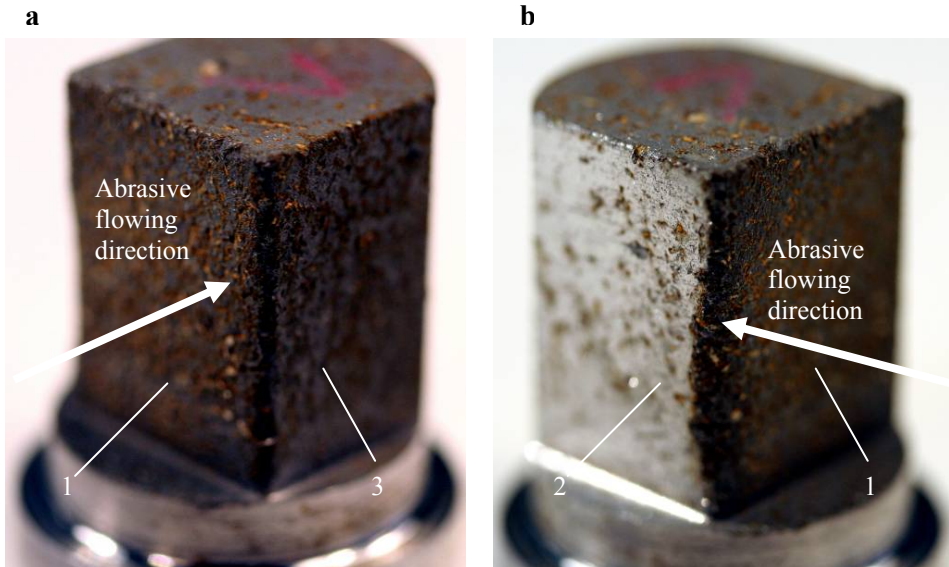
Figure 2.8 SSAB made custom pins. Initial phase of impact (a) and final phase of impact (b): 1 – working surface, 2 – inner facet, 3 – outer facet

2.2.4 Calculation uncertainties

All input random variables X_i are statistically uncorrelated. The determination of real impact angle and real impact velocity started from the calculation of ejection velocity v_{ej} and ejection angle α.

Abrasive movement on the impeller was described by differential equation (2.11). Ejection velocity v_{ej} was calculated by equation (2.21), which was a scalar product of equation (2.19) and equation (2.20). It is very complicated to take partial derivations from equation (2.19) with respect to the variables μ, ω, and ξ. Therefore the relation between the output quantity $\dot{\xi}$ and input quantities μ, ω, and ξ was found experimentally, like it is described in the theoretical part (see subchapter 1.4).

Uncertainty component caused by coefficient of friction μ
Changing input quantity μ while other input quantities are kept constant causes the change in $\dot{\xi}$, and in all other dependent values.

If the COF is assumed to be between $0.1 – 0.6$ and it has a uniform distribution, then the standard deviation is according to equation (1.12)

$$u(\mu) = \frac{0.6 - 0.1}{2 \cdot \sqrt{3}} \approx 0.1.$$

The upper limit of the standard distribution interval is then $0.36 + 0.14 = 0.50 \approx 0.5$ and lower limit is $0.36 – 0.14 = 0.22 \approx 0.2$.

Calculation route is the same as in subchapter 2.2, therefore it is not written out once again. The calculation made twice for both limits of standard tolerance (Table 2.3).

Table 2.3. Calculation results then other input quantities besides COF μ while are held constant

No	μ	ω_1, min^{-1}	ω_2, min^{-1}	ξ, m	Impeller			Impact with the 1st circle of specimens			
					$\dot{\xi}$, m/s	v_{ej}, m/s	α, °	γ_{st}, °	γ_{fin}, °	v_{st}, m/s	v_{fin}, m/s
1	0.2	2830	2830	0.028	17.3	23.1	28.7	87.3	84.0	57.5	59.2
2	0.5				17.4		29.0	87.4	84.1	57.4	59.1

The uncertainty intervals for v_{st} and v_{fin} caused by μ are $2u(v_{st})_\mu$ and $2u(v_{fin})_\mu$. Their values are set equal to the biggest interval given in Table 2.3, i.e. 0.1 m/s.

The uncertainty intervals for γ_{st} and γ_{fin} caused by μ are $2u(\gamma_{st})_\mu$ and $2u(\gamma_{fin})_\mu$.

Their values set are equal to the biggest interval given in Table 2.3, i.e. 0.1°

Uncertainty component caused by rotation velocity ω

The calculation route is the same as it was for μ uncertainty calculation, i.e. the major calculation is made according to subchapter 2.2, and the results of the calculations are given together in Table 2.4.

It is assumed that by the probability of 50% the interval for rotational velocity of the rotors is 2780–2880 min^{-1}. A mean value is 2830 min^{-1} and in case of uniform symmetrical distribution [29]

$$u(\omega) = 1.15 \cdot a(\omega) = 1.15 \cdot \frac{2880 - 2780}{2} \approx 57.7 \quad \text{min}^{-1} \qquad (2.29)$$

A coverage factor $k = 1.653$ corresponds to an expanded uncertainty $U(\omega)$ by the coverage level of 95% [29]

$$U(\omega) = k \cdot u(\omega) = 1.653 \cdot 57.7 \approx 95.4 \text{ min}^{-1}$$

Relative expanded uncertainty $U(\omega)/|\omega|$ necessary for the calculation of uncertainties corresponding to other turning velocities (Table 2.2) is

$$95.4/2830 \approx 33.7 \cdot 10^{-3}.$$

The upper limit of the standard distribution interval is $2830 + 57.7 \approx 2890$ min^{-1}.

The lower limit of the standard distribution interval is $2830 - 57.7 \approx 2770$ min^{-1}.

Four different limiting solutions are presented here. In the first two cases the rotor with impellers and the 2nd circle of the pins is having limiting rotational velocities (ω_1) while the rotor with the 1st circle of pins has 2830 min^{-1} rotational velocity (ω_2). In Cases 3 and 4 the rotor with impellers and the second

circle of pins has 2830 min^{-1} rotational velocity and second rotor has limiting rotational velocities (Table 2.4).

Table 2.4. Calculation results then other input quantities besides ω are held constant

No		Input parameters			Calculated parameters						
					Impeller			Impact with the 1st circle of specimens			
	μ	ω_1, min^{-1}	ω_2, min^{-1}	ξ, m	$\dot{\xi}$, m/s	v_{ej}, m/s	α, °	γ_{st}, °	γ_{fin}, °	v_{st}, m/s	v_{fin}, m/s
1	0.36	2770	2830	0.028	17.0	22.6	29.0	87.1	83.9	57.0	58.7
2		2890			17.7	23.6		87.6	84.2	57.8	59.6
3		2830	2770		17.4	23.1		87.6	84.3	56.6	58.4
4			2890					87.1	83.9	58.2	59.9

The uncertainty intervals for v_{st} and v_{fin} caused by ω_1 are $2u(v_{st})_{\omega_1}$; $2u(v_{fin})_{\omega_1}$ and caused by ω_2 are $2u(v_{st})_{\omega_2}$ and $2u(v_{fin})_{\omega_2}$. Their values are set equal with the biggest corresponding interval given in Table 2.4, i.e. 0.9 m/s for $2u(v)_{\omega_1}$ and 1.6 m/s for $2u(v)_{\omega_2}$.

The uncertainty intervals for γ_{st} and γ_{fin} caused by ω_1 are $2u(\gamma_{st})_{\omega_1}$, $2u(\gamma_{fin})_{\omega_1}$, and caused by ω_2 are $2u(\gamma_{st})_{\omega_2}$ and $2u(\gamma_{fin})_{\omega_2}$. Their values are set equal with to the biggest corresponding interval given in Table 2.4, i.e. 0.5° for $2u(\gamma)_{\omega_1}$ and 0.5° for $2u(\gamma_{fin})_{\omega_2}$.

Uncertainty component caused by the length of impeller ξ
The length ξ is equal with *OB*. If ξ has uniform distribution, it is between (0.025 – 0.031) m, then

$$u(\xi) = \frac{0.031 - 0.025}{2\sqrt{3}} \approx 1.7 \cdot 10^{-3} \text{ m}$$

The upper limit of the standard distribution interval is then

$$\frac{0.031 + 0.025}{2} + 1.7 \cdot 10^{-3} \approx 0.030 \text{ m}$$

The lower limit of the standard distribution interval is then

$$\frac{0.031 + 0.025}{2} - 1.7 \cdot 10^{-3} \approx 0.026 \text{ m}$$

The calculation route is again the same as before, only final results are given here.

The uncertainty intervals for v_{st} and v_{fin} caused by ξ are $2u(v_{st})_{\xi}$ and $2u(v_{fin})_{\xi}$. Their values are set equal to the biggest interval given in Table 2.5, i.e. 0.6 m/s.

Table 2.5. Calculation results then only ξ is changed from input parameters

No	Input parameters				Calculated parameters						
					Impeller			Impact with the 1st circle of specimens			
	μ	ω_1, min^{-1}	ω_2, min^{-1}	ξ, m	$\dot{\xi}$, m/s	v_{ej}, m/s	α, °	γ_{st}, °	γ_{fin}, °	v_{st}, m/s	v_{fin}, m/s
1	0.36	2830	2830	0.026	17.0	23.2	28.1	87.1	83.8	57.7	59.4
2				0.030	17.8	23.0	29.8	87.6	84.3	57.1	58.9

The uncertainty intervals for γ_{st} and γ_{fin} caused by ξ are $2u(\gamma_{st})_{\xi}$ and $2u(\gamma_{fin})_{\xi}$. Their values are set equal to the biggest interval given in Table 2.5, i.e. 0.5°.

Combined uncertainty
Combined uncertainty forms from uncertainties caused by all input parameters. The equation used for the calculation of velocities and impact angles (equation (2.11)) had 4 input parameters: μ, ω_1, ω_2, ξ.
Standard distribution interval is

$$2u(v_{st}) = 2u(v_{fin}) = \sqrt{4u(v)_{\mu}^2 + 4u(v)_{\omega_1}^2 + 4u(v)_{\omega_2}^2 + 4u(v)_{\mu}^2} =$$
$$\sqrt{4 \cdot 0.1^2 + 4 \cdot 0.9^2 + 4 \cdot 1.6^2 + 4 \cdot 0.6^2} \approx 3.9 \text{ m/s}$$

$$2u(\gamma_{st}) = 2u(\gamma_{fin}) = \sqrt{4u(\gamma)_{\mu}^2 + 4u(\gamma)_{\omega_1}^2 + 4u(\gamma)_{w_2}^2 + 4u(v)_{\mu}^2} =$$
$$\sqrt{4 \cdot 0.1^2 + 4 \cdot 0.5^2 + 4 \cdot 0.5^2 + 4 \cdot 0.5^2} \approx 1.9°$$

Because of central limit theorem [29, 30, 31] a normal distribution of v_{st}, v_{fin}, γ_{st}, γ_{fin} is assumed, and if the coverage factor $k = 2$, which corresponds to a coverage level of 95%, the expanded uncertainty is

$$2U(v_{st}) = 2U(v_{fin}) = k \cdot 2u(v_{st}) = 2 \cdot 3.9 = 7.8 \text{ m/s},$$
$$2U(\gamma_{st}) = 2U(\gamma_{fin}) = 2 \cdot 1.9 = 3.8°.$$

$2u(\gamma)$ is suspicious, namely because of small uncertainty of ejection angle α (Table 2.3, Table 2.4 and Table 2.5). This raised suspicions about the measurement model, equation (2.11).

Further investigation of possible reasons for too small uncertainty of ejection angle gave the answer in [9]. The measurement model does not take into account aerodynamical disturbances (mainly air whirls) in the working chamber.

The effect of aerodynamic disturbances for CAK was studied by Kleis [9], who constructed a CAK working under vacuum. The deviations of particle velocity and impact angle decreased to ± 1.5% from their mean values.

The construction of impact wear tester is more complicated than CAK, where the specimens are in standstill position (Figure appendix 1.1). The sand is only accelerated by a rotating rotor in CAK, while two rotors are turning in

impact wear tester (Figure 2.1). It is very complicated to construct the device working under vacuum or to use speed filming for measuring experimental ejection angles because of such construction (like it was done in CAK). It is very hard to evaluate aerodynamical disturbances theoretically.

However, it is possible to use experimental data obtained in [9] for the evaluation of ejection angle. The main conclusions worth mentioning found by speed filming in [9] were:

- the scattering of ejection angle increases if the diameter of particles decreases,
- the trajectory of particles from rotor to specimen is a straight line and the velocity remains constant.

The size ranges of abrasive used for angle determination testing in CAK were (0.3–04) mm and (0.6–1.0) mm. Based on the above information and considering a much bigger size of abrasive particles in impact wear tester, it was concluded that the effect of aerodynamical disturbances is covered by assuming

$$2u(v_{st}) = 2u(v_{fin}) \approx 5 \text{ m/s},$$
$$2u(\gamma_{st}) = 2u(\gamma_{fin}) \approx 3°,$$

Relative expanded uncertainty $u(v_{st})/|v|$ or $u(v_{fin})/|v|$ necessary for the calculation of uncertainties for other turning velocities is

$$2.5/58 \approx 4.3 \cdot 10^{-2}.$$

Real impact velocity and real impact angle depend on the impact stage (Figure 2.5). v_{st}; γ_{st} were determined at the beginning and v_{fin}, v_{fin} at the end of the impact. Real impact velocity v and real impact angle γ values are arithmetic means of v_{st}, v_{fin} and γ_{st}, γ_{fin}. $u(v)$ and $u(\gamma)$ values are calculated by adding half width of v or γ interval to either v_{st}, γ_{st} or γ_{fin}, v_{fin}

$$u(v) = u(v_{st}) + \frac{|v_{fin} - v_{st}|}{2} = 2.5 + \frac{59 - 57}{2} \approx 3 \text{ m/s}$$

$$u(\gamma) = 1.5 + \frac{|84 - 87|}{2} \approx 3°$$

Expanded uncertainties $U(v)$ and $U(\gamma)$ are calculated from equation (1.16) then k = 2. Expanded uncertainty values for other rotational velocities of rotors are calculated on the basis of relative expanded uncertainty. The results were given in Table 2.2.

Kinetic energy calculation uncertainty

The kinetic energy of impact was determined by the equation (2.28), which contained two input random variables X_i: mass and velocity. Mass uncertainty needs to be calculated, velocity uncertainty is already revealed.

The counting is assumed to have a rectangular distribution where width of the interval $2a(n)$ is 10, and from equation (1.12):

$$u(n) = \frac{10}{2\sqrt{3}} \approx 2.9$$

Mass dispersion of 318 particles is assumed to have a rectangular distribution, where the width of interval $2a(m_{abr})$ does not exceed 50 g, from equation (1.12):

$$u(m_{abr}) = \frac{50 \cdot 10^{-3}}{2\sqrt{3}} \approx 14 \cdot 10^{-3} \text{ kg}.$$

Sensitivity coefficients as partial derivatives from equation (2.27) are

$$c_{m_{abr}} = \frac{\partial m_p}{\partial m_{abr}} = \frac{1}{n}, \qquad\qquad c_n = \frac{\partial m_p}{\partial n} = -\frac{m_{abr}}{n^2}.$$

The combined uncertainty of particle mass is

$$u^2(m_{particle}) = c_n^2 \cdot u^2(n) + c_{m_{abr}}^2 \cdot u^2(m_{abr}) = \left(-\frac{m_{abr}}{n^2}\right)^2 \cdot u^2(n) + \frac{u^2(m_{abr})}{n^2} =$$

$$= \left(-\frac{50 \cdot 10^{-3}}{318^2}\right)^2 \cdot 2.88^2 + \frac{14.4^2 \cdot 10^{-3}}{318^2} \approx 4.54 \cdot 10^{-5} \text{ kg}.$$

Combined uncertainty of kinetic energy of a particle is calculated by taking partial derivatives as sensitivity coefficients from equation (2.33)

$$c_{m_p} = \frac{\partial E_k^p}{\partial m_p} = \frac{v^2}{2}, \qquad\qquad c_v = \frac{\partial E_k^p}{\partial v} = mv.$$

The standard uncertainty of the kinetic energy is

$$u\left(E_k^p\right) = c_{m_p}^2 \cdot u^2(m_p) + c_v^2 \cdot u^2(v) = \frac{v^4 u^2(m_p)}{4} + m_p^2 \cdot v^2 \cdot u^2(v) =$$

$$\frac{58.3^4 \cdot 4.54 \cdot 10^{-5}}{4} + (\frac{50 \cdot 10^{-3}}{318} \cdot 58.3^4 \cdot 3.4)^2 \approx 0.083 \text{ J}$$

Although all input quantities had a rectangular distribution, normal distribution according to the central limit theorem, can be assumed for the combined uncertainty [49].

$$U(E_k^p) = k \cdot u(E_k^p) = 2 \cdot 0.083 \approx 0.17 \text{ J}$$

Expanded uncertainty is based on normal distribution and defines an interval estimated to have a coverage probability of 95 %.

The uncertainties of kinetic energies corresponding to other rotational velocities of rotors are calculated in the same way and are drawn together in a Table 2.2.

2.3   Standard quantity of abrasive

Mass losses of the specimens are in direct correlation with the quantity of the tested abrasive. The amount of abrasive should be the smallest possible to give reasonably accurate result, and to ensure the measurement within the stable wear rate behaviour range. Excessive abrasive quantities per test are not

favoured, as it wears the tester excessively. Bayer in [4, 8, 5] names initial wear period for run-in, Kleis in [9] for wear-in, Marcus in [50] and Miyazaki in [51] for incubation period.

The results of uncertainty calculations of several experiments showed that 3 kg of standard granite gravel abrasive is enough for testing steels and coatings (Table 2.6). However, in case of cermets it is not a sufficient amount. GOST standard 23.201-78 developed under supervision of Kleis for CAK testing, claims, that mass loss of a specimen must be at least 5 mg [9]. In our case smaller mass losses may be present at the utmost because weighing accuracy is 0.1 mg. However, the reliability (which is measured by a dispersion) of the result suffers. An example is given below.

A test series was made containing WC-15Co hardmetal and Hardox 600 steel. Steel C 45 was used for reference material. The first test was made with 3 kg of granite gravel, wear loss was determined and then the same specimens were tested again with 3 kg of abrasive. Relative volumetric wear resistance was calculated according to equation (3.3), and test reliability characterised by the uncertainty was found using equation (3.11) and equation (1.16). The results are given in Table 2.6.

Table 2.6. Test results if abrasive quantity varies

Mate-rial	3 kg				3 kg for already by 3 kg worn specimens				6 kg			
	Average mass loss, mg	Mass loss difference, mg	ε_V	$U(\varepsilon_V)$	Average mass loss, mg	Mass loss difference, mg	ε_V	$U(\varepsilon_V)$	Average mass loss, mg	Mass loss difference, mg	ε_V	$U(\varepsilon_V)$
WC-15Co	1.8	1.1	31.0	±11.2	2.7	1.2	30.5	±8.1	4.5	2.3	30.9	±8.3
Har-dox 600	33.3	7.4	1.0	±0.1	38.3	1.4	1.2	±0.1	71.6	8.8	1.1	±0.1

As can be seen from Table 2.6, testing hardmetals with 3 kg of abrasive does not give reliable test results, while the results of Hardox 600 have already small uncertainty. Hardmetal test results using 6 kg of abrasive are already more reliable, although total mass loss is still very small (Table 2.6).

The reasoning for uncertainty decrease while increasing abrasive amount is given below.

According to negligibility criterion [29], a component of uncertainty to the final contribution (equation (3.11)) should be neglected if it is 0.3 times smaller than final contribution. In case of cermets, all other components besides $c_{\Delta m}^2 u^2(\Delta m)$ in equation (3.11) should be neglected. In the sensitivity coefficient $c_{\Delta m}$ we can see that wear loss of investigated material is in the power of two while wear loss of reference material is not powered. From here can be

concluded that if wear loss of investigated material and reference material had increased equally, the uncertainty of volumetric wear resistance would decrease according to square function. In other words a larger amount of abrasive gives better reliability to the results.

Conclusions can be drawn from equation (3.11) and sensitivity coefficient $c_{\Delta m}$: if relative volumetric wear resistance increased, the reliability of the results would decrease. This explains why relative uncertainty of materials with extremely good wear resistance has increased while their mass loss difference is not larger than other materials.

The specimens of WC-5Co and WC-15Co originating from different source were tested with 15 kg of abrasive. In this time the reference material was Hardox 400. Compared to steel C 45 Hardox 400 is slightly worse – its relative volumetric wear resistance is 0.9 (see subchapter 3.3.1). Again, relative volumetric wear resistance was calculated according to equation (3.3), and test reliability, characterised by uncertainty, was found according to equation (3.11) and equation (1.16).The result are given in the Table 2.7.

Table 2.7. Materials tested with 15 kg of granite gravel

Material	Average mass loss, mg	Mass loss difference, mg	ε_V	$U(\varepsilon_V)$
WC-5Co	41	67.1	10.1	±9.3
WC-15Co	28	12.5	13.9	±3.3

Test results (Table 2.7) show, that the reliability is much better compared to testing with 6 kg of abrasive (Table 2.6). WC-5Co had very big mass loss difference – the span was 67.1 mg, bigger than the average mass loss of this material, but still the uncertainty was smaller than in the case of WC-15Co tested with 6 kg of abrasive (Table 2.6). Indeed, smaller uncertainty is also caused by smaller ε_V.

As above experiments and considerations showed, 15 kg of granite gravel is a convenient abrasive amount for conducting impact wear tests of hardmetals and cermets. In most cases it gives the results with moderate uncertainty, but as the wear mechanism of hardmetals and cermets is often unpredictable spalling, it cannot be very small.

The test results given above and the results given in subchapter 3.5 proved that for testing only steels and coatings is 3 kg of granite gravel sufficient amount.

However, when the tests were done using other abrasives (quartzite and limestone), previous knowledge about abrasive behaviour was not available and their quantity was taken to be 15 kg regardless of the tested materials.

3   STUDY OF ABRASIVE IMPACT WEAR RESISTANCE

Abrasive impact wear (AIW) resistance study of steels and cermets was performed in impact wear tester (Figure 2.1). Rotational velocity of rotors was 2830 min^{-1}, which means that the real impact velocity between the abrasive jet and the 1st circle of pins was 60 m/s (Table 2.2), and the abrasive size was (4−5.6) mm.

3.1   The studied materials

Studied materials can be divided into three groups:
  a) steels;
  b) low and high binder content cermets;
  c) hardmetal and metal-matrix coatings.

Studied steels are commonly used in many applications where resistance to the abrasive erosion wear or impact wear is required, for example Hadfield manganese steel was widely used already more than 100 years ago, and chromium-molybdenum steels are proven in impact wear conditions (see subchapter 1.3). The following steels were studied:

  − ordinary commercial carbon steel (C 45) or wear resistant steel Hardox 400 was used as a reference material. The latter is common in mining industry;

  − Hadfield manganese steel (designation in GOST is 110G13L). It is very widely used in Estonian mining industry;

  − Hardox 600 was involved as the world hardest wear plate specifically designed for the extreme wear conditions [52];

  − Vanadis 6, chromium-molybdenum-vanadium alloyed 3rd generation powder metallurgy (PM) tool steel and spray formed (SF) Weartec are both recommended by the producer for wear resistance demanding applications [53]. The producer claims that Weartec offers a combination of very high wear resistance and a good resistance for chipping and cracking [54]. PM tool steels production consist of powder making, capsule filling, hot isostatic pressing (HIP) and mostly rolling or forging [55]. Spray forming used for Weartec production does not involve HIP-ing (although it might be involved in production of other steels). A liquid metal stream is dispersed (atomized) into droplets. These droplets are collected on a rotating disc before full solidification is completed. A finished billet is gradually built up and can then be directly forged or rolled into bars or plates [56, 57];

  − metal-matrix composite (MMC) material, produced by PM/HIP-ing is an experimental steel based on Cr-steel, containing about 20 vol% of

VC micrometrical particles and about 20 vol% of WC reinforcement. The chemical composition and hardness of steels are given in Table 3.1. Figure 3.1 gives the microstructures of the most significant tested steels.
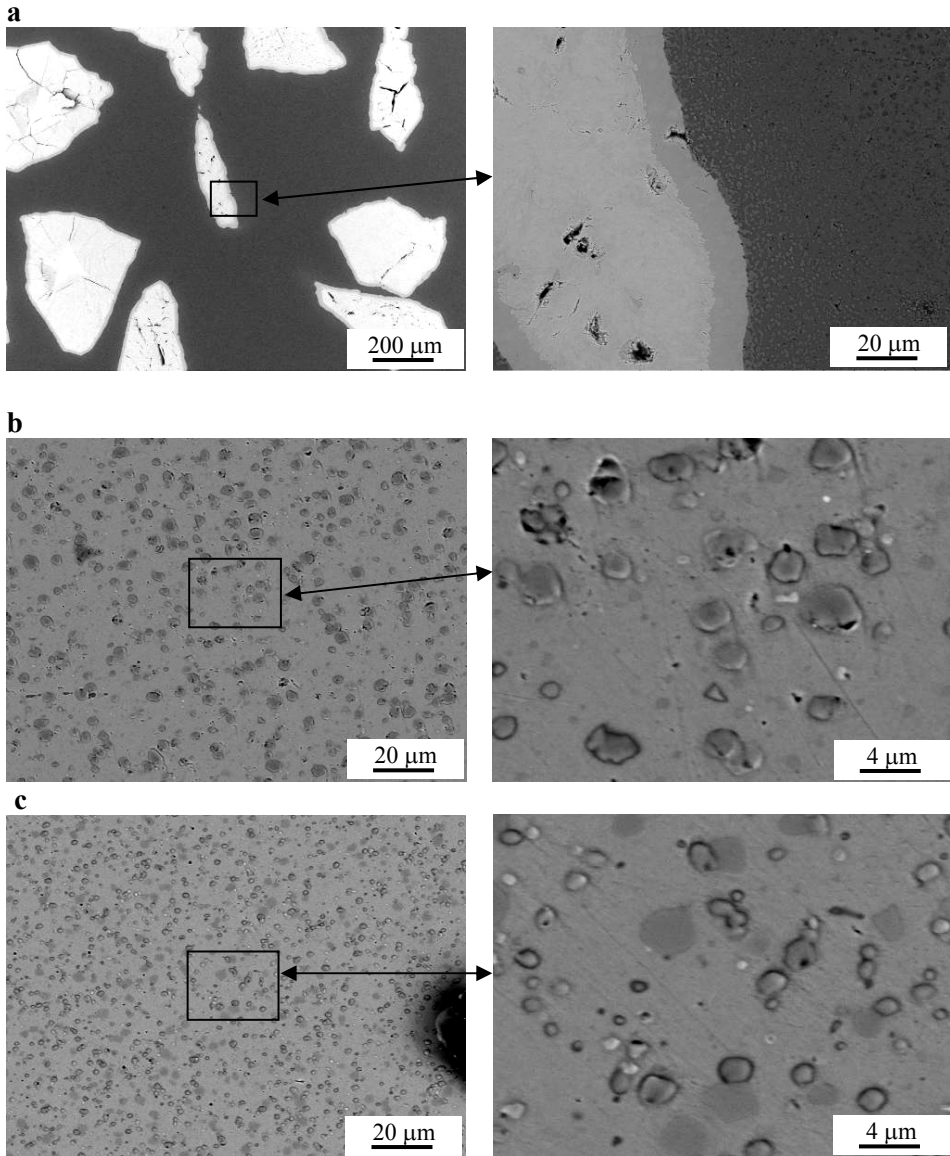
Figure 3.1 Microstructures of the most significant studied steels: MMC (a); Weartec (784 HV30) (b) and Vanadis 6 (834 HV30) (c) at different magnifications

Hardmetals, as traditional wear resistant materials, were most widely tested from cermets because of their unique combination of desired properties like high wear resistance and relatively low production costs. However, tungsten

shortage and poor corrosion resistance has lead to tungsten-free cermets, like cermets based on titanium and chromium carbides [58] and some their representatives are tested here. The hardmetals and cermets studied can be divided into three groups:

- WC-based hardmetals (Co content from 5 to 26 wt%);
- Cr_3C_2 based cermets (Ni binder content from 20 to 50 wt%);
- TiC based cermets (Ni-Mo binder content 30 and 50 wt%; Ni: Mo = 4:1) in the preliminary research.

The chemical composition and hardness of hardmetals and cermets are given in Table 3.1, and the microstructures in Figure 3.2.

Studied coatings were produced by thermal spray processes, namely by high-velocity oxy-fuel spray (HVOFS) followed by possible fusion (F) and by flame spray fusion (FSF).

Used coating materials can also roughly be divided into two groups: nickel based self-fluxing alloy (NiCrSiB) powders and tungsten carbide-cobalt (WC-Co) hardmetal based on commercial and experimental powders.

From commercial hardmetal based coatings was tested in impact conditions proved composition WC-17Co [59].

Experimental recycled (WC-Co)+15Co powder was produced from disintegrator milled hardmetal cutting inserts by using the following production process:

- mechanical mixing of recycled WC-Co and added Co powders,
- compacting by pressing,
- sintering of compacts,
- crushing and classifying.

Further details of experimental powder production are available in [15].

All tested materials with their chemical composition and hardness values are grouped into Table 3.1.
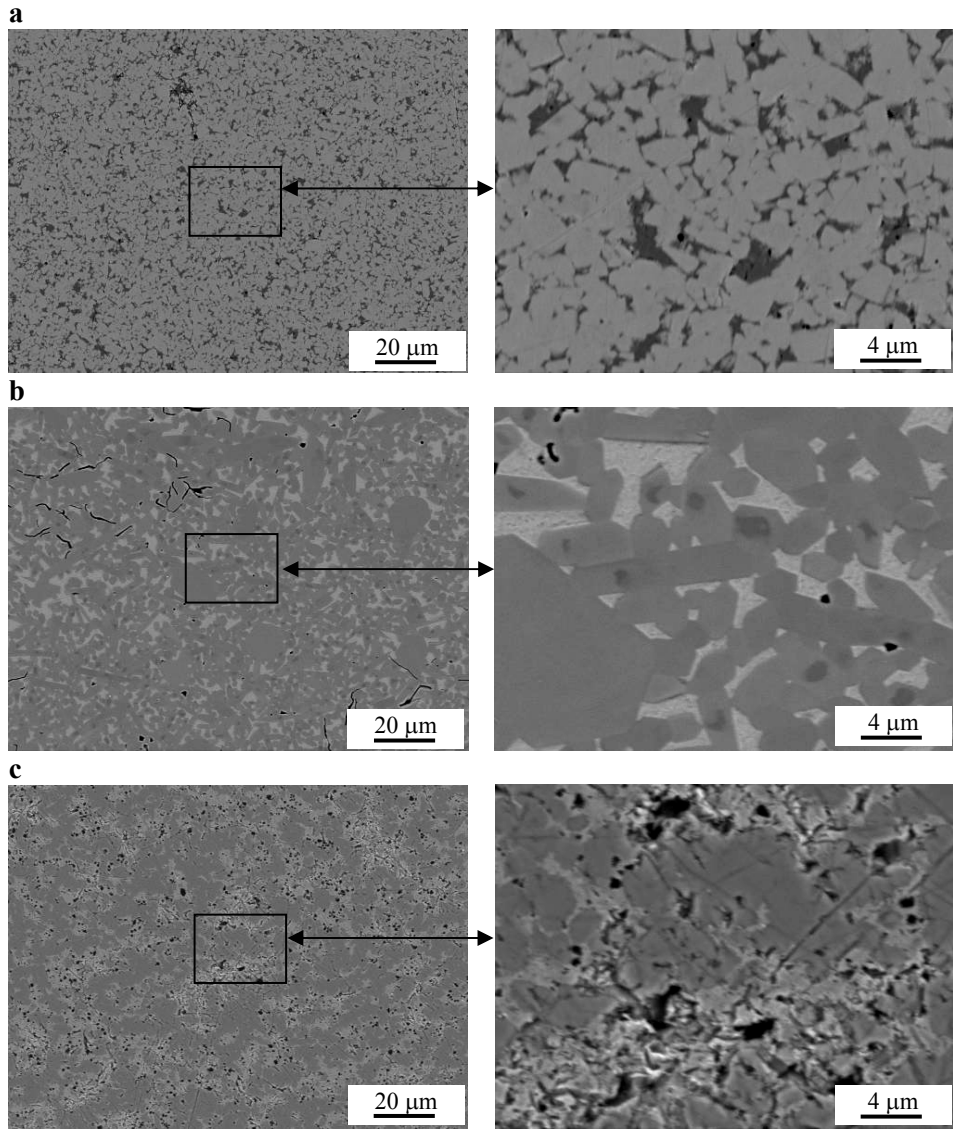
Figure 3.2 Microstructures of the most significant cermets: WC-15Co (a); Cr_3C_2 - 20Ni (b); Cr_3C_2 -50Ni (c)

Table 3.1. Tested materials

Material type	Designation	Composition, wt%	Hardness HV
Steels		Conventional steels	
	C 45	0.45 C	200 HV30
	Hardox 400	0.25 C; 1.60 Mn; 1 Cr; 0.7 Ni; 0.8 Mo	395 HV30
	St 37	0.19−0.23 C	140–150 HV30
	Hardox 600	0.48 C; 1 Mn; 1.2 C; 2.5 Ni; 0.8 Mo	540 HV30
	Hadfield	0.90–1.50 C; 11.5–15.0 Mn; ≤ 1 Cr;	220 HV30
		Powder steels	
	Vanadis 6	Cr-Mo-V alloyed PM steel: 2.1 C; 1.0 Si; 0.4 Mn; 6.8 Cr; 1.5 Mo; 5.4 V	272 HV 402 HV 834 HV30
	Weartec	Spray formed fine grain VC − reinforced Cr-Mo-V steel: 2.8 C; 0.8 Si; 0.7 Mn; 7.0 Cr; 2.3 Mo; 8.5 V	286 HV 458 HV 784 HV30
		Steel based MMC	
	MMC	PM/HIPed (Cr-steel+VC)+WC, reinforcements: ~20% VC (d ~1μm) and ~20% WC d= (200 − 300) μm	680 HV30
Cermets	K05	WC-5Co	2000 HV10
	B10	WC−10Co	1462 HV10
	B15	WC-15Co	1288 HV10
	VK15	WC-15Co'	
	G40	WC-20Co	1110 HV10
	G55	WC-26Co	917 HV10
	J20	Cr_3C_2−20Ni	1214 HV10
	J50	Cr_3C_2−50Ni	385 HV10
	TH30	TiC-30Ni:Mo (4:1)	1360 HV10
	TH50	TiC-50Ni:Mo (4:1)	1050 HV10
HVOFS coatings	Tafa 1275H	16 Cr, 4 Si, 3.5 B, 4 Fe, 0.8 C, rest Ni	
	Tafa 1343V	83 WC; 17 Co	1300 HV1
	Recycled (WC-Co) + 15 Co	60 WC; 23Co; 10Fe	1100 HV1
Spray-fused coatings	HVOFS + F Tafa 1275H	16 Cr, 4 Si, 3.5 B, 4 Fe, 0.8 C, rest Ni	805 HV0.2
	FS+F Castolin 12495	NiCr16Si4B3	560 HV0.2

3.2   Abrasives used in tests

The standard abrasive mineral material for testing is granite gravel (Figure 3.3), classified according to EN 13043, EN 13450 and EN 12620. It originates from Inkoo mine, Finland. Its Los Angeles test coefficient is 22.4 (the test was fulfilled with reduced abrasive fraction (4−6.3) mm according to [60], while common testing fraction is (10−14) mm, (see Appendix 2).

   Distribution polygon and cumulative distribution polygon presented in Figure 3.3 are based on the sieve analysis, where asterisks on the plots designate sieve sizes (Figure 3.3 (c)) or moving averages of adjacent sieve sizes (Figure 3.3 (b)). The size of delivered granite gravel is (4−6) mm. Bigger than 5.6 mm particles are sieved out for the safety reasons − one mistakenly hidden very large particle could destroy the whole testing rig. Finer than 4 mm particles are not separated, but as distribution polygons in Figure 3.3 show, their content is really minimal.
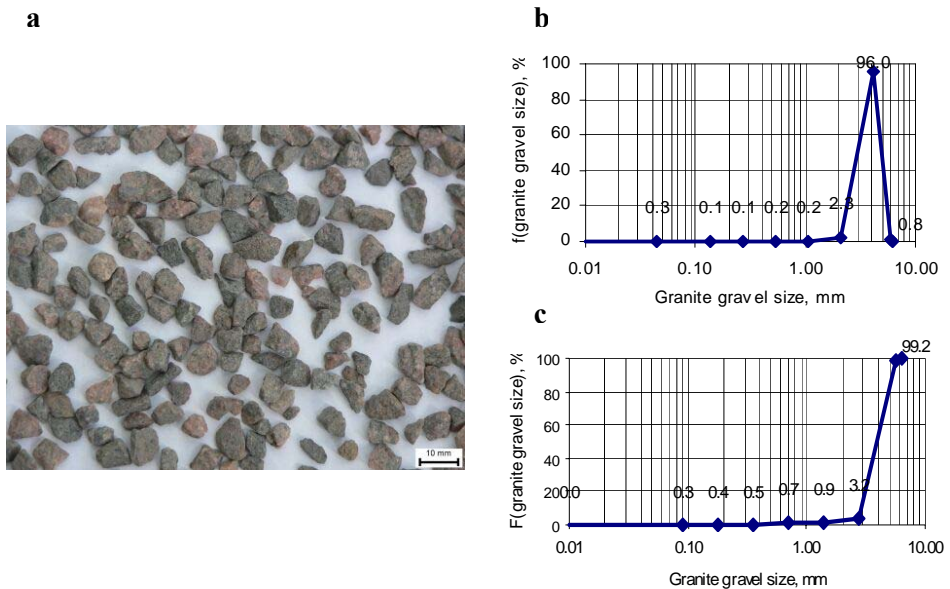
Figure 3.3 Overall picture of the granite gravel (a) with particle size distribution frequency polygon (b) and cumulative frequency polygon (c)

   Granite gravel consists of different minerals (Figure 3.4 and Table 3.2) with different hardnesses. Main components are quartz (black, about 70 vol%) with hardness (1045−1110) HV0.1, feldspar (white mineral, about 10 vol%) with hardness 745−925 HV0.1 and their mix, about 20 vol%.

c

55
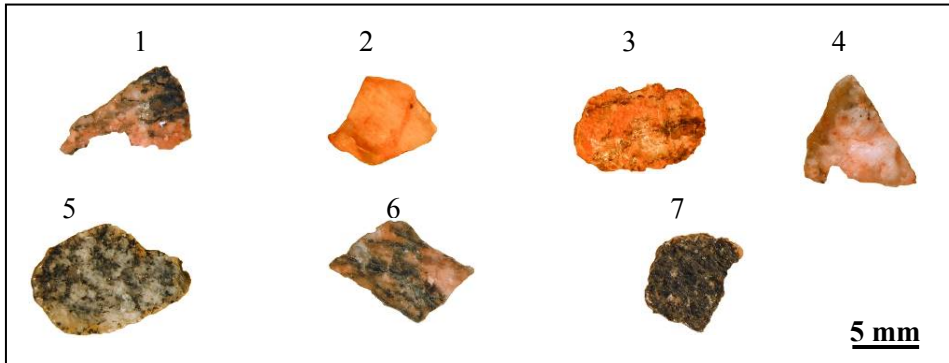
Figure 3.4 Polished cross-sections of granite gravel particles subjected to hardness measurements

Table 3.2. A set of granite particles and their hardness values

Tested granite particle	Hardness of specific measurement, HV 0.1								Average
	1	**2**	**3**	**4**	**5**	**6**	**7**	**8**	
1	1065	1017	1333	882					1074
2	677[1]	666[1]	858[1]	781[1]	677[1]	811[1]			745
3	1027[1]	947[1]	753[1]	967[1]					923
4	766[1]	727[1]	796[1]						763
5	824	946	1187	1169	1288	946	1169	1115	1080
6	908	1288	1248	959	1033	1228			1110
7	1097	1033	1097	814	1002	1227			1045

[1]In these cases HV 0.05 was measured

3.3 Wear characteristics

Measured quantities are mass loss and work surface area. The specimens are weighed before and after each test with an accuracy of 0.1 mg, and mass losses of the specimens are calculated. Usually at least 3 specimens from a material are tested at once. All tests were done with two reference specimens. The specimens were cleaned with technical spirit, ultrasound and compressed air before and after the tests.

Steel C 45 is used as a reference material in almost all tests. Test results with reference specimens in each batch show immediately, if the test has had deviations from standard procedure. Reference specimens are additionally necessary for the calculation of relative volumetric wear resistance which is the best quantity for characterising wear in impact wear tester, although according to the Bayer [3] erosion rates are generally specified in terms of material lost per quantity of abrasive.

Volumetric wear rate and relative volumetric wear resistance

In real life situations volume loss is more important than mass loss, because it describes dimensional changes, and most working details are not usable anymore expressly because of their worn-out dimensions. Operating with volume loss is especially important as the compared materials have a big density span. Materials having equal mass loss but different density have different volume loss (denser materials have less volume loss).

Volume loss ΔV calculation steps are:

- determination of mass loss Δm of the specimen by the accuracy of 0.1 mg,
- determination of unit mass loss Δm_{unit} in mg/mm^2 by dividing mass loss of the specimen with impacted zone area in mm^2,

$$\Delta m_{unit} = \frac{\Delta m}{bh} = \frac{\Delta m}{A} \qquad (3.1)$$

- calculation of mass loss of a standard size specimen (mg) by multiplying unit mass loss with by a standard impacted zone area (15.0 mm x 16.3 mm),
- calculation of volume loss ΔV (mm^3) through dividing mass loss of standard size specimen by the density

$$\Delta V = \frac{\Delta m \cdot b_{st} \cdot h_{st}}{A\rho}, \qquad (3.2)$$

where

Δm – specimen mass loss,
b – impact zone width,
b_{st} – standard impact zone width (15.0 mm),
h – impact zone height,
h_{st} – standard impact zone height (16.3 mm),
A – active surface area of the specimen ($A = bh$, where b – impact zone width, h – impact zone height),
ρ – density.

Unit mass loss calculation decreases the uncertainty of the results caused by the width variation of each specimen (in impact wear tester the width of the hit area of the specimen is not determined by the fixture like it is in CAK [9]). However, unit mass loss does not eliminate width variation completely because wear across the specimens is not uniform – major wear will take place on the edges of the specimen, especially when testing fragile materials.

The relative volumetric wear resistance ε_v was calculated as the volume loss of reference material (steel C 45) divided by the volume loss of studied material

$$\varepsilon_V = \frac{\Delta V_r}{\Delta V} = \frac{bh\Delta m_r \rho}{b_r h_r \Delta m \rho_r}. \qquad (3.3)$$

Relative wear resistance is the most recommended characteristic to describe wear, because it compares the wear loss of the reference material and studied material presented in the same batch. If any input parameter changed (for example the amount of abrasive, the composition of abrasive, feed rate, et

cetera), the results of reference and investigated material would be affected evenly. Additionally, it enables to compare the results of the test made with different abrasive amounts.

Wear rate

Wear rate I_g was determined as the mass loss of the target sample per mass of abrasive particles. Wear rate is not directly influenced by the amount of the abrasive. This enables to easily compare wear losses obtained by different abrasive amounts. Wear rate calculation steps are:

- determination of mass loss Δm of the specimen by the accuracy of 0.1 mg,
- determination of unit mass loss Δm_{unit} in mg/mm^2 by dividing the mass loss of the specimen with impact zone area in mm^2,
- calculation of mass loss of a standard size specimen (mg) by multiplying unit mass loss with a standard impact zone area (15.0 mm x 16.3 mm),
- calculation of wear rate I_g (mg/kg) by dividing the mass loss of standard size specimen by abrasive mass per specimen

$$I_g = \frac{\Delta m \cdot b_{st} \cdot h_{st}}{A \cdot Q}.$$ (3.4)

The volumetric wear rate I_v in mm^3/kg is calculated by dividing I_g with abrasive fraction allocated for a specimen and abrasive density.

$$I_V = \frac{\Delta m \cdot b_{st} \cdot h_{st}}{A \cdot Q \cdot \chi \cdot \rho},$$ (3.5)

where

Δm – average mass loss,

b_{st} – standard working zone width (15.0 mm),

h_{st} – standard working zone height (16.3 mm),

A – average active surface area of the specimen ($A = bh$, where b – average working zone width, h –average working zone height),

ρ – density,

Q – abrasive amount,

χ – the abrasive fraction allocated for a specimen (as it can be deduced from the Figure 2.5, 9.4°/360° from the total abrasive mass is allocated for a specimen).

There is no doubt that an impact wear tester suits perfectly for the determination of relative volumetric wear resistance of a material. However, if the purpose is to determine wear rate I_g (mg/kg) or I_v (mm^3/kg) it fails to provide test results with high accuracy, because the exact amount of the abrasive amount allocated for a specimen cannot be determined precisely. The same disadvantage was noted for CAK [9].

3.3.1 Abrasive impact wear resistance of steels

Table 3.3 gives test results for tested steels. Steel C 45 was the reference material.

Table 3.3. Test results of steels tested with 3 kg of granite gravel

Designation	ΔV, mm^3	ε_V	I_V, mm^3/kg
Reference steel C 45	4.4 ± 0.4	1.0 ± 0.1	56.7 ± 19.1
Hardox 400	4.9 ± 0.6	0.9 ± 0.1	63.2 ± 21.2
Hardox 600	4.5 ± 0.7	1.0 ± 0.1	57.9 ± 19.3
Vanadis 6			
• 272 HV*	4.1 ± 0.4	1.1 ± 0.1	51.9 ± 17.0
• 402 HV	3.8 ± 0.5	1.2 ± 0.1	49.1 ± 16.9
• 834 HV30	2.4 ± 0.3	1.8 ± 0.1	30.5 ± 10.5
Weartec			
• 286 HV*	4.6 ± 0.5	1.0 ± 0.1	58.5 ± 19.3
• 458 HV	3.6 ± 0.3	1.2 ± 0.1	46.4 ± 15.2
• 784 HV30	1.9 ± 0.2	2.3 ± 0.1	24.3 ± 8.1
Hadfield	3.4 ± 0.3	1.3 ± 0.1	43.7 ± 14.3
MMC	2.1 ± 0.3	2.1 ± 0.1	26.4 ± 8.6

*In the delivery condition

Relative volumetric wear resistance and wear rate are given in the Figure 3.5. The columns on the figure indicate relative volumetric wear resistance, and the asterisks indicates volumetric wear rate (the values have to be read from the right vertical axis).
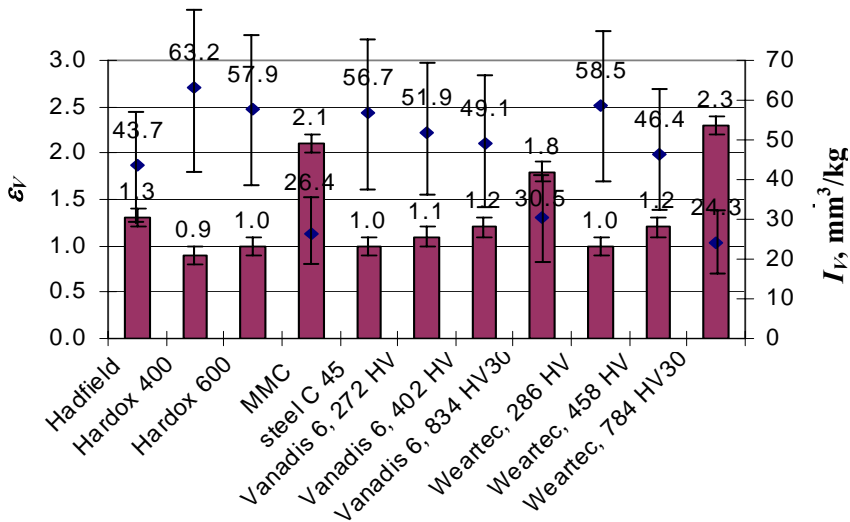
Figure 3.5 Relative volumetric wear resistance ε_V and wear rate I_V of steels

Steels Vanadis 6 and Weartec in soft annealed delivery condition were involved only for comparison (normally these highly alloyed steels are used only in heat treated conditions).

Wear loss of reference steel C 45 and Hardox 400 is quite even. If we compare the pictures of worn surfaces of steel C 45 and Hardox 400, the surface of steel C 45 is plastically more deformed (compare Figure 3.6 and Figure 3.7) because C45 is not so hard and it has higher ductility [61, 62]. Without suffering low cyclic fatigue, plastic deformation of steel C 45 absorbs kinetic energy of the abrasive particles. It seems that steel C 45 has optimum combination between hardness and ductility.
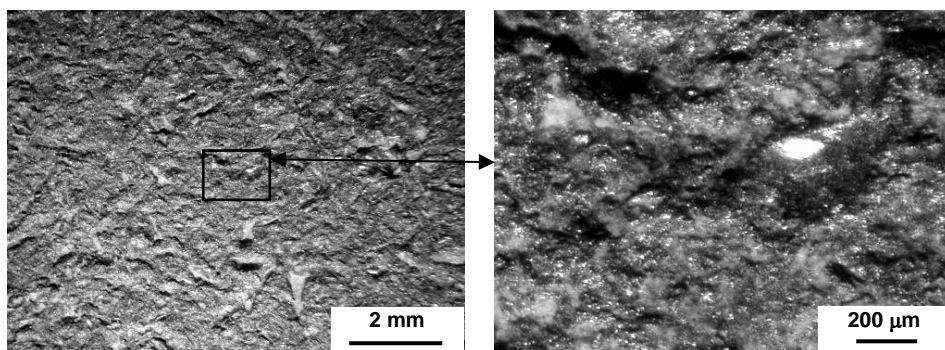
Figure 3.6 Worn surface of reference steel C 45

Hardox 400 is more prone to low cyclic fatigue. The removal of material will take place after a relatively small number of impacts. As it was found by the surface fatigue test, it is about 10−20 impacts [63].
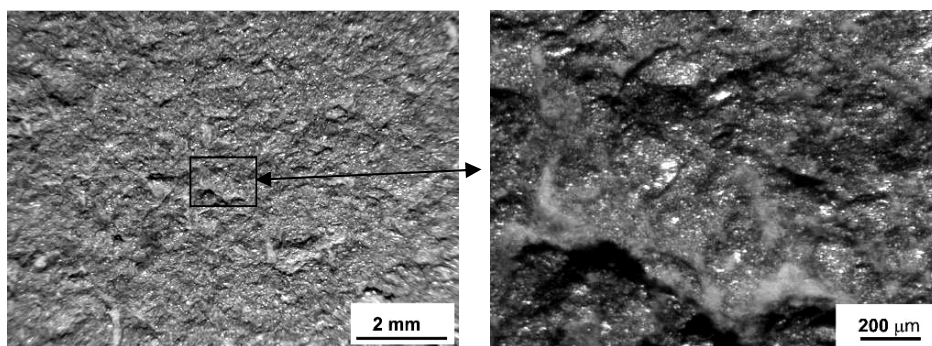
Figure 3.7 Worn surface of Hardox 400 steel

The most wear resistant steel was Weartec. It was tested in different heat treatment conditions and without heat treatment for comparison. It was found, that proper heat treatment increases wear resistance of Weartec up to 2.5 times compared to the soft annealed condition (Figure 3.5). Prevailing wear

mechanisms of 784 HV30 hardened Weartec is low cyclic fatigue. It is evident from numerous craters present on the worn area (Figure 3.8).
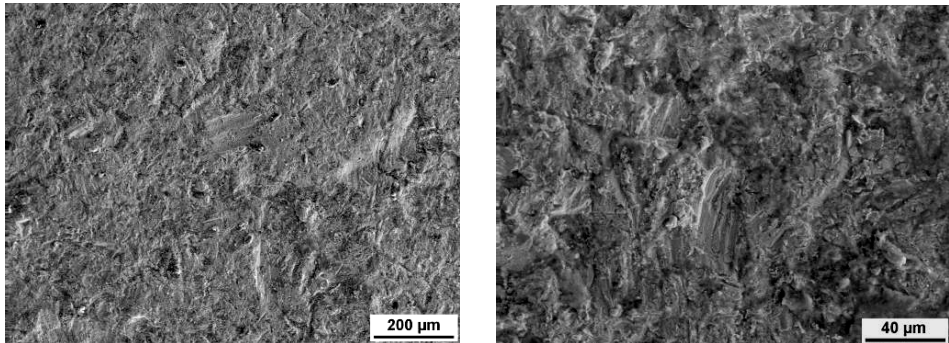
Figure 3.8 Worn surface of Weartec steel hardened and tempered to 784 HV30

However, wear traces on worn area indicate, that despite high hardness, microcutting is also noticeable. Brittle fracture mechanism can be neglected as no cracks were detected.

Next in the sequence of wear resistance was MMC (Figure 3.9), consisting of large and hard tungsten carbide (WC) particles (2450 HV0.1) embedded into a relatively soft matrix of Cr-steel (380 HV0.1). As WC in MMC is relatively resistant to the impact of the abrasive particles of this size and velocity, a wear loss starts from the removal of binder material. Possible carbide removal mechanisms could be:

− WC carbide particles become vulnerable after matrix removal due to microcutting, the metal matrix around the large carbide particles will be removed after a number of impacts and the carbide particle separates finally from the surface of the material;

− a direct fracture of the carbide particles is formed after a number of impacts. Sharp-edged abrasive particles of a size one order larger than those of carbides cause separations of smaller splinters from the carbide grain after multiple strikes. The surface of carbide becomes uneven.

As can be seen from Figure 3.9, microcutting traces on binder phase are visible on the surface of worn specimens, and rare craters are presented in the carbides. Thereby direct fracture of carbides does not take place in the impact wear tester.
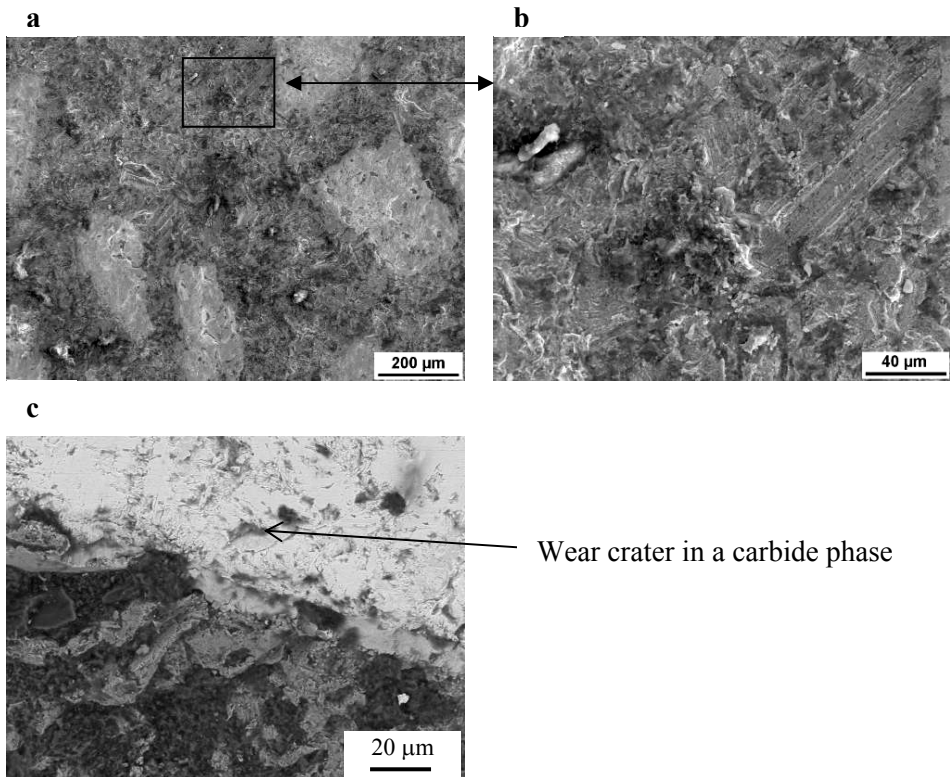
Figure 3.9 Worn surface of MMC at different magnifications

Higher hardness Vanadis 6 (834 HV 30) (Figure 3.10) had only slightly lower wear resistance than Weartec. Compared to Weartec, the hardness of Vanadis 6 was a little higher (see Table 3.1).
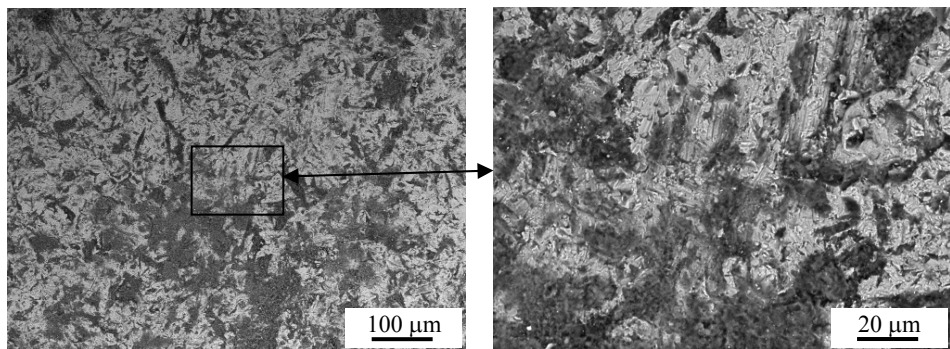
Figure 3.10 Worn surface of Vanadis 6 steel hardened and tempered to 834 HV30

Higher hardness usually means higher resistance to hard particles abrasion, and to surface plastic deformation, debonding, and microploughing [64]. Lower wear resistance can be explained by different structures of Vanadis 6 and

Weartec: Vanadis 6 is produced by PM technique, while Weartec is spray formed. C. Spiegelhauer claims in [56], that spray forming also improves wear resistance due to the larger carbide size achieved by the process compared to PM material. Its larger carbide size is evident in Figure 3.1.

Hadfield manganese steel performed surprisingly well. Considering its low hardness (Table 3.1), it had better wear resistance than the well-known abrasion resistant material Hardox 600. It is the best choice from soft steels. As [65] claims, hadfield is fully austenitic, quench annealed, non magnetic, work-hardening steel with an exceptionally high level of wear resistance when subjected to work-hardening by shock or high impact pressure in service. Severe wear on the surface of Hadfield has a work-hardening effect on the austenitic structure of this steel. This leads to an increase in hardness from the initial hardness up to an in-service hardness of at least 600HB. This work-hardening capability renews itself throughout in-service life. The underlayers not work-hardened maintain an excellent resistance to shock and a very high ductility. That is why Hadfield steel is very commonly used in use of Estonian mining industry (for example by Mäetehnika Ltd).

At the abrasive impact wear, the surface of Hadfield specimens deforms significantly (Figure 3.11) and the abovementioned work-hardening takes place. This is a reason for good wear resistance.
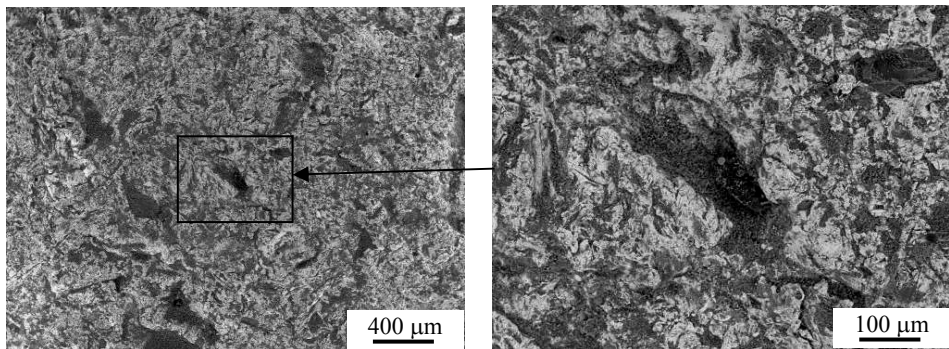
Figure 3.11 Worn sufrace of Hadfield steel

However, as was claimed in the article of J. Mendez et al. [66], plastic deformation has to be remarkable before its work-hardening becomes effective. In certain applications this can be a disadvantage because of undesirable dimensional changes. The growth of Hadfield steel castings to the sideways during wear is noted in [1], and it has to be taken into account when designing the casting and the crushing chambers of crushing machines in order to allow balanced wear and growth. It is also concluded in [1] that replaceable manganese steel castings have proved to be satisfactory wearing surfaces for jaw and gyratory crushers.

3.3.2 Abrasive impact wear resistance of cermets

The widespread use of cermets as wear resistant materials is attributed to their unique combination of desired properties. Cermets are the most promising materials for such hard wear conditions as presented at the abrasive impact wear. WC-based hardmetals are most widely used among cermets because of their excellent wear resistance, strength and toughness properties combination. Impact wear tests showed the superiority of hardmetals – their relative volumetric wear resistance was better than that of Cr_3C_2- or TiC- based cermets. That is why harmetals were tested very thoroughly. Their relative volumetric wear resistance was more than twenty times higher than that of reference steel (Table 3.4 and Figure 3.12).

Table 3.4. Test results of cermets tested with 15 kg of granite gravel

Designation	ΔV, mm^3	ε_V	I_V, mm^3/kg
Steel C 45	26.0 ± 2.6	1.0 ± 0.1	66.5 ± 21.6
WC-5Co	12.6 ± 21.7	2.1 ± 3.6	32.3 ± 56.4
WC-10Co	5.9 ± 9.4	4.4 ± 7.0	15.2 ± 24.5
WC-15Co	1.1 ± 0.1	23.6 ± 1.7	2.7 ± 0.9
WC-15Co'	$0.3' \pm 0.1$	$30.9' \pm 8.3$	$2.1' \pm 0.9$
WC-20Co	2.0 ± 0.2	13.0 ± 0.6	5.2 ± 1.7
WC-26Co	3.5 ± 0.3	7.4 ± 0.4	9.0 ± 2.9
Cr_3C_2-20Ni	2.2 ± 0.2	11.8 ± 0.6	5.6 ± 1.8
Cr_3C_2-50Ni	23.3 ± 2.2	1.1 ± 0.1	59.5 ± 19.2

'Exceptionally tested with 6 kg of abrasive

Relative volumetric wear resistance and wear rate are given in Figure 3.12. The columns in the figure indicate relative volumetric wear resistance and the asterisks indicate volumetric wear rate (the values have to be read from the right vertical axis).
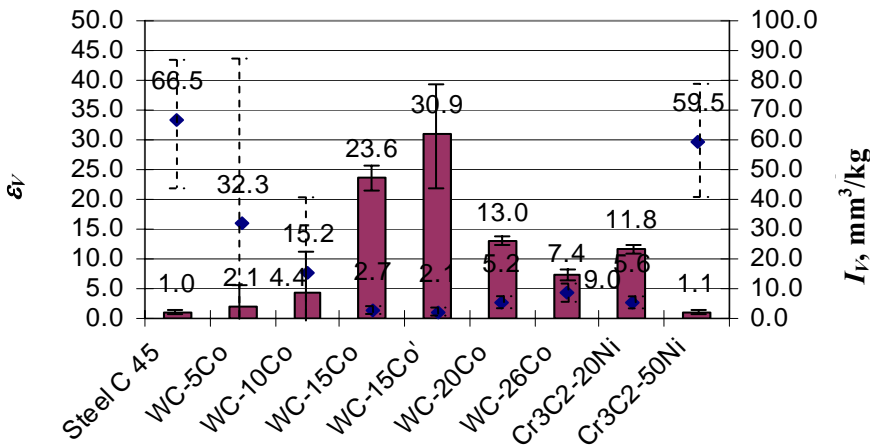
Figure 3.12 Relative volumetric wear resistance ε_V and wear rate I_V of cermets

WC-15Co' was exceptionally tested with 6 kg of the abrasive. This material batch is only included because the same specimens were used in comparative tests carried out in CAK. However, under present comparison the exceptional wear resistance of this test batch should be handled precautionally, because the abrasive amount used was not the same as it was for other materials.

Three specimens from hardmetal consisting of WC-5Co were tested. Two specimens out of 3 had exceptionally low mass loss. The third one had a mass loss exceeding other two specimens over 300 times because serious spalling had occurred. Other 3 specimens from WC-5Co hardmetal produced under different batch were tested. Similar material spalling and large scattering of the results showed clearly that such hardmetal grade is too fragile for such applications.

Three specimens of WC-10Co hardmetal were also tested. Again, 2 specimens out of 3 had a small mass loss while the third one had over 30 times bigger mass loss compared to the others. A big scattering of the results can be seen in relative volumetric wear resistance (ε_V) and wear rate results (I_V) (Figure 3.12). It shows clearly that such hardmetal grade should not be used in constructions working under conditions where any failure must be excluded.

Test results showed that hardmetal consisting of WC-15Co is the best choice for given wear conditions. This material had small mass loss scattering, which leads to small uncertainties of the results (Figure 3.12).

The worn surfaces of the hardmetals and cermets are shown in Figure 3.13
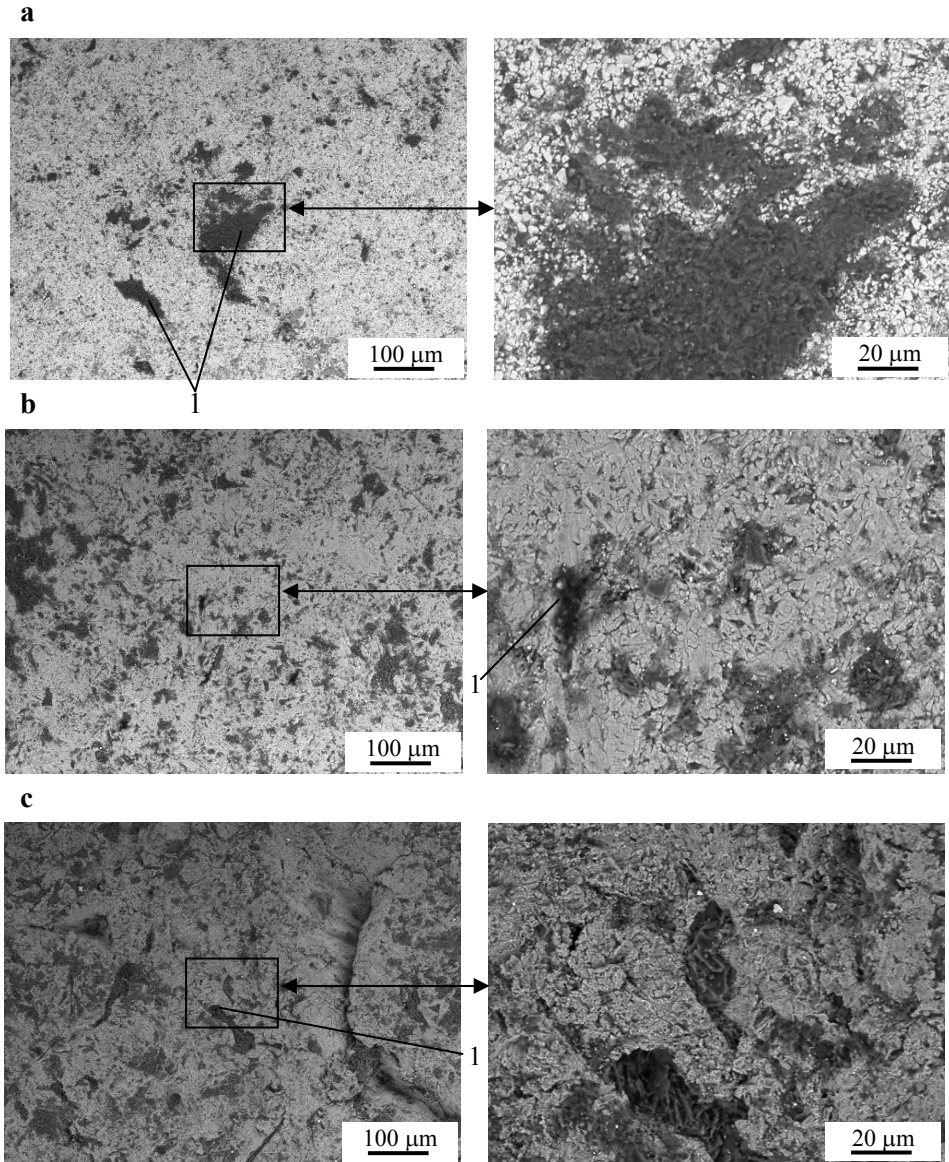
Figure 3.13 Worn surfaces on the WC-15Co hardmetal (a), Cr_3C_2-20Ni cermet (b), and Cr_3C_2-50Ni cermet specimens. 1 –wear scars

No broken carbides can be found in Figure 3.13 (a) because wear tracks are several times bigger. Therefore, material removal takes place by plastic deformation of binder metal, and entire carbide particles will be removed.

From Cr_3C_2 carbide cermets Cr_3C_2-20Ni material (Figure 3.13 (b)) had higher wear resistance. The wear resistance was almost at the same level with WC-20 Co, which has similarly 20% of binder, but the worn surface of Cr_3C_2-20Ni cermet has much deeper scars than WC-15Co hardmetal specimens.

Cr_3C_2-50Ni material had surprisingly low wear resistance. Figure 3.15 (c) shows, that plastic deformation has been very severe. The hardness of this material is not enough for such wear type. Additionally, it must be noted that poor results are probably partly caused from very large initial porosity of the specimens (see Figure 3.2).

Preliminary testing of TiC-NiMo cermets showed very big potential of these materials. The relative volumetric wear resistance of TiC-30Ni:Mo(4:1) was over 18 times better than that of reference steel.

3.3.3 Abrasive impact wear resistance of coatings.

In general, the coatings were worse than reference steel. The amount of the abrasive used for their testing was 3 kg of granite gravel which was found to be their standard testing quantity (see subchapter 2.3). Test results are given in Table 3.5. Relative volumetric wear resistance was calculated according to equation (3.3), and test's reliability characterised by uncertainty was found according to equation (3.11) and equation(1.16).

Table 3.5. Test results of coatings tested with 3 kg of granite gravel

Designation	ΔV, mm^3	ε_V	I_V, mm^3/kg
Reference steel C 45	4.4 ± 0.4	1.0 ± 0.1	56.7 ± 19.1
HVOFS Tafa 1275H	7.8 ± 0.7	0.5 ± 0.1	99.9 ± 32.7
HVOFS Tafa 1275H + F	5.1 ± 0.6	0.8 ± 0.1	65.7 ± 21.9
FS + F Castolin 12495	4.3 ± 0.5	1.1 ± 0.1	54.1 ± 19.2
HVOFS Tafa 1343V	12.3 ± 1.4	0.3 ± 0.1	157.2 ± 52.4
HVOFS Rec (WC-Co)+15Co	3.2 ± 0.9	1.6 ± 0.1	40.4 ± 17.3

Relative volumetric wear resistance and wear rate are given in Figure 3.14. The columns on the figure indicate relative volumetric wear resistance, and the asterisks indicates volumetric wear rate (the values have to be read from the right vertical axis).
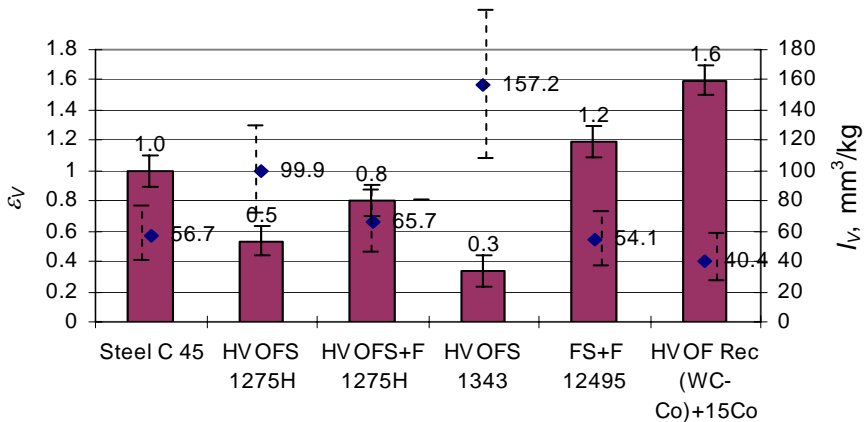
Figure 3.14 Relative volumetric wear resistance ε_V and wear rate I_V of tested coatings

NiCrSiB coating Tafa 1275H had better wear resistance than hardmetal coating Tafa 1343V, especially its fused version. The photos from these worn surfaces are given in Figure 3.15. The coating made from Tafa 1343V powder delaminated from several places and revealed the substrate for direct impact.

Poor performance of 1343V is caused from too thin coating and poor bonding strength. These coatings were thinner than Tafa 1275H. The abrasive particles hit "through"a thin coating and cause its plastic deformations. Such conditions are not favourable for relatively fragile hardmetal coating, and it will be delaminated. From the photos of worn Tafa 1343V coating (Figure 3.15 b) it can be seen that in the regions were coating is not delaminated, wear process is classical – it starts with binder phase extrusion, like in testing solid cermets in abrasive erosion wear conditions [58, 67].

Based on the abovementioned tests, it can be concluded, that thermal spray coatings are not suitable for the applications presented in the impact wear tester, and further testing with quartzite or limestone abrasive was not conducted.
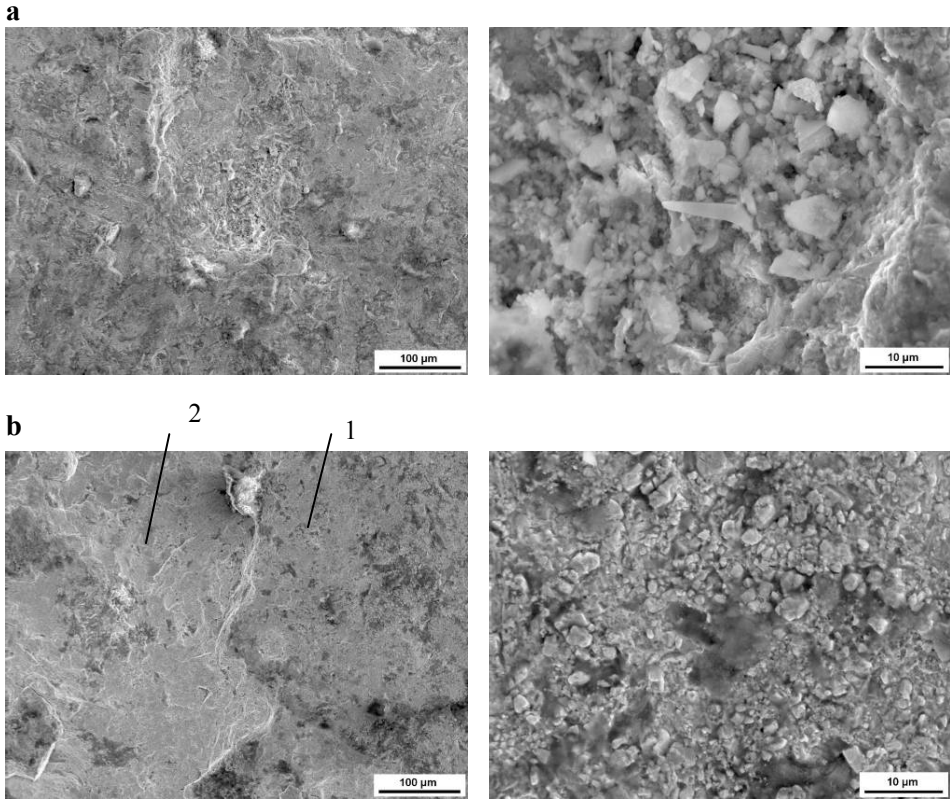
Figure 3.15 Worn surfaces of coatings: HVOFS + F Tafa 1275H (a); HVOFS Tafa 1343V (b). 1 – coating, 2 – revealed steel substrate

3.4 Uncertainty calculation

Uncertainties are calculated for volumetric wear (equation (3.2)), for relative volumetric wear resistance (equation (3.3)), and for wear rate (equation (3.5)). The calculation route is given in a compact form. The calculations were started from the calculation of input quantities uncertainties. Combined experimental variances for three main wear characteristics are found at the end of the calculations.

Height uncertainty of the specimens
Working zone height is considered equal for all specimens, because it is determined by the fixtures and sockets of the rotors of impact wear tester. The heights of the specimens were measured by the vernier calliper (its minimum scale unit was 0.1 mm). The uncertainty of the measurement is determined as combined standard uncertainty (equation (1.6)):

$$u(h) = \sqrt{u_m(h)^2 + u_i(h)^2}$$

(3.6)

$u_m(h)$ – method uncertainty (it takes into account width variations of the specimens)

$u_i(h)$ –instrument's uncertainty

The vernier calliper was not calibrated. It is assumed that its standard uncertainty does not exceed its minimum scale unit, i.e. 0.1 mm.

$$u_i(h) = 0.1 \text{ mm}$$

The variance of working zone height of the specimens was calculated by measuring 32 tested specimens. Instead of measuring one specimen for several times, each specimen was measured only once – 32 different specimens meant 32 measurements.

$$\bar{h} = \frac{1}{n}\sum_{i=1}^{N} h_m \approx 16.3 \text{ mm}$$

Standard deviation for working zone height according to equation (1.8) is:

$$u_m(h) = s(h) \quad = \sqrt{\frac{4.5}{31}} \approx 0.4 \text{ mm}$$

At least 2 specimens, in some cases 3; 4 or even 8 from each material were tested. If 2 specimens were tested from one material, the standard deviation of their arithmetic mean according to equation (1.9) and equation (1.6) is:

$$u(\bar{h}) = \sqrt{\frac{0.38^2}{2} + 0.1^2} \approx 0.3 \text{ mm}$$

For other number of specimens the calculation route is the same and gives:

$$u_3(\bar{h}) \approx 0.2 \text{ mm}$$

$$u_4(\bar{h}) \approx 0.2 \text{ mm}$$

$$u_8(\bar{h}) \approx 0.2 \text{ mm}$$

Width uncertainty

The width of each tested specimen was also measured only once. As the number of specimens in a batch from each material was smaller than 10 (except reference specimens), experimental standard deviation could not be used. The uncertainty is again determined as the combined standard uncertainty from equation (1.6) [3]:

$$u(b) = \sqrt{u_m(b)^2 + u_i(b)^2 + u_\Delta^2(b)}, \qquad (3.7)$$

where

$u_m(b)$ – method uncertainty

$u_i(b)$ – measuring instrument uncertainty

$u_\Delta(b)$ – uncertainty caused by the width variations of the specimens

Method uncertainty $u_m(b)$ and the width variations uncertainty of the specimens $u_\Delta(b)$ are calculated according to equation (1.12). From reading assessment of vernier calliper,

$$u_m(b) = \frac{0.1}{2\sqrt{3}} \approx 0.03 \text{ mm},$$

$$u_i(b) = u_i(h) = 0.1 \text{ mm}.$$

$u_m(b)$ is more than 3 times smaller than $u_i(b)$ and should in this case be neglected according to negligibility criterion [29].

Width uncertainty of the reference specimens
The width of 21 reference specimens was measured in repeatability conditions [29]. Reference specimens used in all tests were cut out at the same time, on the same machine and by the same operator, so experimental standard deviation can be used and $u(b_r)$ calculated when using equation (1.6). Experimental standard deviation $s(b_r)$ counts additional uncertainty caused by the width variation of the specimens

$$u(b_r) = \sqrt{s(b_r)^2 + u_i(b)^2} \ . \tag{3.8}$$

The average width of 21 reference specimens was

$$\overline{b} = \frac{1}{n} \sum_{i=1}^{N} b_i \approx 14.9 \text{ mm}.$$

As two reference specimens were tested from each material, the standard uncertainty of their arithmetic mean calculated by equation (1.9) and equation (3.8) is:

$$u(\overline{b}_r) = \sqrt{\frac{0.067}{2}^2 + 0.1^2} \approx 0.1 \text{ mm}$$

The standard width necessary for the volumetric wear resistance calculation (equation (3.2)) is taken to be equal with 15.0 mm. Its accuracy is 0.1 mm, and its uncertainty is calculated from equation (1.12)

$$u(b_{st}) = \frac{0.1}{2 \cdot \sqrt{3}} \approx 0.03 \text{ mm}$$

Weighing uncertainty
Mettler Toledo AB 204 scales was used for weighing. The scales have a digital 0.1 mg resolution display.

It is stated in the calibration certificate of the scales is that no correction K is needed when weighing 20.0006 g workload, and that the expanded uncertainty is $U(K) = 0.2$ mg by 95% of coverage probability. As the masses of our specimens are roughly the same, we can take $K = 0$ and

$$u(m) = \frac{0.2}{2} = 0.1 \text{ mg}.$$

The weighing is done twice, firstly before the test and secondly after the test. According to equation (1.15), a full correlation between two weightings is assumed and the uncertainty is

$$\text{u}(\Delta \text{m}) = \sqrt{[u(m_b) + u(m_a)]^2 + u_\Delta(m)^2} \ , \tag{3.9}$$

where, $u(m) = u(m_b) = u(m_a)$
m_b – mass of the specimen before the test
m_a – mass of the specimen after the test

$u_\Delta(m)$ - uncertainty caused by different mass losses of the specimens.

$u_\Delta(m)$ is the biggest uncertainty component in combined mass loss uncertainty equation and is calculated according to equation (1.12).

Density uncertainty

Density values were partly taken from the literature and partly determined experimentally. The uncertainty is calculated from rectangular distribution (equation (1.12)) [33]

$$u(\rho) = \frac{0.01}{\sqrt{3}} \approx 0.006.$$

Abrasive weighing uncertainty

The Abrasive (Q) was weighed by analogue scales and its minimum scale interval was 50 g. Considering poor condition of scales method uncertainty is taken to be 150 g. The standard uncertainties are calculated from uniform distribution (equation (1.12)).

$$u(Q) = \sqrt{u_m(Q)^2 + u_i(Q)^2} = \sqrt{\frac{50^2}{12} + \frac{150^2}{12}} \approx 88 \text{ g}$$

$u_m(Q)$ – method uncertainty

$u_i(Q)$ – scales uncertainty

Uncertainty of abrasive fraction hitting a specimen

The abrasive fraction for a specimen (χ) is deduced from Figure 2.5. Its expanded uncertainty $U(\chi)$ is taken to be equal with expanded uncertainty of $U(\gamma)$ calculated in subsection 2.2.4.

$$U(\chi) = U(\gamma) = 5°, \text{ by } k = 2$$

Combined experimental variance of relative volumetric wear resistance ε_V

Calculation of ε_V was made according to equation (3.3). Quantities Δm_r and Δm are in correlative relation because these were determined by the same scales. If the uncertainties of Δm_r and Δm are equal [33] then

$$u(\Delta m_r, \Delta m) \cong u^2(\Delta m_r) \cong u^2(\Delta m), \tag{3.10}$$

and from equation (1.13)

$$r(\Delta m_r, \Delta m) \cong 1$$

Quantities b_r, b and h_r, h in equation (3.3) correlate with each other because they are measured by the same vernier calliper (but their measuring method was different). The width (b and b_r) was measured by usual procedure – the specimens were placed between the "fork" of the vernier calliper. Working zone height (h and h_r) measurement was complicated because only one end of each specimen was possible to put against vernier calliper's upper jaw of the "fork". The lower jaw was positioned by eye. It was concluded that in all covariances only instrument's uncertainty is common:

$r(h, h_r)$, $r(h, b_r)$ and $r(h_r, b_r)$ do not change if the no of specimens and reference specimens is constant.

Example. If 2 reference specimens and 4 specimens from the tested material were used, then:

$$r(h, h_r) = \frac{0.1 \cdot 0.1}{0.21 \cdot 0.29} \approx 0.2$$

$$r(h, b_r) = \frac{0.1 \cdot 0.1}{0.21 \cdot 0.11} \approx 0.4$$

$$r(h_r, b_r) = \frac{0.1 \cdot 0.1}{0.29 \cdot 0.11} \approx 0.3$$

$r(h, b)$; $r(h_r, b)$ and $r(b, b_r)$ values change from material to material because $u(b)$ calculated by equation (3.7) varies.

In equation (3.3) there are 8 quantities, 6 from these are in correlation, 2 are not. The combined experimental variance of ε_V is:

$$u^2(\varepsilon) = c_\rho^2 u^2(\rho) + c_{\rho_r}^2 u^2(\rho_r) + c_h^2 u^2(h) + c_{h_r}^2 u^2(h_r) + c_b^2 u^2(b) + c_{b_r}^2 u^2(b_r) +$$
$$+ \left[c_{\Delta m_r}^2 u^2(\Delta m_r) + c_{\Delta m}^2 u^2(\Delta m) \right]^2 + 2 c_h c_{h_r} u(h) u(h_r) r(h, h_r) + 2 c_h c_b u(h) u(b) r(h, b) +$$
$$+ 2 c_h c_{b_r} u(h) u(b_r) r(h, b_r) + 2 c_{h_r} c_b u(h_r) \cdot u(b) r(h_r, b) + 2 c_{h_r} c_{b_r} u(h_r) u(b_r) r(h_r, b_r) +$$
$$+ 2 c_b c_{b_r} u(b) u(b_r) r(b, b_r) \qquad (3.11)$$

Sensitivity coefficients from equation (3.3) are found according to equation (1.7):

$$c_\rho = \frac{\partial \varepsilon}{\partial \rho} = \frac{bh\Delta m_r}{b_r h_r \Delta m \rho_r} \qquad\qquad c_{\rho_r} = \frac{\partial \varepsilon}{\partial \rho_r} = -\frac{bh\Delta m_r \rho}{b_r h_r \Delta m \rho_r^2}$$

$$c_{\Delta m_r} = \frac{\partial \varepsilon}{\partial \Delta m_r} = \frac{bh\rho}{b_r h_r \Delta m \rho_r}$$

$$c_{\Delta m} = \frac{\partial \varepsilon}{\partial \Delta m} = -\frac{bh\Delta m_r \rho}{b_r h_r \Delta m^2 \rho_r}$$

$$c_h = \frac{\partial \varepsilon}{\partial h} = \frac{b\Delta m_r \rho}{b_r h_r \Delta m \rho_r} \qquad\qquad c_{h_r} = \frac{\partial \varepsilon}{\partial h_r} = -\frac{bh\Delta m_r \rho}{b_r h_r^2 \Delta m \rho_r}$$

$$c_b = \frac{\partial \varepsilon}{\partial b} = \frac{h\Delta m_r \rho}{b_r h_r \Delta m \rho_r} \qquad\qquad c_{b_r} = \frac{\partial \varepsilon}{\partial b_r} = -\frac{bh\Delta m_r \rho}{b_r^2 h_r \Delta m \rho_r}$$

In later experiments the width of specimens was measured by another vernier calliper, and equation (3.11) was simplified:

$$u^2(\varepsilon) = c_\rho^2 u^2(\rho) + c_{\rho_r}^2 u^2(\rho_r) + c_h^2 u^2(h) + c_{h_r}^2 u^2(h_r) + c_b^2 u^2(b) + c_{b_r}^2 u^2(b_r) +$$
$$\left[c_{\Delta m_r}^2 u(\Delta m_r) - c_{\Delta m}^2 u(\Delta m) \right]^2 . \qquad (3.12)$$

Combined experimental variance of volumetric wear ΔV
Volumetric wear was calculated according to equation (3.2). The combined experimental variance of ΔV is:

$$u^2(\Delta V) = c_b^2 \cdot u^2(b) + c_h^2 \cdot u^2(h) + c_{\Delta m}^2 \cdot u^2(\Delta m) + c_\rho^2 \cdot u^2(\rho) + c_{b_{st}}^2 \cdot u^2(b_{st}) +$$
$$+ c_{h_{st}}^2 u^2(h_{st}) \tag{3.13}$$

Sensitivity coefficients from equation (3.2) are found according to equation (1.7):

$$c_b = \frac{\partial \Delta V}{\partial b} = -\frac{b_{st} \cdot h_{st} \cdot \Delta m}{b^2 h \rho} \qquad\qquad c_h = \frac{\partial \Delta V}{\partial h} = -\frac{b_{st} \cdot h_{st} \cdot \Delta m}{b h^2 \rho}$$

$$c_{\Delta m} = \frac{\partial \Delta V}{\partial \Delta m} = \frac{b_{st} \cdot h_{st}}{b h \rho} \qquad\qquad c_\rho = \frac{\partial \Delta V}{\partial b} = -\frac{b_{st} \cdot h_{st} \cdot \Delta m}{b h \rho^2}$$

$$c_{b_{st}} = \frac{\partial \Delta V}{\partial b_{st}} = \frac{h_{st} \cdot \Delta m}{b h \rho} \qquad\qquad c_{h_{st}} = \frac{\partial \Delta V}{\partial h_{st}} = \frac{b_{st} \cdot \Delta m}{b h \rho}$$

Combined experimental variance of volumetric wear rate I_V
Volumetric wear rate was calculated according to the equation (3.5). The combined experimental variance of I_V is:

$$u^2(I_V) = c_b^2 \cdot u^2(b) + c_{b_{st}}^2 \cdot u^2(b_{st}) + c_h^2 \cdot u^2(h) + c_{h_{st}}^2 \cdot u^2(h_{st}) + c_{\Delta m}^2 \cdot u^2(\Delta m) + ,$$
$$+ c_Q^2 \cdot u^2(Q) + c_\rho^2 \cdot u^2(\rho) + c_\chi^2 \cdot u^2(\chi) \tag{3.14}$$

Sensitivity coefficients from equation (3.5) are found according to equation (1.7):

$$c_b = \frac{\partial I_v}{\partial b} = -\frac{\Delta m \cdot b_{st} \cdot h_{st}}{b^2 \cdot h \cdot Q \cdot \alpha \cdot \rho} \qquad\qquad c_{b_{st}} = \frac{\partial I_v}{\partial b_{st}} = \frac{\Delta m \cdot h_{st}}{b \cdot h \cdot Q \cdot \alpha \cdot \rho}$$

$$c_h = \frac{\partial I_v}{\partial h} = -\frac{\Delta m \cdot b_{st} \cdot h_{st}}{b \cdot h^2 \cdot Q \cdot \alpha \cdot \rho} \qquad\qquad c_{h_{st}} = \frac{\partial I_v}{\partial h_{st}} = \frac{\Delta m \cdot b_{st}}{b \cdot h \cdot Q \cdot \alpha \cdot \rho}$$

$$c_{\Delta m} = \frac{\partial I_v}{\partial \Delta m} = \frac{b_{st} \cdot h_{st}}{b \cdot h \cdot Q \cdot \alpha \cdot \rho} \qquad\qquad c_Q = \frac{\partial I_v}{\partial Q} = -\frac{\Delta m \cdot b_{st} \cdot h_{st}}{b \cdot h \cdot Q^2 \cdot \alpha \cdot \rho}$$

$$c_\rho = \frac{\partial I_v}{\partial \rho} = -\frac{\Delta m \cdot b_{st} \cdot h_{st}}{b \cdot h \cdot Q \cdot \alpha \cdot \rho^2} \qquad\qquad c_\chi = \frac{\partial I_v}{\partial \chi} = -\frac{\Delta m \cdot b_{st} \cdot h_{st}}{b \cdot h \cdot Q \cdot \chi^2 \cdot \rho}$$

3.5 Variance analysis of reference steel

The impact wear tester was developed during this work. As this is a new testing method, the reliability of its results had to be proved. During the first test period, reference specimens were used obligatorily. It was necessary to determine whether the tests made in a long time period are comparable and how often are the outliers, if any, present. The conditions in the situation where time has changed considerably between the tests are categorised as reproducibility conditions. A statistical procedure known as one-factor analysis of the variance basing of F-test was used for evaluating the possible influence of repeated

measurement for mass loss variance of unit surface area. The aim is to find whether the results of the same material, which are tested in different batches in a long time interval, are comparable.

Test series of Hardox 400

In a period of two and a half years, 2 specimens of Hardox 400 were presented in 9 tests. The abrasive amount was 15 kg. Thus, the number of series is $J = 9$ and the number of repetitions in each series is $K = 2$. The results of different series J are shown in a Table 3.6. The outline of the analysis of variance is as follows.

The arithmetic mean of the *j*-th series of measurement is calculated from equation (1.17), for example, on 18 November 2005, two specimens of Hardox 400 were tested,

$$(\overline{\Delta m_{unit}})_j = \frac{0.892 + 0.760}{2} = 0.826 \text{ mg/mm}^2.$$

In order to calculate the mass loss to surface area uncertainty, sensitivity coefficients as partial derivatives from equation (3.1) have to be found according to equation (1.7). Sensitivity coefficients are

$$c_{\Delta m} = \frac{\partial(\Delta m_{unit})}{\partial \Delta m} = \frac{1}{b \cdot h},$$

$$c_b = \frac{\partial(\Delta m_{unit})}{\partial \Delta b} = -\frac{\Delta m}{b^2 h},$$

$$c_h = \frac{\partial(\Delta m_{unit})}{\partial \Delta h} = -\frac{\Delta m}{bh^2}.$$

Within the series J uncertainty of mass loss to surface area is calculated according to the equation (1.6) as a combined standard uncertainty.

$$u(\overline{\Delta m_{unit}})_j = \sqrt{c_{\Delta m}^2 \cdot u^2(\Delta m) + c_b^2 \cdot u^2(b) + c_h^2 \cdot u^2(h)} \quad (3.15)$$

The average width of all the 18 Hardox 400 specimens used within the series and between the series is

$$\overline{b} = \frac{1}{n} \sum_{i=1}^{N} b_i = 14.9$$

$u(\Delta m)$, $u(b)$ and $u(h)$ calculation is done according to the subchapter 3.4.

The experimental within test series variances were calculated From the standard uncertainties of each test series

$$s^2(\Delta m_{unit})_{jk} = K \cdot u^2(\overline{\Delta m_{unit}})_j.$$

Calculation results are given in Table 3.6.

Table 3.6. Arithmetic means of 9 series measurements of material Hardox 400 and corresponding standard uncertainties and deviations

Day j	18.11.05	18.11.05	21.11.05	14.08.06	25.10.06	25.10.06	7.11.06	17.05.07	24.05.07
$(\overline{\Delta m_{unit}})_j$, mg/mm^2	0.826	0.876	0.861	0.845	0.823	0.852	0.915	0.857	0.846
$u(\overline{\Delta m_{unit}})_j$, mg/mm^2	0.041	0.017	0.017	0.020	0.017	0.029	0.021	0.018	0.017
$s^2(\Delta m_{unit})_{jk}$, mg^2/mm^4	$3.4 \cdot 10^{-3}$	$6.0 \cdot 10^{-4}$	$5.6 \cdot 10^{-4}$	$7.9 \cdot 10^{-3}$	$5.9 \cdot 10^{-4}$	$1.7 \cdot 10^{-3}$	$8.7 \cdot 10^{-4}$	$6.6 \cdot 10^{-4}$	$5.9 \cdot 10^{-4}$

$$\sum (\overline{\Delta m_{unit}})_j = 7.701 \text{ mg/mm}^2,$$
$$\sum s^2 (\Delta m_{unit})_{jk} = 9.79 \cdot 10^{-3} \text{ mg}^2/\text{mm}^4.$$

In our case, the number of observations K is very small. In these situations Cochran's C test may be used which has been designed for testing the homogeneity of a set of experimental variances (see subchapter 0).

A visual inspection of the data shows that the experimental variance of the test 18.11.05 is larger than others

Cohran's C test value calculated from equation (1.26) is

$$C = \frac{3.41 \cdot 10^{-3}}{9.79 \cdot 10^{-3}} = 0.348.$$

Cohran's critical values $C_{Cr\,p}\,(K, J)$ for significance levels $p = 5\%$ and $p = 1\%$ are

$$C_{Cr\,0.05}\,(2, 9) = 0.638,$$
$$C_{Cr\,0.01}\,(2, 9) = 0.754.$$

The ratio C is smaller than $C_{Cr\,0.05}\,(K, J)$, therefore the result obtained by all tests should be considered homogeneous (see subchapter 0). The best estimate for the mass loss per surface area is obtained as the arithmetic mean by using equation (1.17)

$$(\overline{\overline{\Delta m_{unit}}}) = \frac{7.701}{9} = 0.856 \text{ mg/mm}^2.$$

In order to evaluate the difference between the result within a series and between the series, as well as their significance, the experimental variances s_a^2 and s_b^2 are calculated from equation (1.20) and equation (1.21), yielding

$$s_a^2 = \frac{2}{9-1} \sum_{j=1}^{J} (\overline{\Delta m_{unit}})_j - 0.856)^2 = 1.52 \cdot 10^{-3} \text{ mg}^2/\text{mm}^4$$

$$s_b^2 = \frac{9.79 \cdot 10^{-3}}{9} = 1.09 \cdot 10^{-3} \text{ mg}^2/\text{mm}^4$$

The ratios of the variances are found by equation (1.22)

$$F(v_a, v_b) = 1.40$$

Corresponding numbers of degrees of freedom are $v_a = J-1 = 8$ and $v_b = J(K-1) = 9$. From quantiles table in [29] can be found, that $F_{0.95}(8, 9) = 3.23$ and $F_{0.99}(8, 9) = 5.47$. As the calculated ratio is much smaller than the quantities of the F distribution at both the 5% and the 1% significance level, we can conclude that there is no significant effect between the tests series, that is all observations $(\Delta m_{unit})_{jk}$ are samples taken from the same distribution. That means that the variance between the series and within the series is the same and the experimental average variance calculated from equation (1.23) is

$$u(\Delta \overline{m}_{unit}) = \sqrt{\frac{8 \cdot 1.52 \cdot 10^{-3} + 9 \cdot 1.09 \cdot 10^{-3}}{18 \cdot 17}} = 8.47 \cdot 10^{-3} \ \mathrm{mg/mm^2}$$

By normal distribution and coverage level of 95% ($k = 2$) an expanded uncertainty is

$$U(\Delta \overline{m}_{unit}) = k \cdot u(\Delta \overline{m}_{unit}) = 2 \cdot 8.47 \cdot 10^{-3} = 1.69 \cdot 10^{-2} \ \mathrm{mg/mm^2}$$

Thus, based on the results obtained at all 9 test series, unit mass loss of Hardox 400 surface area with a coverage probability of 95% ($k = 2$) is

$$\Delta m_{unit} = (0.86 \pm 0.02) \ \mathrm{mg/mm^2}.$$

F-test proved that all experiments are made in equal conditions and have been carried out according to the same, well-defined measurement method and are all under statistical control. They are not time-dependent, that is, all the test results of the impact wear tests can be used for pooling (equation (1.10)).

Test series of reference steel C 45
In the last section it was showed, that if 15 kg of the abrasive is used then the test results do not depend on a specific test. What happens when the amount of the abrasive is smaller? A reference material steel C 45 was tested during a one year period by 3 kg of the abrasive in 4 tests. Again two reference specimens were presented in each test. Thus, the number of series is $J = 4$ and the number of repetitions in each series is $K = 2$. The results of different series J are shown in Table 3.7. The outline of the analysis is the same as it was for Hardox 400. The sections which are different from Hardox 400 F-test calculation are written out the here.

Table 3.7. Arithmetic means of 4 series measurements of reference material steel C 45 and corresponding standard uncertainties and deviations

Day j	26.04.05	20.05.05	15.06.05	19.05.06
$(\overline{\Delta m}_{unit})_j$, mg/mm^2	0.134	0.162	0.132	0.142
$u(\overline{\Delta m}_{unit})_j$, mg/mm^2	0.007	0.016	0.007	0.009
$s^2(\Delta m_{unit})_{jk}$, mg^2/mm^4	$9.7 \cdot 10^{-5}$	$5.0 \cdot 10^{-4}$	$9.6 \cdot 10^{-5}$	$1.8 \cdot 10^{-4}$

$$\sum (\overline{\Delta m}_{unit})_j = 0.570 \ \mathrm{mg/mm^2},$$

$$\sum s^2 (\Delta m_{unit})_{jk} = 8.69 \cdot 10^{-4} \, \text{mg}^2/\text{mm}^4.$$

A visual inspection of the data shows that the experimental variance of the test 20.05.05 is larger than others.

Cohran's C test value calculated from equation (1.26) is

$$C = \frac{4.97 \cdot 10^{-4}}{8.69 \cdot 10^{-4}} = 0.572.$$

Cohran's critical values $C_{Cr\,p}\,(K, J)$ for significance levels $p = 5\%$ and $p = 1\%$ are

$$C_{Cr\,0.05}\,(2, 4) = 0.906$$
$$C_{Cr\,0.01}\,(2, 4) = 0.968$$

Ratio C is smaller than $C_{Cr\,0.05}\,(K, J)$, therefore the result obtained by all tests should be considered as homogeneous (see subchapter 0). The best estimate of the mass loss per surface area is obtained as the arithmetic mean by using equation (1.17).

$$(\overline{\Delta m}_{unit}) = \frac{0.570}{4} = 0.143 \, \text{mg/mm}^2$$

To evaluate the difference between the results within a series and between the series, as well as their significance, the experimental variances s_a^2 and s_b^2 are calculated from equation (1.20) and equation (1.21), yielding

$$s_a^2 = \frac{2}{4-1} \sum_{j=1}^{J} ((\overline{\Delta m}_{unit})_j - 0.143)^2 = 3.74 \cdot 10^{-4} \, \text{mg}^2/\text{mm}^4$$

$$s_b^2 = \frac{8.69 \cdot 10^{-4}}{4} = 2.17 \cdot 10^{-4} \, \text{mg}^2/\text{mm}^4$$

The ratios of the variances are found by equation (1.22)

$$F(v_a, v_b) = 1.72$$

The corresponding numbers of degrees of freedom are $v_a = J{-}1 = 3$ and $v_b = J(K{-}1) = 4$. From the table of quantiles in [29] it can be found that $F_{0.95}(3, 4) = 6.59$ and $F_{0.99}(3, 4) = 16.7$. As the calculated ratio is much smaller than the quantities of the F distribution at both the 5% and the 1% significance level, we can conclude that there is no significant effect between the tests series, that is, all observations $(\Delta m_{unit})_{jk}$ are samples taken from the same distribution. It means that the variances between the series and within the series are the same and the experimental average variance calculated from equation (1.23) is

$$u(\Delta \overline{m}_{unit}) = \sqrt{\frac{3 \cdot 3.74 \cdot 10^{-4} + 4 \cdot 2.17 \cdot 10^{-4}}{8 \cdot 7}} = 5.96 \cdot 10^{-3} \, \text{mg/mm}^2$$

In the case of normal distribution, the coverage level is 95% ($k = 2$), an expanded uncertainty is

$$U(\Delta \overline{m}_{unit}) = k \cdot u(\Delta \overline{m}_{unit}) = 2 \cdot 5.96 \cdot 10^{-3} = 1.19 \cdot 10^{-2} \, \text{mg/mm}^2$$

Thus, based on the results obtained in all 9 test series, the unit mass loss of Hardox 400 surface area with a coverage probability of 95% ($k = 2$) is

$$\Delta m_{unit} = (0.57 \pm 0.01) \text{ mg/mm}^2.$$

F test proved again that all experiments are made in equal conditions. They are not time-dependent, that is all these impact wear tests can be used for pooling (equation(1.10)).

3.6   Comparison of abrasive impact wear and erosive wear

Comparative abrasive erosive wear (AEW) testings were carried out with CAK [9], which is a well-known erosive wear tester for testing in finer abrasives. The abrasives used at AEW and AIW were the same in order to compare the results. Granite gravel (GG) is a standard abrasive for testing in the impact wear tester, while quartzite gravel (QG, see chapter 4) is the hardest abrasive used. The fractions of (0.13−0.63) mm granite sand (GS) and quartzite sand (QS) were sieved out for AEW tests (Figure 3.16).

a   **b**
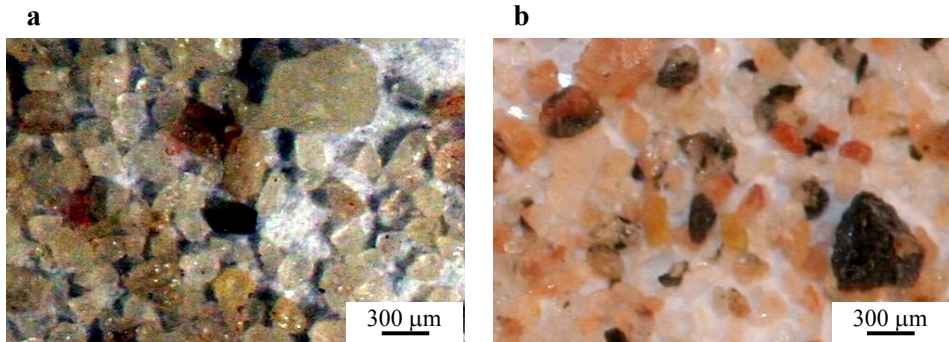
Figure 3.16 (0.13−0.63) mm abrasives used for AEW tests: quartzite sand (a), granite sand (b)

Frequency and cumulative frequency polygon were made from the sieve analysis of the abrasives. In Figure 3.17 these curves are drawn along with sieve analysis curves of (4.0−5.6) mm feed fraction of impact wear tests. Asterisks on the cumulative frequency plot designate sieve opening sizes, and on the frequency plots, moving averages of adjacent sieve opening sizes.

The angularity of sand particles was evaluated by the quadratic fit that is by the "spike parameter". "Spike parameter − quadratic fit" (*SPQ*) is based on the quadratic polynomial approximation; those spikes are considered that are outside the circle with equal particle area, centred over the particle centroid.

The angularity parameter *SPQ* was calculated as an arithmetical mean of spike values:

$$SPQ = \text{SV average}, \tag{3.16}$$

where SV = cos θ / 2 and θ is spike's apex [68].
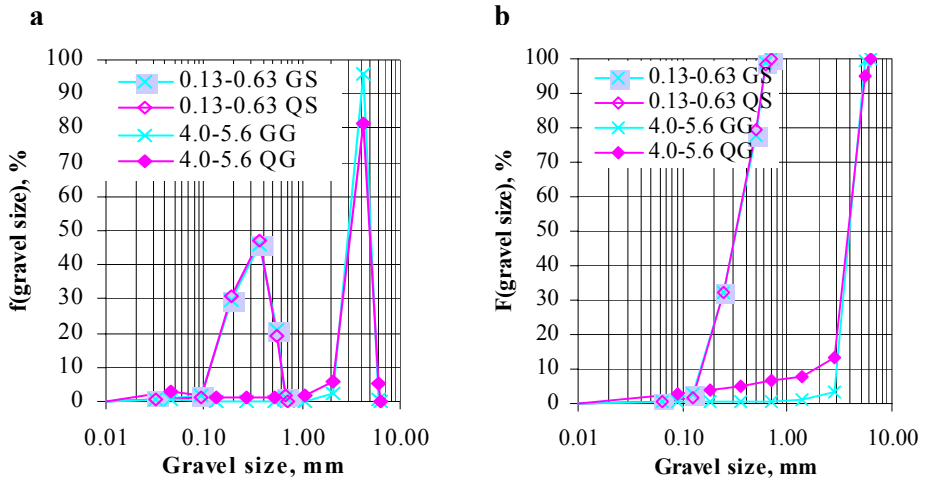
Figure 3.17 Frequency polygon (a) and cumulative frequency polygon (b) of abrasives used for AIW and AEW tests

As closer is *SPQ* value for 1, as bigger is the angularity. The *SPQ* values of sieved out (0.13−0.63) mm fractions where 0.686 for granite sand and 0.680 for quartzite sand (corresponding values for granite and quartzite gravel are 0.611 and 0.543 given in the Table 4.1).

The selected materials from steels, hardmetals and cermets were chosen for testing. For eliminating possible effects of different specimens, the same specimens were tested in AEW conditions as were tested in the impact wear tester. At AEW tests the velocity of particles was 80 m/s, and the impact angle was 90 degrees. The test results are drawn together in Table 3.8

Table 3.8. AEW test results with granite and quartzite sand

Designation	Granite sand			Quartzite sand		
	ΔV	ε_V	I_V, mm^3/kg	ΔV	ε_V	I_V, mm^3/kg
Reference steel C 45	3.1 ± 0.5	1.0 ± 0.2	22.0 ± 6.1	3.4 ± 0.2	1.0 ± 0.1	24.0 ± 5.8
Cr_3C_2-20Ni	1.6 ± 0.1	2.0 ± 0.3	11.1 ± 2.7	2.6 ± 0.1	1.3 ± 0.1	18.2 ± 4.4
Vanadis 6, 834 HV30	3.6 ± 0.4	0.9 ± 0.2	25.7 ± 6.6	4.1 ± 0.3	0.8 ± 0.1	28.9 ± 7.1
Weartec, 784 HV30	3.3 ± 0.1	0.9 ± 0.1	23.6 ± 5.6	4.5 ± 0.4	0.8 ± 0.1	31.5 ± 7.9
WC-15Co	0.5 ± 0.3	5.8 ± 3.0	3.9 ± 2.1	0.9 ± 0.3	3.9 ± 1.5	6.2 ± 2.8
Hardox 400	3.1 ± 0.1	1.0 ± 0.2	21.6 ± 5.1	3.3 ± 0.1	1.0 ± 0.1	23.4 ± 5.6

The graphical presentation of AEW test results tested with granite sand is shown in Figure 3.18 and with quartzite sand test in Figure 3.19. The columns in the figure indicate a relative volumetric wear resistance, and the asterisks

indicate a volumetric wear rate (the values have to be read from the right vertical axis).
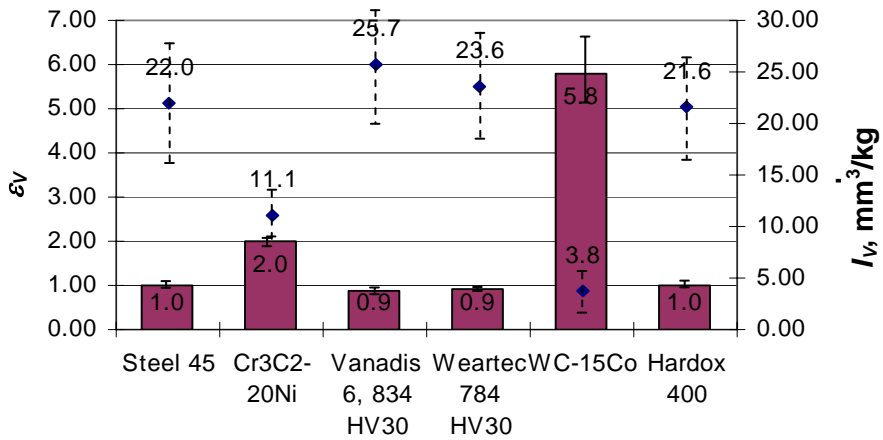
Figure 3.18 Relative volumetric wear resistance ε_V and wear rate I_V of materials tested at AEW conditions by using granite sand as abrasive
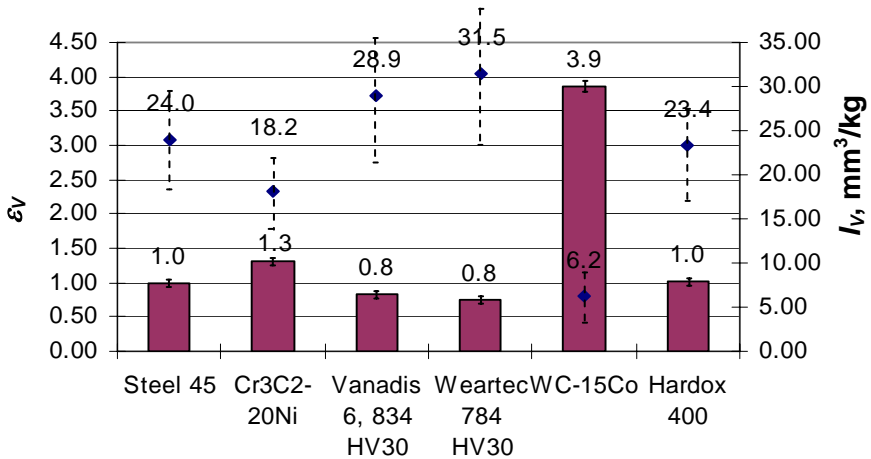
Figure 3.19 Relative volumetric wear resistance ε_V and wear rate I_V of materials tested at AEW conditions by using quartzite sand abrasive

Quartzite sand caused expectedly bigger material loss than granite sand (compare Figure 3.18 and Figure 3.19). The proportions between the relative volumetric wear resistance of tested materials stayed practically the same, except for WC-15Co, whose superior value in granite sand decreased by one third times in quartzite sand.

When comparing AIW results fulfilled with granite gravel (Figure 3.12) and relevant AEW results (Figure 3.18) of cermets, it can be seen, that although

WC-15Co hardmetal was the most wear resistant in both cases, its advantage decreased in the AEW test. It is explainable by the smaller fractional size of the abrasive, and thereby it has better access to softer binder material. The same trend is noticeable for Cr_3C_2-20Ni which contains similarly softer binder and harder carbide phase. The wear mechanism itself is classical; at first the softer binder metal is removed, and then carbide particles start to fall out (Figure 3.20) [58, 67]. The similar erosion wear mechanism of ceramics was found by Marcus in [50].

a

b
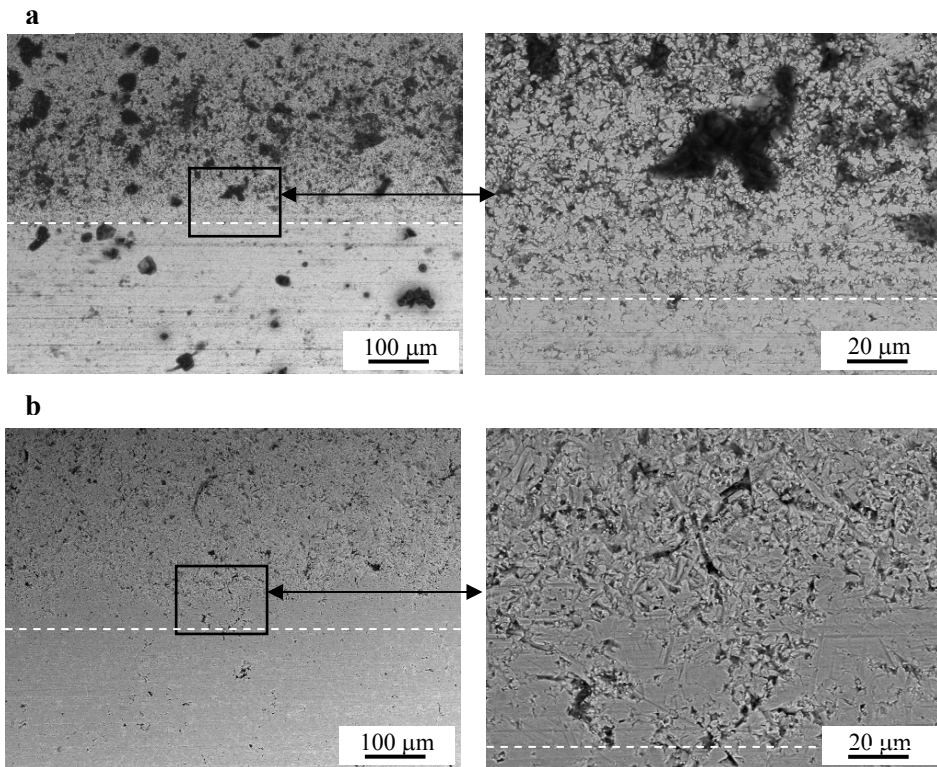
Figure 3.20 Worn sufraces of eroded WC-15Co (a) and Cr_3C_2-20Ni (b) specimens at different mangifications (the area under dashed line has not been subjected to erosion

When comparing AIW test results fulfilled with quartzite gravel (Figure 4.7) and relevant AEW results (Figure 3.19) of cermets, the same wear resistance drop can be noticed AEW tests, as by comparing impact wear and AEW results made by granite gravel. Consequently, the abovementioned classical wear mechanism takes place regardless of the hardness and abrasive type.

When comparing AIW and AEW test results of steels, a similar behaviour as for cermets has occurred. In the AIW test, powder steels Vanadis 6 and Weartec had about 2 times higher wear resistance than reference steel C 45 (compare Figure 3.5 and Figure 4.7), while in AEW tests they were outperformed by reference steel C 45 (Figure 3.19). Figure 3.21 presents SEM

photos of the worn surface area of reference steel C 45 in AEW tests and spray formed powder steel.
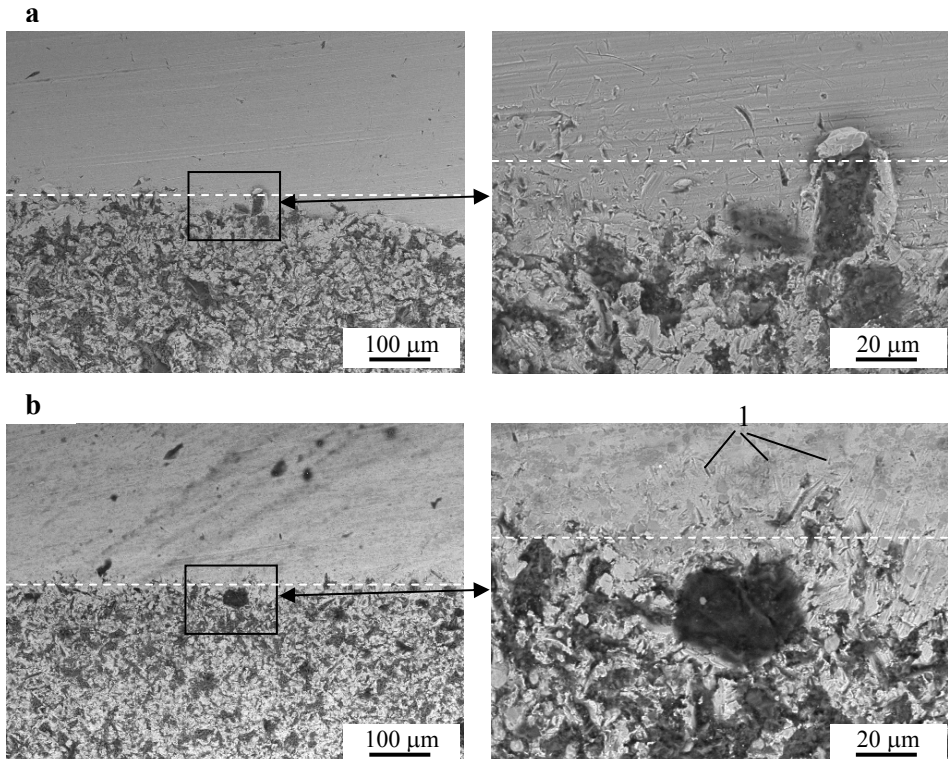
Figure 3.21 SEM pictures of top surface of eroded steel C 45 (a) and Weartec (784 HV30) (b) specimens at different mangifications (the area above dashed line was not subjected to erosion).1- possible carbides

An explanation for the drop of wear resistance in powder steels Vanadis 6 and Weartec is given below:

1. Plastic deformation of the surface of the specimens has occurred regardless of the hardness of tested steels. On the surface of Weartec (784 HV30) there are clearly visible wear craters, like in the case of soft (see Table 3.1) reference steel C 45. A bigger magnification of the worn surface of Weartec does not show plastic nature of the deformation like in the case of reference steel C 45. Reference steel C 45 has better ductility, thereby, its resistance to numerous local plastic indentations of the surface is better than that of high hardness steel Weartec or Vanadis 6 [61, 62].

2. High wear resistance of these steels is caused by the composite structure, namely by carbides (Figure 3.1 b). Although the distribution density of these carbides is much smaller than carbides are in cermets (compare Figure 3.1 b and Figure 3.2), the wear resistance drop in AEW tests is explainable similarly to cermets wear mechanism. The

wear crater of finer abrasive particles covers a smaller number of wear resistant carbides than in the case of impact wear, and consequently the wear rate will increase.

Erosive wear tests with silica and SiC abrasive carried out in CAK under the impact angles of 75° showed similarly, that out of cermets, the most wear resistant material is hardmetal [69].

4 STUDY OF GRINDABILITY AND ABRASIVITY

Grindability and abrasivity studies were done by five different minerals. The abrasives ranged from soft limestone to hard quartzite gravel. Their composition and designation is given in Table 4.1.

Table 4.1. Mineral abrasive materials used in grindability studies

Type of the abrasive	Designation	Composition, vol %/ HV	Los Angeles coefficient	Weighted hardness HV'[**]	Angularity parameter *SPQ*
Granite gravel	GG	quartz, 70/~1100 feldspar, 10/940 others 20/their mix	22.4[*]	1070	0.611
Quartzite gravel	QG	quartz, 100/1180	26.0[*]	1100	0.543
Limestone gravel	LG	Calcite, 70/109 Others (dolomite et al), 30	24.8[*]	170	0.628
Mica-rich gravel	MG	amphibole, 42/950 plagioclase, 37/880 others 21	24	930	0.572
Green-grey gravel	GGG	amphibole, 49/950 plagioclase, 35/880 others (chlorite et al.) 16	14–17	930	0.609

[*]These values were obtained by reduced sample fraction size of L.A. test (see appendix 2)
[**] $HV' = HV_1 \cdot V_1 + HV_2 \cdot V_2 + HV_3 \cdot V_3$, where HV_1, HV_2 and HV_3 are hardnesses of the components, V_1, V_2 and V_3 are relative weight amounts of components.

The initial abrasives classified by the sieving were (4−5.6) mm. Frequency and cumulative frequency polygons of the initial abrasives are based on sieve analysis. The particle size of tested minerals was practically the same (Figure 4.1). Asterisks in the cumulative frequency plot designate sieve opening sizes and in the frequency plots the moving averages of adjacent sieve opening sizes.
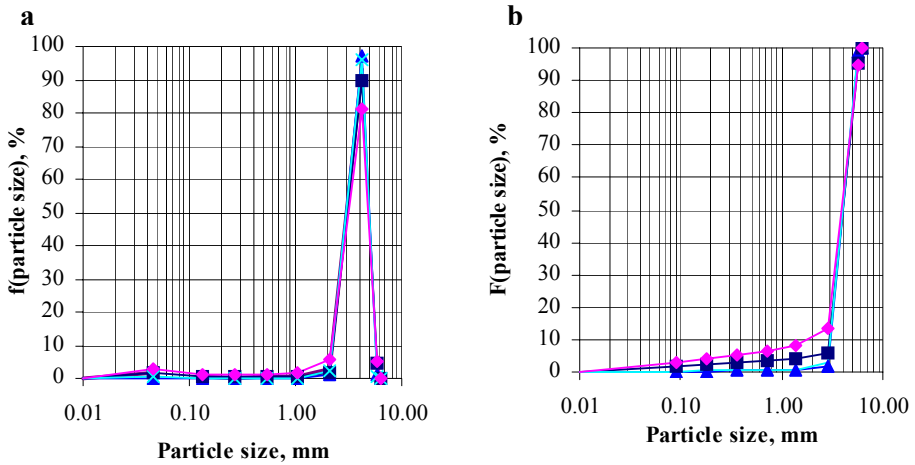
Figure 4.1 Frequency polygon (a) and cumulative frequency polygon (b) of abrasives used as feed materials in impact wear tests: —▲—MG, —■—GGG, —◆—QG, —✳—GG, —+—LG

4.1 Grindability

Eloranta in [10] writes strikingly that although all crushing parameters, crushers, screens, settings, etc., may be the same, there is always one parameter which is different practically every time, and that is the rock itself.

Grindability is particle size reduction study of the abrasives, was mainly done in the 1st circle of pins mode (Figure 2.1), only granite gravel was tested additionally in both circle modes.

Three different rotational velocities of rotors were used for grindability testing: 2025 min^{-1}; 2830 min^{-1}; and 3965 min^{-1} (in all cases both rotors rotated with equal velocity). Corresponding impact velocities to the 1st circle of pins were roughly 40 m/s, 60 m/s and 80 m/s (Table 2.2).

Three abrasives were tested by 40 m/s of impact velocity between the 1st circle of pins and the abrasive jet: mica-rich, green-gray and quartzite gravel (Figure 4.2). Asterisks in the cumulative frequency plot designate sieve opening sizes and in the frequency plots moving averages of adjacent sieve opening sizes.

Initial abrasive size decreases considerably after an impact with the 1st circle of specimens. Median particle size d_{50} of all the initial abrasives was about 4 mm (Figure 4.1 (b)). The median of a population is the value of the random variable at which the cumulative distribution function $F(x)$ is 0.50 [70].

The mica-rich abrasive was refined relatively more. After an impact with the 1st circle of pins, d_{50} was 0.5 mm for mica-rich and 1.5 mm for green-gray and quartzite gravel (see Table 4.1). Green-gray and quartzite gravel contained a similar amount of coarser fraction after the test.
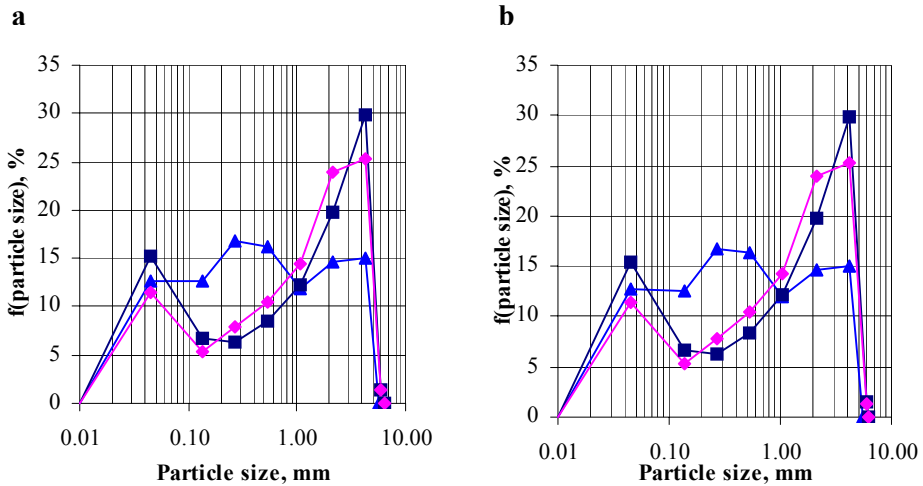
Figure 4.2 Frequency polygon (a) and cumulative frequency polygon (b) of grinded abrasives tested in 1st circle of specimens mode when impact velocity onto 1st circle of specimens was 40 m/s: ▲ MG, ■ GGG, ◆ QG

Frequency polygon distribution of refined green-gray and quartzite gravel contained a distinctive peak, clearly indicating the selective forming of fine fraction. The peak of coarse fraction shows proportion of particles staying relatively intact after the test. Such behaviour is especially noticeable for green-gray gravel. It seems to be that the peak in fine fraction region is induced from gradual fragmentation of coarse particles, which it is, is the debris of this process. This would explain the lack of middle fraction between two peaks. This correlates with Gorham et al experiments in [71], where they studied failure of various spherical particles under impact.

The breakage of the abrasive particles instead of polishing (smoothening) was approved by the increase of angularity parameter *SPQ*. The *SPQ* values of pre-test abrasives are given in Table 4.1. The fractions (0.13−0.63) mm of granite and quartzite sand abrasives used for AEW tests were sieved out from the abrasive tested in the impact wear tester. *SPQ* values of these sands (given in the subchapter 3.6) are bigger (that is the particles became more angular) than that of initial (4−5.6) mm fractions.

Two abrasives were tested by 60 m/s of impact velocity between the 1st circle of pins and the abrasive jet: granite and quartzite gravel; the former was tested additionally in both circle modes (Figure 4.3). Asterisks in the cumulative frequency plot designate sieve opening sizes and in the frequency plots the moving averages of adjacent sieve opening sizes.

From Figure 4.3 it can be seen, that the 2nd circle of pins does not cause considerable size reduction compared to the 1st circle of pins (in order to understand the circles of pins, see Figure 2.1).
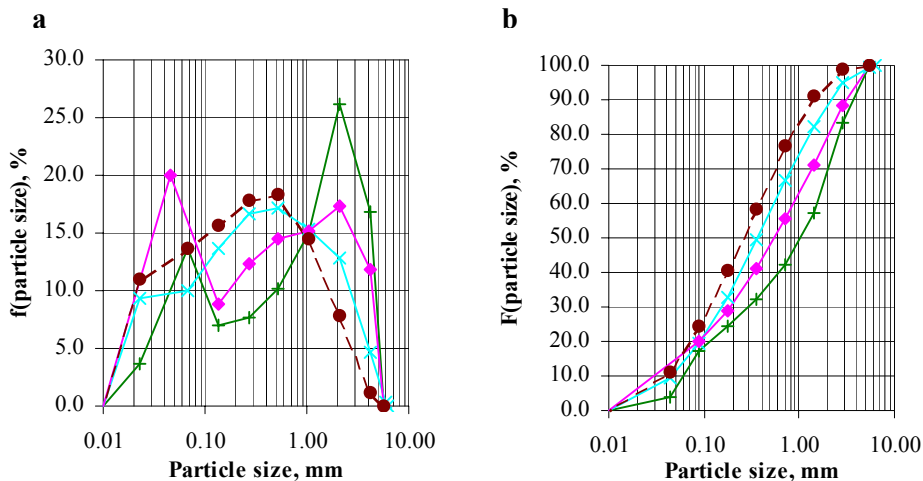
Figure 4.3 Frequency polygon (a) and cumulative frequency polygon (b) of grinded abrasives tested in both circles of specimens mode, when impact velocity onto the 1st circle of specimens was 60 m/s: ──┼── *Limestone,* ──✕── *Granite gravel after an impact with the 1st circle of specimens* ──◆── *Quartzite gravel,* ──●── *Granite gravel after an impact with the 2nd circle of specimens*

The refinement of granite gravel has been different from the refinement of limestone and quartzite gravel. The frequency polygon distributions of refined limestone and quartzite gravel contained two distinctive peaks as in tests made by 40 m/s (Figure 4.2), while the curves of granite gravel were roughly similar to the normal distribution.

For the shake of clarity, it is really important to note, that a 0.045 mm sieve has not been used for obtaining quartzite gravel curve (used sieve sizes are indicated by the asterisks on the curves of Figure 4.3 (b)). It means that the high peak in the fine fraction region of quartzite gravel is not genuine, as we do not have so much information about its distribution in this region, like for the limestone and both circle of granite gravels. For example, if we artificially took away 0.045 mm sieve from the results of granite gravel after the 2nd circle of pins, we would have to add its portion to the portion on the next 0.090 mm sieve, and instead of two first initial points, there would be only one point in Figure 4.3 (a) at the 25 % frequency polygon level. As such approach would degrade accuracy of the result, it is not favoured.

Limestone proved to be surprisingly intact after the test. In present case it was refined the least from all the tested abrasives. The particles of the limestone are tough and will be polished (smoothened) instead of fragmentation. L.A. coefficient predicted early integrity loss of limestone (see Table 4.1), but energies presented in the L.A. test are higher, whereby it does not describe the present situation adequately. Moreover, Wu and others [72] found, that L.A. abrasion loss was unable to predict field performance of the abrasives used as road pavements aggregates. They tested 16 aggregates, the performance of

which was evaluated by the service history and by the customers. They found, that the test may not be satisfactory for some types of aggregates, e.g. slag and some limestones tend to have high L.A. abrasion loss, but perform adequately well in the pavements.

Three abrasives were tested by 80 m/s of impact velocity between the 1st circle of pins and the abrasive jet: mica-rich, green-gray and quartzite gravel (Figure 4.4). Asterisks in the cumulative frequency plot designate sieve opening sizes, and in the frequency plots the moving averages of adjacent sieve opening sizes.
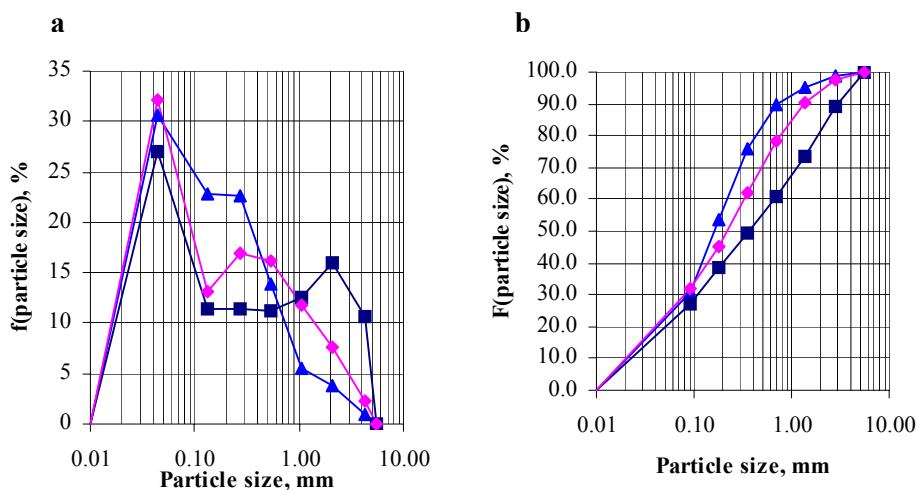
Figure 4.4 Frequency polygon (a) and cumulative frequency polygon (b) of grinded abrasives tested in both circles of specimens mode, when impact velocity onto 1st circle of specimens was 80 m/s: ▲ *MG,* ■ *GGG,* ◆ *QG*

Again, frequency polygon distributions of the refined green-gray and quartzite gravel contained two distinctive peaks, clearly indicating the selective forming of limiting fractions. Compared to 40 m/s (Figure 4.2), green-gray gravel contained considerably more of the larger fraction than quartzite gravel. It shows that certain components of multicomponent green-gray gravel are tougher and more fragmentation resistant than monolithic quartzite gravel (Table 4.1), and probably failure by Herzian cone cracks as it is found to be in [71]. The effect of these tough particles is also clearly emphasized by d_{50} of green-gray gravel (about 0.35 mm), which was the largest of all tested abrasive mineral materials.

The refinement of mica-rich gravel by 80 m/s has not been considerably severer compared to other the abrasives as it was at 40 m/s (Figure 4.2). The median diameter d_{50} of mica-rich and quartzite gravel did not differentiate more than 0.05 mm. The energy of impact in 40 m/s tests was probably enough for refining the mica-rich abrasive, but not for green-gray and quartzite gravel refinement, like it is in 80 m/s tests.

The results of the grindability tests of 80 m/s approximate to the L.A. test results. The bigger is the energy of impact, the more highlighted is the green-gray gravel, like it was shown by L.A. coefficients (Table 4.1). It is explainable by the bigger energy of impact which will be closer to the L.A. test energy levels.

To study the grindability of mineral ores and to estimate the size reduction dependence on the specific energy of treatment, the milling experiments with quartzite gravel at different velocities (40 m/s, 60 m/s and 80 m/s, that is Figure 4.2, Figure 4.3 and Figure 4.4) were summarised (Table 4.2).

Table 4.2. Influence of the velocity on the particle size reduction of quartzite gravel

Parameter	Initial	Impact velocity, m/s		
		40	60	80
Median particle size d_{50}, mm	4.0	1.5	0.5	0.2
Size reduction ratio (initial size/final size), times	−	2.5	7.3	17.3

The size reduction of quartzite gravel correlates with work-energy theorem − by increasing the particles velocity 2 times, their size decreases 4 times.

Work energy theorem is [7]:

$$W_{net} = K_f - K_i, \text{ where} \tag{4.1}$$

K_i and K_f − initial and final kinetic energy of a particle ($K = \dfrac{1}{2}mv^2$).

The initial kinetic energies of different abrasive velocities are given in the Table 2.1.

Based on grinding results on the various velocities of quartzite gravel, a grindability curve was constructed (Figure 4.5). The asterisks show the actual values of d_{50} measurements.

The grindability curve shows, that the dependence of the median particle size on the specific energy of treatment E_s is exponentially decreasing.
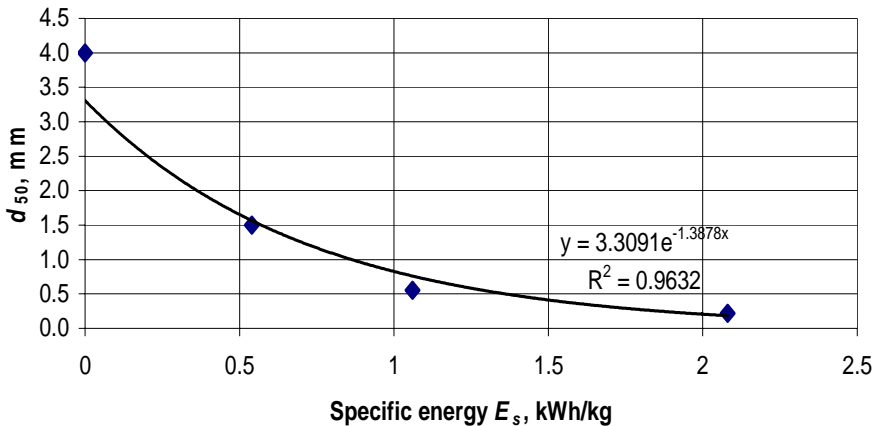
Figure 4.5 Grindability curve − dependence of median particle size on the specific energy of treatment of quartzite gravel

4.2 Abrasivity

The comparison of impact wear results of similar investigated materials tested with various abrasive mineral materials gives abrasivity (A_C). Based on the abrasive wear studies of steels (St 37, C45 and Hardox 400), the abrasivity of the studied mineral ores was found (Table 4.3). Wear rate I_V is given above the fraction line, abrasivity below it

Table 4.3. Wear rate of steels and abrasivity of studied minerals

Reference steels	Quartzite gravel		Granite gravel		Mica-rich gravel	Green-gray gravel	Lime-stone gravel
	$v = 60$ m/s	$v = 80$ m/s	$v = 60$ m/s	$v = 80$ m/s	$v = 80$ m/s	$v = 80$ m/s	$v = 60$ m/s
St37	-	156.4/1.0	-	-	72.6/0.5	97.7/0.6	-
C45	81.1/1.0	-	56.7/0.7	-	-	-	3.1/0.04
Hardox 400	83.3/1.0	132.8/1.0	63.2/0.8	111.5/0.8	50.5/0.4	43.8/0.3	2.0/0.02

The dependence of the abrasivity on the hardnesses of abrasives are given in Figure 4.6. The asterisks in the figure show actual values of specific steels, and the curve is an exponential trendline basing on these values.

It was demonstrated, that there is a direct correlation between the hardness and the abrasivity of tested minerals; the values of abrasivity rise deeply when abrasive hardness H_a is more than 800–900 HV', and in general do not depend on steel grade or impact velocity. The shape of curve correlates with the theory given in [2], where it is claimed, that the resistance of a material to abrasive wear is fairly constant when the abrasive is much harder than the material. As
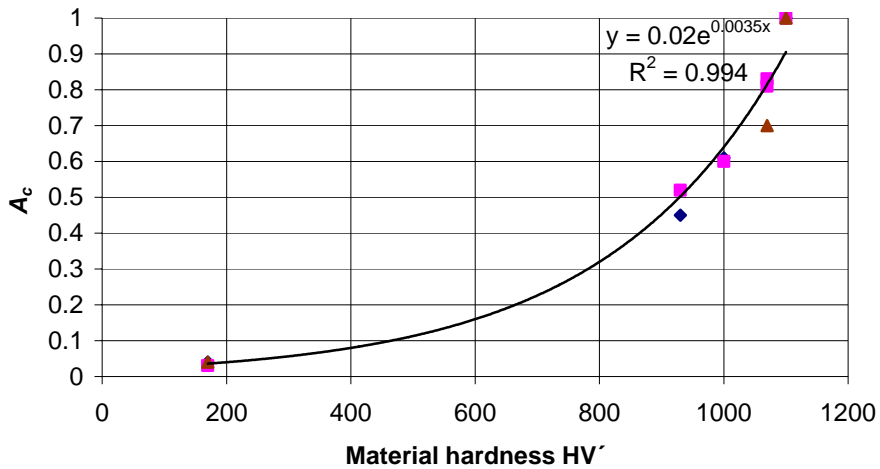
Figure 4.6 Dependence of abrasivity on the hardness of minerals. Determined on steels: ■ *– Hardox 400,* ▲ *– C45,* ◆ *– St37*

the hardness of both becomes similar, and the abrasive action approaches polishing, wear resistance generally improves by one to two orders of magnitude.

The correlation between grindability and abrasivity of abrasives is not clear. The dependence is valid for quartzite and granite gravel: the median particle size of granite decreased about 11 times while that of quartzite decreased 7 times (see Figure 4.1 and Figure 4.3); at the same time abrasivity of granite was about 20% lower than that of quartzite (Table 4.3). However, the behaviour of limestone and green-gray gravel show that an evident correlation between grindability and abrasivity cannot be proved: the abrasivity of limestone was less than 5 % of quartzite gravel abrasivity, but still its median particle size was ca 2 times more than of quartzite gravel.

4.2.1 Wear resistance of prosperous materials in various abrasives

To select materials for similar conditions as are presented in the impact wear tester like grinding elements of the disintegrator mills, various impact-based milling crushers (see subchapter 1.2.1), concrete crushers, etc, the wear resistance study of different steels and cermets was carried along with grindability experiments. Results of the wear resistance study at 60 m/s of impact velocity between the 1st circle of pins and abrasive jet are given in Table 4.4 and Figure 4.7. Wear resistance results in granite gravel were already given in chapter 3, but are repeated here for a better overview.

Table 4.4. AIW rates I_v (mm^3/kg) and relative wear resistance ε_v of the studied steels and cermets in different abrasives

Abrasive mater. / Tested material	Quartzite gravel		Granite gravel		Limestone gravel	
	ε_v	I_v, mm^3/kg	ε_v	I_v, mm^3/kg	ε_v	I_v, mm^3/kg
Steel C 45	1.0 ± 0.1	81.1 ± 26.1	1.0 ± 0.1	56.7 ± 19.1	1.0 ± 0.1	3.1 ± 1.1
Hardened steel Hardox 400	1.0 ± 0.1	83.3 ± 26.8	0.9 ± 0.1	63.2 ± 21.2	1.5 ± 0.1	2.0 ± 0.7
Powder steels Vanadis 6	1.9 ± 0.1	42.5 ± 13.7	1.8 ± 0.1	30.5 ± 10.5	2.7 ± 0.1	1.1 ± 0.4
Weartec	2.2 ± 0.1	37.6 ± 12.1	2.3 ± 0.1	24.3 ± 8.1	2.3 ± 0.1	1.3 ± 0.4
Cermets WC-15Co	17.8 ± 1.4	4.5 ± 1.5	23.6 ± 1.7	2.7 ± 0.9	2.3 ± 0.2	1.3 ± 0.4
Cr$_2$C$_3$-20Ni	5.3 ± 0.3	15.3 ± 4.9	11.8 ± 0.6	5.6 ± 1.8	3.1 ± 0.2	1.0 ± 0.4

As volumetric wear rate I_V depends very much on specific abrasive, relative wear resistance ε_V is a better universal characteriser for the present task, and is separately presented in the Figure 4.7.
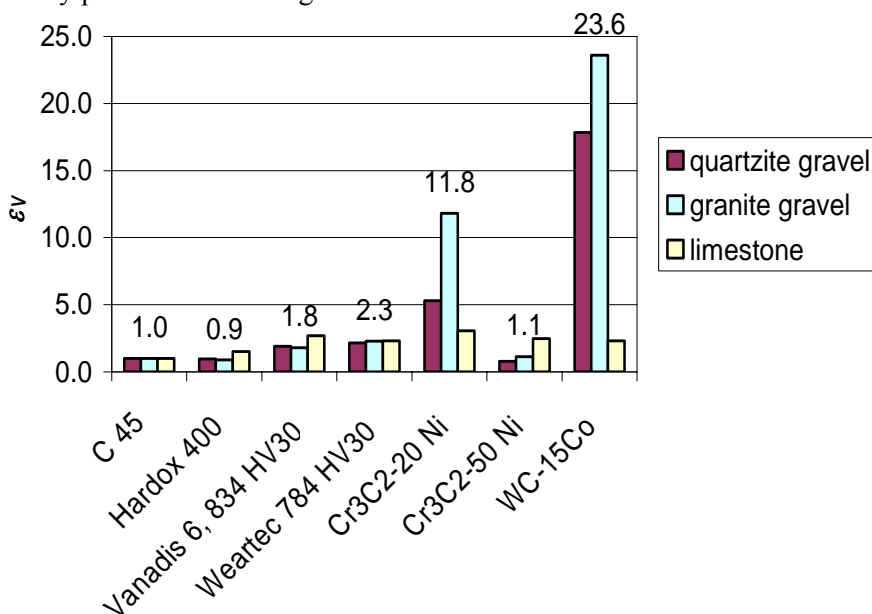
Figure 4.7 Relative wear resistance ε_V of materials for grinding media in different minerals

Figure 4.7 shows the dependence of wear resistance on a specific abrasive. The hardness of quartzite and granite gravel is similar (Table 4.1), and in both

cases low binder content cermets of tungsten and chromium carbide would be an obvious choice for making wear resistant working details.

If it is known, that abrasive mineral material is soft like limestone, powder steels would be a good choice, especially considering their advance over cermets because of relatively easier manufacturing process. A typical usage example would be disintegrators working in Estonians limestone mines, like in Quarry of Harku Ltd.

4.2.2 Calculation of size of wear craters

In order to be able to predict the size of wear craters theoretically, elastic-plastic contact model, proposed by Beckmann and developed by Kleis and Kulu [9], was used. The calculations based on the following equations for volumetric wear rate I_V (mm^3/kg):

$$I_V = \frac{3}{4\pi\rho_2} \cdot \frac{\tau_0}{e_s} \left[6.81 \left(\frac{2h_p}{D_2} \right)^{0.5} \cdot \frac{2\rho_2}{3H_1} v^2 \cdot \cos^2 \gamma + 0.85 \left(\frac{2h_p}{D_2} \right)^2 \right], \qquad (4.2)$$

where
v is the velocity of particles,
γ is the real impact angle,
H_1 is the hardness of the material,
ρ_2 is the density of erodent particle,
h_p is the depth of the wear crater after single impact of the particle,
D_2 is the mean diameter of the erodent particle,
τ_0 / e_s according to Beckmann and Kleis [9] is a dimensionless universal parameter used to determine wear resistance of metals.

It is assumed, that solid spherical particles used in this erosion model are homogeneous and elastically deformable, and particle velocity before the impact is constant. Rotational movement of particles was eliminated, because the impact angle is close to 90° (Table 2.2). Plastic penetration depth of the impact crater h_p was determined by the following relation:

$$h_p = \frac{D_2}{2} \sqrt{\frac{2\rho_2}{3H_1} \left[v^2 \sin^2 \gamma - \frac{4E'}{5\pi\rho_2} \left(\frac{H_1}{E'} \right)^5 \right]}, \qquad (4.3)$$

where E' is the reduced modulus of elasticity

$$E' = \left[(1 - \mu_1^2)/E_1 + (1 - \mu_2^2)/E_2 \right]^{-1}, \qquad (4.4)$$

and E_1 and E_2 are Young's modulus of the target material and the abrasive particle, μ_1 and μ_2 are Poisson's ratios for the same materials.

Following from the depth of the impact crater h_p (equation (4.3)), the corresponding diameter of the wear crater was calculated:

$$d = 2D_2 \sqrt{\frac{h_p}{D_2} - \left(\frac{h_p}{D_2}\right)} . \qquad (4.5)$$

In order to guarantee that the measured wear tracks on the specimens are not overlayed by other impacts, a special test was made, where only 50 g of abrasive was used for obtaining wear tracks on the polished specimens. The tracks were investigated by a tabletop scanning electron microscope Hitachi TM-1000 and measured under Vickers hardness measurement tester. The topography of worn surfaces is presented in Figure 4.8, Figure 4.9, and Figure 4.10.
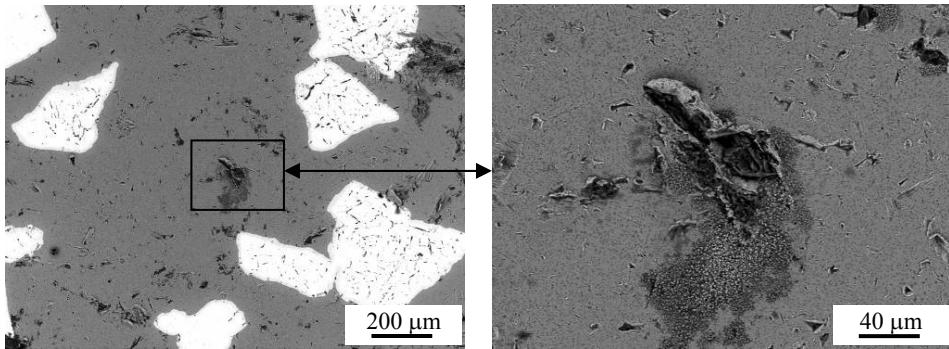
Figure 4.8 Abrasive footprints on the MMC steel specimen
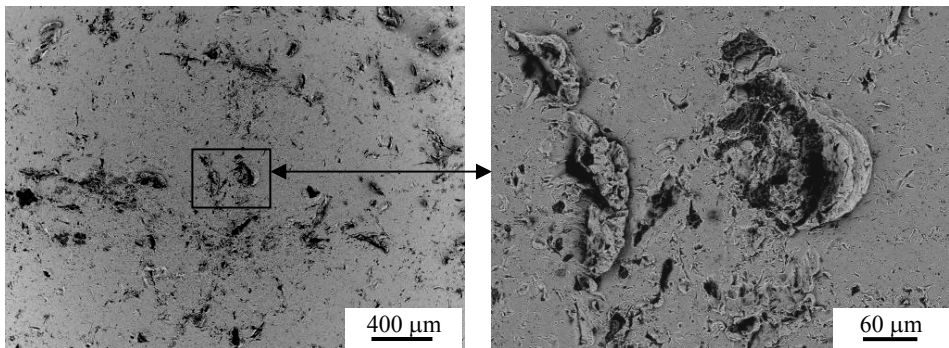
Figure 4.9 Abrasive footprints on the Hardox 400 steel specimen

It is known, that the shape of Vickers hardness measurement indenter originates from the ideal spherical Brinell hardness measurement impression [73]. The spherical shape of abrasive particles was assumed in the elastic-plastic contact model described in equation (4.2) too. Therefore, Vickers hardness measurement impressions suit very well for wear crater comparison.
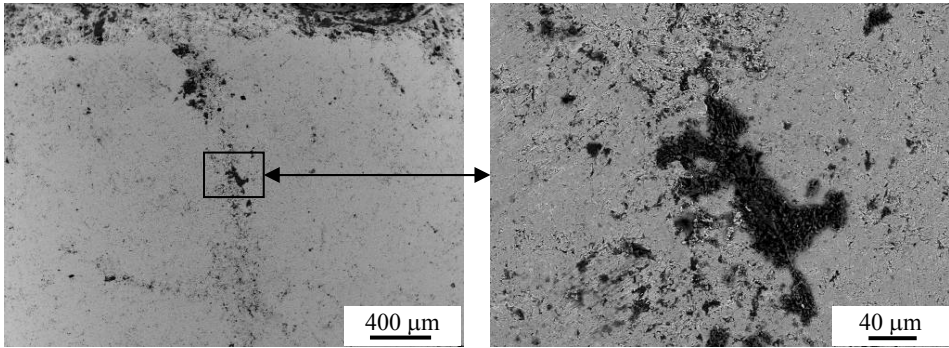
Figure 4.10 Abrasive footprints on the Cr₃C₂-20Ni cermet specimen

To find the best Vickers hardness measurement load for characterising the real size of wear craters on the specimens, various loads were used (Table 4.5).

Table 4.5. The sizes of hardness impressions, experimental wear craters, and calculated indents, when input parameters were $D_2 = 4$ mm, $v = 60$ m/s

Material	From hardness measurement		Experimentally obtained wear crater	Calculated by using eq. (4.5)
	HV1	HV30		
MMC	48	270	340	1166
Hardox 400	68	377	620	1334
Cr₃C₂-20Ni	41	242	380	974

Table 4.5 shows, that Vickers hardness scale HV30 suits for the characterization of hardness of materials with composite structure and subjected to AIW. The sizes of hardness measurement impressions and wear craters are comparable.

CONCLUSIONS

1. In the frames of the thesis was developed abrasive impact wear tester which is protected by the Estonian utility model no U200600001. It is suitable for simultaneous study of impact wear resistance of materials for grinding media and the grindability and abrasivity of mineral materials. The available velocities are up to 220 m/s, kinetic energy of the impact is up to 0.15 J for a particle, and impact angle is close to normal.
2. In the result of uncertainty focused wear resistance study media was shown that 15 kg of granite gravel is a convenient abrasive amount for conducting impact wear tests of hardmetal-type materials. For testing of steels and coatings is 3 kg of granite gravel sufficient amount.
3. The results of wear resistance testing demonstrated that for the selection of materials for conditions similar to the impact wear tester (for example grinding elements of disintegrator mills and various impact-based milling devices, concrete crushers, etc), is necessary to know the properties of abrasive mineral materials:
    − for the milling of mineral material with hardness about 1000 HV and more, low binder content cermets of tungsten and chromium carbide are recommended to be used as working elements (the relative volumetric wear resistance of WC-15Co is over 23 times, and of Cr_3C_2-20Ni material 12 times higher than that of reference steel C 45). Preliminary testing of TiC-NiMo cermets showed their big potential (relative volumetric wear resistance of TiC-30Ni:Mo(4:1) was over 18 times better than that of reference steel);
    − for the milling of mineral materials with low hardness (like limestone), powder steels like Weartec, etc are preferable (their relative volumetric wear resistance is on the same level with hardmetals, more than 2 times higher than that of reference steel);
    − thermal spray coatings are not suitable for the applications presented in the impact wear tester.
4. The relative volumetric wear resistance of hardmetals, cermets, and powder steels was better in abrasive impact wear tests compared to abrasive erosion wear tests. It is explainable by the smaller fractional size of abrasive, and thereby it has a better access to softer binder material. The wear mechanism itself at both cases is classical; at first the softer binder metal is removed, and then carbides start to fall out.
5. Grindability dependence between the median particle size and the specific energy of treatment E_s is exponential.
6. Highly efficient size reduction was demonstrated in the developed abrasive impact wear tester (depending on milling parameters one step milling gives size reduction up to 5−10 times). There is a direct correlation between the hardness and the abrasivity of the tested abrasive minerals; the values of

97

abrasivity rise deeply when abrasive hardness H_a is more than 800–900 HV', and in general do not depend on steel grade or impact velocity.

The correlation between grindability and abrasivity of abrasives is not clear. The dependence is valid for quartzite and granite gravel and their grindability, but not for limestone and green-gray gravel.

The bigger the energy of impact, the more the grindability coincides with the L.A. test. In case of smaller impact energies, the correlation between the grindability and L.A. coefficient was not found.

Future plans
1. To measure the kinetics (impact angles, velocities, and kinetic energies) of impact wear tester practically.
2. To study and improve the design of impact-based milling tester (find optional impact angles from the point of grindability and shape of working pins to minimize wear).
3. To study new prospective materials and coatings for grinding media.
4. To study the relation between the grindability and L.A test more thoroughly for proposing alternative test method enabling grindability and abrasivity investigation simultaneously.

REFERENCES

1. **A.J. Lynch, C.A. Rowland**. The History of Grinding. Society for Mining, 2005. 207 p.

2. **R.G. Bayer**. Wear Testing. – ASM Handbook: Mechanical Testing Vol. 8, Joseph R. Davis (Senior Technical Editor), 1992, p. 601−608.

3. **P. A. Engel**. Impact wear of materials. New York: Elsevier Science Publishers, 1986. 339 p.

4. **R.G. Bayer**. Mechanical Wear Fundamentals and Testing. 2nd Edition. New York: Marcel Dekker, Inc, 2004. 399 p.

5. **R.G. Bayer**. Wear Analysis for Engineers. New York: HNB Publishing, 2002. 360 p.

6. **P.J. Blau.** Glossary of Terms: ASM Handbook, Friction, Lubrication and Wear Technology ,Vol. 18, 1992, 942 p.

7. **R. A. Serway**. Physics For Scientists & Engineers with Modern Physics. Fourth Edition. USA: 1996. 1442 p.

8. **R. G. Bayer**. Engineering Design for Wear. 2nd Edition. New York: Marcel Dekker, Inc, 2004. 422 p.

9. **I. Kleis, P. Kulu**. Solid Particle Erosion: Occurrence, Prediction and Control. Springer-Verlag New York Limited, 2007. 206 p.

10. **J. Eloranta**. Influence of Crushing Process Variables on the Product Quality of Crushed Rock. Doctoral work, 1995. 118 p.

11. **The official home page of Metso Minerals**, the leading global supplier of technology and services for the mining and construction industries**, http://www.metsominerals.com, 26.03.09.

12. **The brochure for Metso Minerals Barmac B Series VSI crusher**, http://www.metsominerals.com/inetMinerals/MaTobox7.nsf/DocsByID/154FD 75456A4C75442256B10004546C4/$File/1122-02-08_english_20pp.pdf, 26.03.09.

13. **A. Pramstig**. Manufacturing Concrete Aggregates with a good Particle Shape. Septieme Congres des Grandes Barrages, Rome, 1961.

14. **A. Svensson**. Cubical shape crushing. A better shape for aggregates. – Concrete Plant and Production, 1990, vol. 8, no 4, pp. 141 – 144.

15. **R. Tarbe**. Thermal Spray Coatings from Recycled Hardmetal: Master of Science work, 2004. 93 p (in Estonian).

16. **M. Vierula**. Developing design of transportability of Lokotrack Mobile Crushers. Engineering thesis, 2007. 76 p (in Finnish).

17. **Aubema machinenfabrik GMBH impact mill data sheet,** http://www.aubema.cn/datasheet/Impact%20Mill.pdf, 27.03.09.

18. **The brochure for Metso Minerals Nordberg series impact crusher**, http://www.metsominerals.com/inetMinerals/MaTobox7.nsf/DocsByID/F8EAC 8D77753A11141256B410031202D/$File/NP_English.pdf, 27.03.09.

19. **The brochure for Metso Minerals Barmac VI Series VSI crusher,** http://www.metsominerals.com/inetMinerals/MaTobox7.nsf/DocsByID/9B67B A93ABC565CC41256B3B004758B0/$File/VI_English.pdf, 25.03.09.

20. **Wikipedia, the free encyclopedia**, Johannes Hint, http://et.wikipedia.org/wiki/Johannes_Hint, 8.04.09.

21. **B. Tamm, A. Tümanok**. Impact grinding and disintegrator. – Proc. Estonian Acad. Sci. Eng. No 2, 1996, pp. 209–223.

22. **The brochure for Metso Minerals Nordberg C Series jaw crushers**, http://www.metsominerals.com/inetMinerals/MaTobox7.nsf/DocsByID/C456E D9F5C9B39B7C2256DAC00206B4D/$File/CseriesEnglish.pdf, 28.03.09.

23. **Wikipedia, the free encyclopedia**, Rock crusher, http://en.wikipedia.org/wiki/Cone_crusher, 24.03.09

24. **The brochure for Metso Minerals Nordberg Superior® primary gyratory crushers**, http://www.metsominerals.com/inetMinerals/MaTobox7.nsf/DocsByID/1AF19 BA4A65DA68586256B48006565BE/$File/Superior.pdf, 31.04.09.

25. **The brochure for Metso Minerals GP series cone crushers**, http://www.metsominerals.com/inetMinerals/MaTobox7.nsf/DocsByID/4045B6 C4E0154A79C22573F3002E2216/$File/GPseries_English.pdf, 31.04.09.

26. **T. Deng, M.S. Bingley, M.S.A. Bradley.** Understanding particle dynamics in erosion testers—A review of influences of particle movement on erosion test conditions. – Wear, 2009, (Available online, in press).

27. **T. Deng, M.S. Bingley, M.S.A. Bradley, S.R. De Silva.** A comparison of the gas-blast and centrifugal-accelerator erosion testers: The influence of particle dynamics. – Wear 265, 2008, pp 945–955.

28. **Wikipedia, the free encyclopedia**, Measurement, http://en.wikipedia.org/wiki/Measurement, 8.06.08.

29. **R. Laaneots, O. Mathiesen.** An Introduction to Metrology. Tallinn: TUT Press, 2006. 271 p.

30. **D.R. Anderson, D.J. Sweeny, T.A. Freeman, E. Shoesmith**. Statistics for business and economics. London: Thomson Learning, 2007. 904 p.

31. **D.C. Motgomery, G.C. Runger**. Applied statistics and probability for engineers. 3 Ed. New York: Wiley, 2003. 706 p.

32. **Wikipedia, the free encyclopedia**, Covariance, http://en.wikipedia.org/wiki/Covariance, 26.05.08.

33. **R. Laaneots.** Measurement. Tallinn: TUT press, 1998. 135 p. (in Estonian)

34. **R.J. Hyndman, Y. Fan.** Sample quantiles in statistical packages. – The American Statistician,1996, Vol. 50, No. 4, pp 361–365.

35. **J. Li, T. Deng, M.S. Bingley, M.S.A Bradley**. Prediction of particle rotation in a centrifugal accelerator erosion tester and the effect on erosion rate. – Wear 258, 2005, pp 492–502.

36. **T. Deng, M.S. Bingley, M.S.A. Bradley**. The influence of particle rotation on the solid particle erosion rate of metals. – Wear 256, 2004, pp 1037–1049.

37. **J. Sarandi**, **R. Tarbe**. Estonian utility model Desintegraatorveski löökkulumise uurimiseks. 17.07.2006.

38. **E. Topnik**. Theoretical Mechanics 2: Dynamics. Tallinn: TUT press, 1995, 63 p (in Estonian).

39. **J. Kirs**. Engineering Mechanics II: Lectures and Exercises in Kinematics, 2008, http://www.mh.ttu.ee/jkirs/Kinemaatika/, 26.09.08 (in Estonian).

40. **J. Kirs**. Engineering Mechanics III: Lectures and Excercises in Dynamics, 2004, http://www.mh.ttu.ee/jkirs/Dynaam/, 25.09.08 (in Estonian).

41. **A. Bedford, W. Flower**. Engineering Mechanics: Dynamics. 2nd edition, USA, 1999. 588 p.

42. **F. Millard, Jr. Beatty**. Principles of Engineering Mechanics: Volume 2 Dynamics—The Analysis of Motion. USA: Springer. 595 p.

43. **E. Topnik.** Engineering Mechanics Exercises III: Dynamics. Tallinn: TUT press, 2001, 112 p (in Estonian).

44. **T. Deng, M.S. Bingley, M.S.A. Bradley.** Infuence of particle dynamics on erosion test conditions within the centrifugal accelerator type erosion tester. – Wear 249, 2001, pp 1059−1069.

45. **N. Piskunov.** Differential and Integral Calculation: 2. Tallinn: Valgus, 1983. 576 p (in Estonian).

46. **L. Råde, B. Westergren**. Mathetamics Handbook. Berlin, Heidelberg, New York, Springer-Verlag, 2004. 562 p.

47. **K.N. Berk, P. Carey**. Data Analysis with Microsoft Excel. Southbank, Australia; Belmont, CA: Brooks/Cole. 580 p.

48. **Solid Works Design homepage,** http://www.solidworks.com/, 3.02.09**.**

49. **Wikipedia, the free encyclopedia**, Central limit theorem, http://en.wikipedia.org/wiki/Central_limit_theorem, 15.11.08.

50. **K. Marcus**. Tribology in coal-fired power plants. – Ninth International Tribology Conference of the South African Institute of Tribology. South Africa, 2008.

51. **N. Miyazaki.** Solid Particle Erosion Behaviour of FRPs with Prior Impact Damage. – Journal of Composite Materials, Vol. 00, No. 00, 2006.

52. **SSAB Hardox web page**, http://www.hardox.com/templates/Page____517.aspx, 29.11.08.

53. **C. Spiegelhauer**. Industrial production of tool steels using the spray forming technology. Proceedings of the 6th International Tooling Conference, 10−13 september 2002, pp1101−1106

54. **Böhler-Uddeholm.** The producer of Vanadis 6 and Weartec SF. http://www.bucorp.com/, 29.11.08

55. **T. Hillskog**. Powde-Metallurgy tool steels: An overview. Metalforming magazine, January 2003, pp 48−51.

56. **C**. **Speiegelhauer**. Industrial Production of Tool Steels Using the Spray Forming Technology. Proceedings of the 6th International Tooling Conference. 2002. pp. 1101−1109.

57. Spray forming, http://www.metsomaterialstechnology.com, 16.12.08

58. **H Klaasen, J. Kübarsepp**. Abrasive wear performance of carbide composites. Wear 262, 2006, pp 520−526.

59. **C. Deng, M. Liu, C. Wu, K. Zhou, and J. Song**. Impingement Resistance of HVAF WC-Based Coatings. – Journal of Thermal Spray Technology Vol. 16, 2007, pp 604−609.

60. **Standard EVS-EN 1097-2:2007**. Tests for mechanical and physical properties of aggregates. Methods for the determination of resistance to fragmentation. 2007. 22 p.

61. **W.D. Callister, Jr**. Materials science and engineering an Introduction. Sixth edition. USA: John Wiley & Sons, Inc., 2002. 820 p.

62. **W.D. Callister, Jr**. Fundamentals of Materials science and engineering an Interactive. Sixth edition. USA: John Wiley & Sons, Inc., 2001. 524 p.

63. **R. Tarbe, P. Kulu, M Saarna, R. Veinthal, H. Käerdi**. Mechanisms and Prediction of Abrasive Impact Wear of Powder Materials. – 16th IFHTSE (The International Federation for Heat Treatment and Surface Engineering) Congress, 30.10 – 2.11.2007, Brisbane (Australia).

64. **Z. Fang, S Tool**. Wear Resistance of Powder Metallurgy Alloys. ASM Handbook vol. 7: Powder Metal Technologies and Applications. USA, pp. 965−977.

65. **Material property data**, Hadfield steel, http://www.matweb.com/search/DataSheet.aspx?MatGUID=2fe94d5bf4914b51 83b9affb2f43dfc8&ckck=1, 17.12.08

66. **J. Mendez, M. Ghoreshy, W.B.F. Mackay, T.J.N. Smith and R.W. Smith**. Weldability of austenitic manganese steels. Journal of Materials Processing Technology 153−154. Elsevier, 2004, pp. 596−602.

67. **I. Hussainova, J. Pirso**. Microstructure and erosive wear in ceramic based composites. Wear 258, 2005, pp 351−365.

68. **G. W. Stachowiak.** Particle angularity and its relationship to abrasive and erosive wear. Wear 241, 2000, pp 214−219.

69. **I. Hussainova, J. Kübarsepp, J. Pirso**. Mechanical properties and features of erosion of cermets. Wear 250, 2001, pp. 818−825.

70. **Richard C. Rice**. Stastics and Data Analysis: Introduction. − ASM Handbook: Mechanical Testing Vol. 8, Joseph R. Davis (Senior Technical Editor), 1992, p. 623−627.

71. **D.A. Gorham, A.D. Salman**. The failure of spherical particles under impact. – Wear 258, 2005, pp. 580−587.

72. **Y. Wu, F. Parker, K. Kandhal**. Aggregate Toughness/Abrasion Resistance and Durability/Soundness Tests Related to Asphalt Concrete Performance in Pavements. National Center of Asphalt Technology Report No. 98-4: 1998. 23 p.

73. **Wikipedia, the free encyclopedia**, Vickers hardness test, http://en.wikipedia.org/wiki/Vickers_hardness, 2.02.09.

74. Los Angeles Abrasion Test, http://www.pavementinteractive.org/index.php?title=Los_Angeles_Abrasion, 5.02.09.

75. **Standard BS EN 1097-2**. Tests for mechanical and physical properties of aggregates. Methods for the determination of resistance to fragmentation. 1998, 22 p.

LIST OF PUBLICATIONS

Veinthal, R.; Tarbe, R.; Kulu, P.; Käerdi, H. (2009). Abrasive erosive wear of powder steels and cermets . Wear, xx−xx. [in press]

Kulu, P.; Tarbe, R.; Käerdi, H.; Goljandin, D. (2009). Abrasivity and grindability study of mineral ores. Wear, xx−xx. [in press]

Kulu, P.; Veinthal, R.; Käerdi, H.; Tarbe, R. (2008). Abrasive wear resistance of Powder Composites at Abrasive Erosion and Abrasive Impact Wear. Materials Science (Medžiagotyra), 14(4), 328−332.

Tarbe, R.; Kulu, P. (2008). Impact Wear Tester for the Study of Abrasive Erosion and Milling Processes. Küttner, R. (Toim.). Proceedings of the 6th International Conference of DAAAM Baltic Industrial Engineering, 24-26th april, Tallinn, Estonia (561−566). Tallinn: Tallinn University of Technology

Veinthal, R.; Kulu, P.; Pirso, J.; Käerdi, H.; Tarbe, R. (2008). Abrasive Wear Resistance of Powder Composite Materials: Characterization and Prediction. In: Tribology 2008 : Proceedings of the 9th International Tribology Conference: 9th International Tribology Conference, University of Pretoria, South Africa, 2−4 April 2008. (Editor.) Vaal, PL de.; Fuller, G.. South Africa: South African institute of Tribology, 1.3 (1) - 1.3(10).

Kulu, P.; Veinthal, R.; Käerdi, H.; Tarbe, R. (2008). Abrasivity study of materials used at abrasive tests. In: Tribology 2008 : Proceedings of the 9th Inernational Tribology Conference: 9th Inernational Tribology Conference, University of Pretoria, South Africa, 2−4 April 2008. (Toim.) Vaal, PL de.; Fuller, G.. South Africa: South African institute of Tribology, 3.4(1) - 3.4(10).

Kulu, P.; Veinthal, R.; Saarna, M.; Tarbe, R. (2007). Surface fatigue processes at impact wear of powder materials. Wear, 263(1-6), 463−471.

Kulu, P.; Tarbe, R.; Veinthal, R (2007). Erosion and impact wear resistance of thermal sprayed coatings. In: Proceedings of the 20th International Conference on Surface Modification Technologies: Surface Modification Technologies, September 2006, Vienna. (Toim.) Sudarshan, T.S; Stiglich, J. J.. Asm International, 94−99.

Peetsalu, P.; Zimakov, S.; Pirso, J.; Mikli, V.; Tarbe, R.; Kulu, P. (2006). Characterization of WC-Co composite thermal spray powder and coating. Proc. Estonian Acad. Sci. Eng., 12(4), 435−444.

Peetsalu, P.; Zimakov, S.; Pirso, J.; Mikli, V.; Tarbe, R.; Kulu, P. (2006). Characterizationa of WC-Co thermal spray coatings based on the composite powders. Powder Metallurgy Progress : Journal of Science and Technology of Particle Materials, 6(1), 34−41.

Saarna, M.; Kulu, P.; Veinthal, R.; Tarbe, R. (2006). Study of surface fatigue of wear resistant powder metallurgical materials. Proc. Estonian Acad. Sci. Engineering, 12(4), 377−387.

Tarbe, R.; Zimakov, S.; Peetsalu, P.; Kulu, P.; Mikli, V. (2006). Experimental spray powders and coatings produced from recycled hardmetal by various Mechanical Methods. In: Euro PM2006 Congress & Exhibition Proceedings, Hard Materials: Euro PM2006, Ghent, Belgium, 23-25 October 2006. (Toim.) European Powder Metallurgy Association. European Powder Metallurgy Association, 259−264.

Kulu, P.; Tarbe, R.; Zimakov, S. (2006). Application of composite thermal sprayed coatings. . In: Proceedings of the International Surface Engineering Congress (ISEC), 15-18 May 2006, Seattle, USA: International Surface Engineering Congress (ISEC), 15-18 May 2006, Seattle, USA. Seattle: Asm International, 2006, 19−25.

Peetsalu, P.; Pirso, J.; Mikli, V.; Tarbe, R.; Kulu, P. (2006). Characterization of WC-Co composite thermal spray powder and coating. . In: Proceedings of 15th International Baltic Conference Engineering Materials & Tribology : BALTMATTRIB 2006: The 15th International Baltic Conference Engineering Materials & Tribology, BALTMATTRIB 2006, Tallinn, Estonia, 5-6 Oct. 2006, 52−53.

Saarna, M.; Kulu, P.; Veinthal, R.; Tarbe, R. (2006). Study of surface fatigue of wear resistant powder materials. . In: Proceedings of 15th International Baltic Conference Engineering Materials & Tribology : BALTMATTRIB 2006: The 15th International Baltic Conference Engineering Materials & Tribology, BALTMATTRIB 2006, Tallinn, Estonia, 5-6 Oct. 2006., 66−68.

Kulu, P.; Tarbe, R.; Vallikivi, A. (2005). Abrasive wear of powder materials and coatings. Materials Science (Medžiagotyra), 11(3), 230−234.

Peetsalu, P.; Zimakov, S.; Pirso, J.; Mikli, V.; Tarbe, R.;Kulu, P. (2005). Technology and characterization of composite thermal spray powders. Materials Science (Medžiagotyra), 11(4), 385−389.

Tarbe, R.; Zimakov, S.; Mikli, V.; Kulu, P.; Veinthal, R. (2005). Wear resistant powder coatings on the base of recycled hardmetal. Powder Metallurgy Progress, 3, 148−157.

Peetsalu, P.; Zimakov, S.; Pirso, J.; Mikli, V.; Tarbe, R.; Kulu, P. (2005). Characterization of Composite Thermal Spray Powders. In: Euro PM2005 Powder Metallurgy Congress & Exhibition : Proceedings: Euro PM2005 Powder Metallurgy Congress & Exhibition, Prague Congress Centre, Czech Republic 2 - 5 Oct. 2005. EPMA, 87−92.

Mikli, V.; Kulu, P.; Tarbe, R.; Peetsalu, P.; Zimakov, S. (2004). Recycled hardmetal based powders for thermal spray. Proceedings of the Estonian Academy of Sciences. Engineering, 10(4), 315−325.

Mikli, Valdek; Kulu, Priit; Tarbe, Riho; Peetsalu, Priidu (2004). Double-cemented recycled hardmetal based powders for thermal spray. Proceedings of the 4th International Conference "Industrial engineering - new challenges to SME" : 29-30th April 2004, Tallinn, Estonia, 211−214.

Zimakov, S.; Mikli, V.; Kulu, P.; Tarbe, R. (2004). Wear resistant sprayed coatings on the base of recycled hardmetal powder. In: Proc. of 13th Int. Conf. Engineering Materials& Tribology, 2004, Riga:, 83−88.

Zimakov, S.;Tarbe, R.; Kulu, P. (2003). New composite coatings on the base of recycled hardmetals. In: Thermal Spray 2003 : Advancing the Science and Applying the Technology : Proceedings of the 2003 International Thermal Spray Conference: 2003 International Thermal Spray Conference, Orlando (Florida), 5-8 May 2003. (Toim.) Marple, B. R.; Moreau, Chr.. Asm International, 2003, 455−459.

Zimakov, S.; Tarbe, R.; Kulu, P. (2002). Thermally sprayed WC-Co hardmetal based coatings. Materials Science (Medžiagotyra), 8(4), 409−412.

Zimakov, S., Tarbe, R., Veinthal, R., Kulu, P. (2002). Optimization of structure of Sprayed WC-Co Hardmetal based Coatings. In: Proceedings of the 3rd International Conference "Industrial Engineering - New Challenges to SME" : 3rd international DAAAM conference industrial engineering - new challenges to SME, Tallinn (Estonia), 25-27 april 2002. (Editors.) Papstel, J.; Katalinic, B.. Tallinn: Tallinn Technical University, 224−227.

KOKKUVÕTE

Löögil baseeruvate jahvatusmeetoditega saavutatakse üldiselt soovitav etteantud omadustega kuubiline lõpp-produkt, kus osakeste purunemine toimub mööda defektseid tasandeid, kusjuures lõpp-produkt on defektivaba. Löögil baseeruva jahvatuse puuduseks on seadmete või nende osade suur kulumine. Sellest tulenevalt on oluline katseaparatuuri loomine jahvatusseadmete materjalide käitumise kui ka mineraalsete materjalide jahvatatavuse uurimiseks, sest enamiku erosioonkatsetusseadmetega ei ole võimalik katsetada üle 2 mm suuruseid osakesi.

Antud töö käigus konstrueeritud löökveski võimaldab löögi tingimustes uurida paralleelselt jahvatusseadmete materjalide käitumist koos mineraalsete materjalide jahvatatavusega.

Esimeses peatükis tutvustatakse lühidalt tööstuslikke jahvatusmeetodeid. Põhjalikumalt on käsitletud löögil baseeruvaid meetodeid kui konstrueeritud löökveskis häid tulemusi näidanud materjalide ühte võimalikku kasutusvaldkonda. Samuti on lühidalt käsitletud jahvatusseadmetes kasutatud materjale ning töös teostatud mõõtemääramatuste arvutuste aluseid. Peatüki lõpetusena on formuleeritud töö eesmärgid, mis on järgmised:

1. Luua mitmeotstarbeline löökjahvatusseade, mis võimaldab uurida jahvatusseadmes sobivaid materjale kui ka materjalide jahvatatavust samaaegselt.
2. Määrata sobilikud kulutamise katsetusparameetrid piisavalt väikese määramatusega tulemuste saavutamiseks pulbermaterjalide ja –pinnete korral.
3. Uurida erinevate materjaligruppide kulumiskindlust sobilike löökulumise tingimustes töötavate materjalivaliku põhimõtete väljatöötamiseks.
4. Erinevate mineraalsete materjalide jahvatatavuse ja abrasiivsuse uurimine.
   Nimetatud eesmärkide täitmiseks on kavandatud järgmised tegevused:
   1) löökjahvatusseadme konstrueerimine materjali liikuvuse parameetrite (kiirus, energia, lööginurgad) määramine;
   2) pulbermaterjalide ja –pinnete kulumiskindluse uuringud määramatust arvestades;
   3) abrasiivlöök- ja erosioonkulumiskindluse tulemuste võrdlus;
   4) erinevate mineraalsete materjalide jahvatatavuse uurimine (graniit, kvarts- ja lubjakivi);
   5) jahvatatavate materjalide abrasiivsuse uurimine.

Teine peatükk käsitleb eksperimentaalse seadme konstruktsiooni ja katsetusmetoodikat ning seadme kinemaatika (lööginurgad ja põrkekiirused) arvutusi. Olulise osa antud peatükist moodustavad lööginurkade ja põrkekiiruste määramatuse arvutus. Samuti on leitud määramatusel põhinevalt optimaalsed abrasiivide kogused teraste, kermiste ja pinnete kulumiskindluse uuringuteks.

Kolmas peatükk on pühendatud erinevate materjaligruppide (pulberterased, kõvasulamid ja kermised) kui ka pulberpinnete kulumiskindluse uurimisele.

Pulberterastest olid vaatluse all pulbermetallurgia meetodil toodetud terased Vanadis 6 ja Weartec, ning Cr-terasest metallmaatriksiga karbiidtugevdatud komposiitmaterjalid. Kermistest olid vaatluse all volfram-, kroom- ja põgusalt titaankarbiidsed materjalid. Pinnetest kiirleekpihustuspinded iseräbustuvate sulamite ja kõvasulampulbri baasil. Abrasiivse materjalina kulumiskindluse uuringutes kasutati graniit- ja kvartskillustikku osise suurusega 4−5.6 mm. Etalonmaterjalina kasutati süsinikterast C45 ja St 37 aga ka eriteraseid Hardox 400 ja 600 ning Hadfieldi terast. Kulumisnäitajaina kasutati suhtelist mahulist kulumiskindlust (võrrelduna etalonmaterjalidega) ja kulumise intensiivsust (mm^3/kg). Toodud on teraste, kermiste ja pihustuspinnete abrasiivkulumiskindlus ning erinevate materjalide kulumismehhanismid. Võrreldi abrasiivlöökkulumist ja abrasiiverosioonkulumist.

Neljas peatükis on vaatluse all mitmete mineraalsete materjalide (graniit, kvartsiit, lubjakivi) jahvatatavus ning nende materjalide abrasiivsus. Toodud on põhiliste mineraalsete materjalide (graniit ja kvartsiit) osiseline koostis. Materjalide jahvatatavuse uuringud üherootorsüsteemi kasutades viidi läbi kiirustel 40 m/s, 60 m/s ja 80 m/s. Lisaks uuriti graniidi jahvatatavust kaherootorsüsteemis kiirusel 60 m/s. Analüüsiti jahvatusprodukti osiselt koostist ning koostati jahvatatavuse kõver – keskmise osise suuruse sõltuvus jahvatuse energiast. Materjalide abrasiivsuse uuringud viidi läbi kasutades erinevaid etalonmaterjale ning koostati graafik iseloomustamaks abrasiivsuse teguri sõltuvust abrasiivide kõvadusest. Mõõdetud on kulumisjäglede "suurusi" ja arvutatud need lähtudes Kleisi ja Kulu kulumisteooriast [9] ning võrreldud Vickersi vastavate kõvaduse määramise meetoditega (HV 1 ja HV 30) saadud jälgede suurustega.

Töö põhitulemused on järgmised:
1. Välja on töötatud originaalne desintegraatorjahvatusseadmel baseeruv eksperimentaalne löökveski (kasuliku mudeli tunnus nr U200600001), mis on mõeldud materjalide kulumiskindluse kui ka jahvatusprotsesside samaaegseks uurimiseks. Seadme piirparameetrid on järgmised: maksimaalne põrkekiirus abrasiivse mineraaliga 220 m/s, osakeste suurus kuni 7 mm, nende kineetiline energia 0.15 J, põrkenurk 90°.
2. Määramatusel põhineva materjalide kulumiskindluse uurimise tulemusena selgitati välja minimaasled abrasiivi kogused graniidi korral: 15 kg abrasiivi kõvasulamite ja kermiste katsetamiseks, 3 kg – teraste ja pinnete katsetamiseks, teiste abrasiivide puhul 15 kg sõltumata katsetatava materjali liigist.
3. Materjalide kulumiskindluse uurimise tulemused näitasid, et löökveskile sarnastes tingimustes (näiteks erinevad desintegraatorite ja löögil baseeruvate jahvatusseadmete tööorganid jne) kasutatavate materjalide valikuks on vajalik teada kasutatava abrasiivmineraalsete materjalide omadusi:
    − materjalide kõvadusega üle 1000 HV töötlemiseks sobivamaks jahvatusseadmete osade materjaliks on madala sideaine sisaldusega

(10−15 mahu%) kõvasulamid ja kermised, millede suhteline kulumiskindlus (teras C 45 suhtes) on 12 (kroomkarbiidsed kermised) kuni 23 korda enam (kõvasulamid);

- väikese kõvadusega, näiteks lubjakivi (200 HV) materjalide töötlemiseks on sobivad pulberterased (näit. Weartec), millede kulumiskindlus on ca 2x suurem etalonterastest ja võrreldav kõvasulamite omega;
- termopinded tulenevalt nende struktuuri iseärasustest, pole sobivad jahvatusseadmete löögielementide valmistamiseks.

4. Võrreldes abrasiivlöök- ja erosioonkulumiskindlust, on erosioonkulumise tingimustes materjalide (kõvasulamid, kermised ja pulberterased) kulumine intentsiivsem. Seda võib seletada eelkõige väiksema abrasiivosakese suurusega erosioonil, mis põhjustab kõvasulam-tüüpi struktuuride korral sideaine väljakulumise, millele järgneb kõvafaasi eraldumine hapra purunemise tagajärjel.

5. Jahvatatavuse sõltuvus osakeste mediaani ja erienergia E_s vahel on eksponentsiaalne.

6. Loodud seade on kasutatav ka jahvatusprotsesside uurimiseks ning jahvatuse efektiivsus (jahvatatavus) on eelõige sõltuv jahvatamise erienergiast ja seda eksponentsiaalses sõltuvuses. Tulenevalt jahvatuspara-meetritest on selliste mineraalsete materjalide korral, nagu graniit ja kvartsiit saavutatav peenenemise effekt üherootorsüsteemi korral 5−10 x. Eksisteerib otsene seos jahvatatava materjali kõvaduse ja abrasiivsuse vahel − abrasiivsus kasvab järsult kõvaduse 800−900 HV (taandatud kõvadus) juures ja ei sõltu oluliselt jahvatuskiirusest. Ühest seost materjalide jahvatatavuse ja abrasiivsuse vahel ei täheldatud: kui graniidi ja kvartsiidi korral oli see täheldatav, siis pehmete abrasiivide korral (lubjakivi) käitusid materjalid vastu ootusi. Suurematel jahvatuskiirustel materjalide jahvatatavus ühtib L.A. testiga.

Uurimistöös saadud originaaltulemused ja esilekerkinud probleemid on andnud ainet tulevasteks uuringuteks, mis võiks olla pühendatud järgmistele küsimustele:

- seadme kineetika (osakeste liikumine, nurgad, kiirus, eriti mitmerootorsüsteemi korral) katseline uurimine;
- konstruktsiooni täiustamine põrkenurkade jahvatatavuse ja tööorganite kulumise optimaalsest seosest lähtudes;
- täiendavate löökkulumise tingimustes perspektiivsete materjalide uurimine;
- meetodi kui alternatiivi L.A. meetodile täiustamine, mille põhiline eelis peale materjali jahvatatavuse on abrasiivsuse määramise võimalus.

ABSTRACT

Impact-based milling tends to produce a favourable cubical product. The drawback of impact-based milling is a high wear rate of the mills, which raises the importance of a good testing apparatus for studying the behaviour of the crusher materials.

Due to the need for abrasive impact wear tester enabling to test bigger abrasive mineral particles than 2 mm, and considering good properties of centrifugal-accelerators, is the first part of this work solely devoted to disintegrator type tester development, which enables to study simultaneously impact wear resistance of materials for grinding media and grindability of mineral materials. The available velocities are up to 220 m/s, kinetic energy of the impact is up to 0.15 J for a particle and impact angle is close to normal. A proper wear characteristics and testing conditions have been proposed.

The wear resistance of the common powder materials (steels and cermets) and thermally sprayed coatings is studied. A proper testing route regarding reasonable uncertainty values was found and a comparison between abrasive impact wear and abrasive erosive wear was carried out. The abrasive mineral material was (4–5.6) mm granite gravel, but for grindability and abrasivity tests quartzite gravel, limestone, mica-rich gravel and green-gray gravel from the same size range were used.

The results of wear resistance testing demonstrated that for the selection of materials for conditions similar to the impact wear tester is necessary to know the properties of abrasive mineral materials: low binder content cermets of tungsten and chromium carbide are recommended to be used in case when abrasive mineral hardness is about 1000 HV, but when crushing low hardness abrasive minerals like limestone, powder steels (Weartec, etc) are preferable.

Keywords: impact wear, impact-based milling, erosion, wear resistance, grinding, grindability, abrasivity, abrasive hardness, uncertainty,

FRICTION COEFFICIENT IN CAK

Fifty years ago prof. Kleis made the first centrifugal accelerator (CAK) in Tallinn University of Technology (TUT). In these times, TUT became known as a major research centre in the Soviet Union engaged in studies of erosive processes, in elaboration of new testers, and in investigating materials resistant to erosion. A version of CAK made in 1980, received a gold medal at a major USSR trade fair. A standard GOST 23.201-78 *Gas abrasive wear testing of materials and coatings with a centrifugal accelerator* basing on the CAK was developed in TUT [9]. Particle ejection angle β of CAK was tested thoroughly and is 55° (Figure appendix 1.1 (a)).

a   b
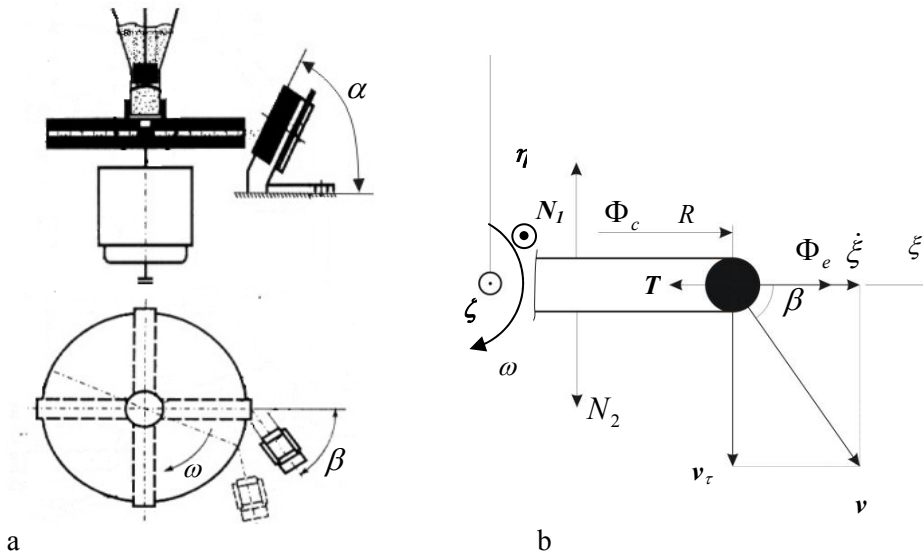
Figure appendix 1.1 General scheme of desintegrator CAK (a) and forces acting on ejecting abrasive particle (b)

Friction coefficient calculation bases on the proved ejection angle β and on the main equation of relative movement in dynamics, equation (2.1). Moreover, as the calculation bases on ejection angle β, it takes into account rolling and sliding of particles in the tube. The calculation was made according to the theory given in [6, 8,39].

$\xi\eta\zeta$ is a body fixed reference frame. Axle ξ coincides with abrasive channel. All axles originate from the centre of the rotor. Angular velocity of the rotor $\omega = 6000$ min^{-1} (628.3 rad/s).

The projections on the indicated axles are (Figure appendix 11 (b))

$$\xi \qquad m\ddot{\xi} = \Phi_e - T$$
$$\eta \qquad 0 = \Phi_c - N_2$$
$$\zeta \qquad 0 = N_1 - mg.$$

We can reveal radial velocity $\dot{\xi}$ from tangential velocity v_τ

$$\Phi_c = \frac{2\omega \cdot v_\tau m}{\tan \beta} = \frac{2\omega^2 \xi \cdot m}{\tan \beta} = N_2 \,.$$

From equation

$$m\ddot{\xi} = m\omega^2 \xi - \mu N_2 = m\omega^2 \xi - \frac{2m\mu\omega^2 \xi}{\tan \beta}$$

$$\ddot{\xi} = \omega^2 \xi - \frac{2\mu\omega^2 \xi}{\tan \beta} = \xi(\omega^2 - \frac{2\mu\omega^2}{\tan \beta})$$

$$\dot{\xi} \frac{d\dot{\xi}}{d\xi} = \xi(\omega^2 - \frac{2\mu\omega^2}{\tan \beta}) \,, \quad \int_0^{\dot{\xi}} \dot{\xi} d\dot{\xi} = (\omega^2 - \frac{2\mu\omega^2}{\tan \beta}) \int_0^{\xi} \xi d\xi$$

$$\frac{\dot{\xi}^2}{2} = (\omega^2 - \frac{2\mu\omega^2}{\tan \beta}) \frac{\xi^2}{2} \,, \quad \dot{\xi}^2 = (\omega^2 - \frac{2\mu\omega^2}{\tan \beta})\xi^2 = \xi^2 \omega^2 - \frac{2\mu\xi^2 \omega^2}{\tan \beta}$$

$$\frac{2\xi^2 \mu\omega^2}{\tan \beta} = \xi^2 \omega^2 - \dot{\xi}^2$$

$$\mu = \frac{\xi^2 \omega^2 \tan \beta}{2\xi^2 \omega^2} - \frac{\dot{\xi}^2 \tan \beta}{2\xi^2 \omega^2}$$

After substituting $\dot{\xi} = \dfrac{\omega\xi}{\tan \beta}$

$$\mu = \frac{\tan \beta}{2} - \frac{\omega^2 \xi^2 \tan \beta}{2\omega^2 \xi^2 \tan^2 \beta} = \frac{\tan \beta}{2} - \frac{1}{2\tan \beta} = \frac{\tan^2 \beta - 1}{2\tan \beta}$$

$$\mu = \frac{\tan^2 55 - 1}{2\tan 55} = 0.36$$

LOS ANGELES TEST

The Los Angeles (L.A) abrasion test is a common test method used to indicate aggregate toughness and abrasion characteristics [74].

The L.A. abrasion test measures the degradation of a coarse aggregate sample that is placed in a rotating drum with steel spheres. As the drum rotates the aggregate degrades by abrasion and impact with other aggregate particles and the steel spheres (called "charge") [74]. According to [75], L.A. test method involves at least 15 kg of test aggregate sample between (10-14) mm in size.

A reduced test sample of (5000 ± 5) g is obtained from the test aggregate. The reduced sample is rotated in a steel drum, which contains a projecting shelf inside, with a specified quantity of steel balls, at a speed of 31 to 33 revolutions per minute for 500 revolutions [72]. The quantity of steel balls depends from the size fraction of the test aggregate. For general (10−14) mm size fraction of the sample of aggregate are used eleven balls. For reduced fraction (4−6.3) mm sample of aggregate are used seven balls [60].

The L.A. Coefficient is calculated from the proportion of the sample reduced to less than 1.6 mm in size [75]:

$$LA = \frac{5000 - m}{50}, \text{ where}$$

m – is the mass retained on a 1.6 mm sieve, in grams.
Basically, the LA coefficient value indicates a percentage of the total aggregate weight that has broken down to smaller than 1.6 mm [74].

ELULOOKIRJELDUS

1. Isikuandmed
    Ees- ja perekonnanimi   Riho Tarbe
    Sünniaeg ja -koht   18.08.1978, Aegviidu, Eesti
    Kodakondsus   eestlane

2. Kontaktandmed
    Aadress   Ehtitajate tee 5, 19086, Tallinn
    Telefon   +3726 203 371
    E-posti aadress   rihot@staff.ttu.ee

3. Hariduskäik

Õppeasutus (nimetus lõpetamise ajal)	Lõpetamise aeg	Haridus (eriala/kraad)
Tallinna Tehnikaülikool	2004	Tootmistehnika, MSc.
Tallinna Tehnikaülikool	2004 -	Masina- ja aparaadiehitus, Doktoriõpe
Tallinna Tehnikaülikool	2001	Tootmistehnika, BSc.

4. Keelteoskus (alg-, kesk- või kõrgtase)

Keel	Tase
Eesti	emakeel
Inglise	kesktase
Soome	algtase
Vene	algtase
Saksa	algtase

5. Täiendusõpe

Õppimise aeg	Täiendusõppe läbiviija nimetus
2007	Mittepurustava kontrolli kursus. Visuaalkontrolli meetod II tase.
2005	Suvekool pulbermetallurgias,

	Euroopa pulbermetallurgia ühing (EPMA)

6. Teenistuskäik

Töötamise aeg	Tööandja nimetus	Ametikoht
2004–	Tallinna Tehnikaülikool, Mehaanikateaduskond, Materjalitehnika instituut, Materjaliõpetuse õppetool;	Teadur
2006–2007	Tehnokontrollikeskus	Surveseadmete tugevusarvutus
2005–2008	Keemia ja materjalitehnoloogia teaduskond, Uute tootmistehnoloogiate ja -prots.doktorikool; Erakorraline teadur (0.25)	Teadur
2000–2004	Tallinna Tehnikaülikool, Mehaanikateaduskond, Materjalitehnika instituut, Materjaliõpetuse õppetool;	Insener

7. Teadustegevus

8. Kaitstud lõputööd

9. Teadustöö põhisuunad

Pulbermaterjalide ja -pinnete löökkulumine

10. Teised uurimisprojektid

CURRICULUM VITAE

1. Personal data

   Name   Riho Tarbe
   Date and place of birth   18.08.1978

2. Contact information

   Address   Ehitajate tee 5, 19086, Tallinn Estonia
   Phone   +3726 203 371
   E-mail   rihot@staff.ttu.ee

3. Education

Educational institution	Graduation year	Education (field of study/degree)
Tallinn University of Technololgy	2004	Production Engineering/ MSc.
Tallinn University of Technololgy	2004–	Mechanical and instrumental engineering/PhD student
Tallinn University of Technololgy	2001	Production Engineering/ BSc.

4. Language competence/skills (fluent; average, basic skills)

Language	Level
Estonian	mother language
English	average
Finnish	basic skills
Russian	basic skills
German	basic skills

5. Special Courses

Period	Educational or other organisation
2007	Course on non-destructive testing.

	Visual testing (II level)
2005	Powder metallurgy training courses, European Powder Metallurgy Association (EPMA)

6. Professional Employment

Period	Organisation	Position
2004–	Tallinn University of Technology, Faculty of Mechanical Engineering, Department of Materials Engineering, Chair of Materials engineering	Reasearch Scientist
2006–2007	Technical Inspection Centre	Strength calculation of pressure vessels
2005–2008	Tallinn University of Technology , Faculty of Chemical and Materials Technology, Doctoral School of new production technologies and processes	Reasearch Scientist
2000–2004	Tallinn University of Technology, Faculty of Mechanical Engineering, Department of Materials Engineering, Chair of Materials engineering	Engineer
Period	Organisation	Position

7. Scientific work

8. Defended theses

9. Main areas of scientific work/Current research topics

Impact wear of powder materials and coatings

10. Other research projects